Nuclear Physics

Todd H. Rider thor@riderinstitute.org 13 November 2019

Any suggestions for improvements would be greatly appreciated.

...The intense atom glows
A moment, then is quenched in a most cold repose.

–Percy Bysshe Shelley
Adonais: An Elegy on the Death of John Keats
Stanza XX (1821)

The Germans have in recent times carried out two large-capacity bomb explosions in Thuringia. The explosions took place in a forest area, under conditions of strictest secrecy. Trees fell at a distance of 500–600 meters from the center of the explosion. Buildings and fortifications specially constructed for the tests have been destroyed.

Prisoners of war who were near the epicenter of the explosion died, often without leaving a trace. Prisoners of war who were in the area beyond the center of the explosion have burns on their face and body, the strength of which depends on their position in relation to the epicenter of the explosion. The tests were carried out in a remote deserted area. The regime of secrecy at the test site was at maximum level. Entrance and exit from the territory are by special pass only. SS soldiers have surrounded the area of tests and interrogated any person approaching the area.

The bomb, supposedly filled with uranium 235 and weighing approximately two tons, was brought to the test site on a specially constructed truck. Dewars of liquid oxygen were delivered together with it. The bomb was permanently guarded by 20 guards with dogs. The bomb explosion was accompanied by a large explosive wave and high temperature. In addition, a massive radioactive effect was observed. The bomb is a sphere with a diameter of 130 cm.

–Soviet military intelligence report to Joseph Stalin (March 23, 1945)

Overview

Nuclear physics concerns the behavior of atomic nuclei, which are composed of protons and neutrons held together by the strong nuclear force. To avoid many-body calculations involving complicated forces, one can use simplified theoretical models, including the liquid drop model, Fermi gas model, and shell model. As will be shown, these models correctly describe processes such as radioactive decay, in which a nucleus emits an alpha, beta, or gamma particle to reach a more stable state. The models also describe nuclear reactions such as fusion (joining of two nuclei) and fission (splitting of a nucleus). Methods by which the alpha, beta, gamma, and neutron radiation from nuclei can be attenuated and detected will be presented. Finally, medical and other applications of radiation will be discussed.

Contents

1 Nuclear Structure

This section will examine the structure of atomic nuclei [1-4]. After considering the component particles within nuclei, we will present theoretical models that greatly simplify the interactions of the large number of particles inside typical nuclei. These models include: (1) the liquid drop model, which treats the nucleus as a continuous blob of matter, (2) the Fermi gas model, which explains how like particles within a nucleus avoid being in exactly the same state as each other, and (3) the shell model, in which protons and neutrons orbit within a nucleus just as electrons orbit around an atom. These models will be used to analyze nuclear masses, spins, and electromagnetic moments in this section, as well as nuclear decays and reactions in Sections 2 and 3.

1.1 Nuclear Processes Versus Chemical Processes

Whereas chemical reactions are due to rearrangement of electrons in atomic orbitals, nuclear decays and reactions are due to rearrangement of nucleons (protons and neutrons) in the nucleus. The difference in size between atomic electron orbits and nucleon spacing in the nucleus has a profound effect on the energies involved in chemical and nuclear processes (Fig. 1). Electron orbits are typically measured in units of Angstroms, 1 A = 10^{-10} m. Nuclear sizes are typically measured in units of **fermis** or femtometers, 1 fm = 10^{-15} m, roughly the diameter of a proton or neutron.

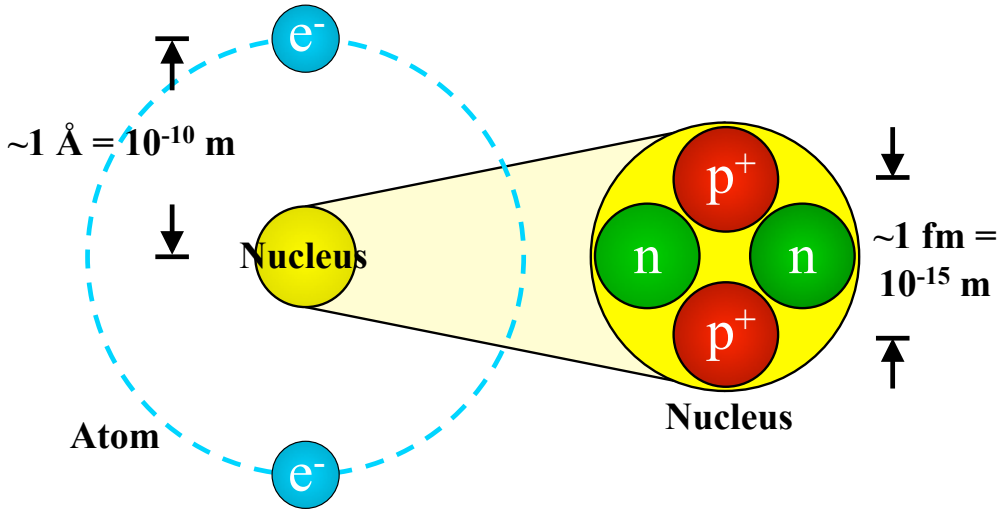

Figure 1. Size matters. The nucleus is $\sim 10^5$ smaller than atomic electron orbits, so nucleons (protons and neutrons) have $\sim 10^5$ more energy than electrons.

Energies in nuclear physics and related fields are often measured in electron volts (eV), where 1 eV = 1.602×10^{-19} J, as well as multiples such as kilo-electron volts (keV) and mega-electron volts (MeV). Temperatures T are frequently converted to an equivalent thermal energy $k_B T$ in electron volts, where $k_B = 1.3807 \times 10^{-23}$ J/^{o}K $= 8.618 \times 10^{-5}$ eV/^{o}K is the Boltzmann constant.

The effect of size on reaction energies may be estimated from Coulomb's law, in which the attractive or repulsion electrostatic potential energy between two particles is inversely proportional to the separation r between those particles:

$$E \sim \frac{e^2}{4\pi\epsilon_0 r} = \frac{14.4 \text{ eV}}{r \text{ [in A]}} \tag{1}$$

$$\frac{E_{\text{nucl}}}{E_{\text{chem}}} \sim \frac{r_{\text{atom}}}{r_{\text{nucl}}} \sim 10^5 \tag{2}$$

Because nuclei are $\sim 10^5$ smaller than atomic electron orbits, the energies of nuclear processes E_{nucl} are typically $\sim 10^5$ larger than those of chemical processes E_{chem}. As will be seen, the strong nuclear force also plays a vital role in nuclear processes, yet this simple estimate is still valid since the strong force is comparable to the Coulomb force in nuclei.

Alternatively, the effect of size on reaction energies may be estimated from the **Heisenberg uncertainty principle** for the uncertainty Δx in a particle's position and the uncertainty Δp in that particle's momentum (*Nonrelativistic Quantum Physics* ?.?):

$$(\Delta x)\,(\Delta p) \sim \hbar \tag{3}$$

where $\hbar \approx 1.055 \times 10^{-34}$ J·sec $\approx 6.582 \times 10^{-16}$ eV·sec is **Planck's constant**. Using the uncertainty principle, the minimum energy E of a particle depends on the particle's mass m and the space Δx within which the particle is confined:

$$E \sim \frac{(\Delta p)^2}{2m} = \frac{\hbar^2}{2m(\Delta x)^2} \tag{4}$$

$$\frac{E_{\text{nucl}}}{E_{\text{chem}}} \sim \frac{m_e}{m_p}\left(\frac{r_{\text{atom}}}{r_{\text{nucl}}}\right)^2 \sim 10^6 \tag{5}$$

Thus both of these simple estimates show that nuclear processes have $\sim 10^5 - 10^6$ more energy than chemical chemical processes (energies of MeV vs. eV). This also means that a nuclear particle has enough energy to break $\sim 10^5 - 10^6$ chemical bonds. As a result, radiation from nuclear decays or reactions can damage hardware components, depending on the particle type and component material. Similarly, radiation is especially bad for DNA and other biological molecules. These issues will be addressed in Sections 4 and 6.

1.2 Quarks, Gluons, and Pions, Oh My!

We will now consider in more detail the particles and forces that are involved in atomic nuclei. Nuclei are composed of protons, which have a positive electric charge e, and neutrons, which have no net electric charge. Sometimes protons and neutrons are lumped together under the generic names of nucleons or **baryons**. Scrutinized more closely, a proton is composed of two **up quarks** (electric charge $+\frac{2}{3}e$) and one **down quark** (charge $-\frac{1}{3}e$), whereas a neutron contains two down quarks and one up quark. These particles experience electromagnetic forces because of their electric charges.

A second force is particularly important for the particles in nuclei. Quarks interact with each other via the **strong nuclear force**, which is mediated by the exchange of **gluons** (*Relativistic Quantum Field Theory* Section 4). This force binds together the three quarks within each proton and neutron. In addition, it binds together pairs of various types of quarks and antiquarks to form different **mesons**, the most common of which are charged or neutral **pions** (π^+, π^-, and π^0).

The exchange of mesons produces a mutual attraction between nucleons. This attraction is actually an indirect manifestation of the strong nuclear force. For example, Fig. 2(a) shows two protons exchanging a neutral pion, revealing all of the quark and gluon interactions involved in that process.

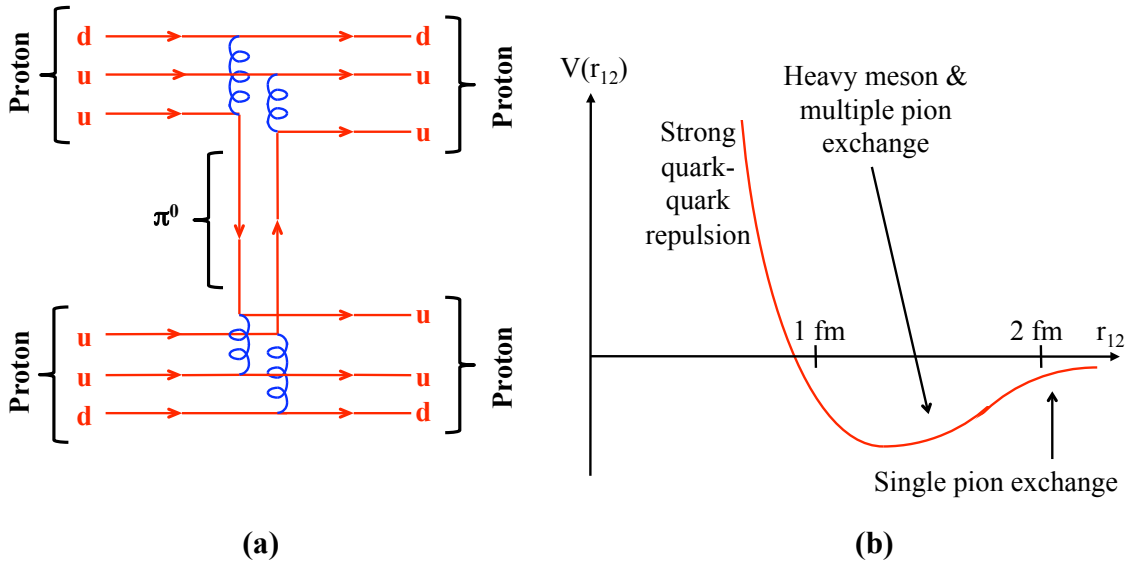

Figure 2. Strong force between nuclei. **(a)** The strong force, caused by gluon exchange (coiled lines) between quarks (lines with arrows), manifests itself indirectly as mesons that bind nuclei together. Time advances to the right and the vertical direction is spatial separation. **(b)** The strong force potential between two nucleons is dominated by single pion exchange for separations $r_{12} > 2$ fm, heavy meson and multiple pion exchange for 1 fm $< r_{12} <$ 2 fm, and quark-quark repulsion for $r_{12} < 1$ fm.

Throughout this summary, we will ignore these underlying quark-gluon interactions and consider only the net forces among protons and neutrons. Quantum chromodynamics (QCD), which describes quark-gluon interactions and is explained in the field theory summary, is so complicated that it can scarcely be used to calculate practical results even for just two or three quarks. Applying QCD to all the quarks in a nucleus would be obscenely complicated. As will be shown, our simpler approach yields sufficiently accurate results. "Pay no attention to that man behind the curtain..."

Just to sound impressive, nuclear physicists sometimes mention **isospin** [1, 2], a measure of whether something is more like a proton or like a neutron. Just as a spin-$\frac{1}{2}$ particle can be in $+\frac{1}{2}$ or $-\frac{1}{2}$ spin states, a nucleon has $+\frac{1}{2}$ isospin if it is a proton and $-\frac{1}{2}$ isospin if it is a neutron. Since absorption of a positive pion changes a neutron into a proton, π^+ has +1 isospin. A negative pion effects the opposite change and thus has -1 isospin, while π^0 has 0 isospin. If you simply keep track of electric charges or quark content, you can ignore isospin without missing any important physical principles.

For a meson of mass m_{meson} to exist officially, its total energy must at least equal the rest energy $m_{\text{meson}}c^2$, where c is the speed of light. The mesons that effectively transmit the strong nuclear force between nucleons do not have that much energy and are therefore called **virtual** particles. From quantum physics, a virtual meson with zero energy can violate the conservation of energy by an amount $\Delta E = m_{\text{meson}}c^2$ for a duration Δt given by the other Heisenberg uncertainty principle between energy and time (*Nonrelativistic Quantum Physics* ?.?):

$$(\Delta E)\,(\Delta t) \;\sim\; \hbar \qquad \Longrightarrow \qquad \Delta t \;\sim\; \frac{\hbar}{m_{\text{meson}}c^2}\,. \tag{6}$$

Even if the virtual mesons move at nearly the speed of light, during their brief existence they can only travel a distance

$$\Delta x \sim c\Delta t \sim \frac{\hbar}{m_{\rm meson}c} = \frac{197.3}{m_{\rm meson,\ MeV/c^2}} \text{ fm} . \tag{7}$$

In nuclear and particle physics, particle masses are often given in units of MeV/c^2 ($\approx 1.783 \times 10^{-30}$ kg). The numerical factor in Eq. (7) is frequently useful for evaluating results in nuclear physics:

$$\hbar c \approx 197.3 \text{ MeV} \cdot \text{fm} . \tag{8}$$

Pions have a mass $m_\pi \sim 140$ MeV/c^2, so from Eq. (7) the range of virtual pions is only ~ 1.4 fm. Other mesons have higher masses and hence even shorter ranges.

The mass of an isolated proton is $m_p \approx 938.28$ MeV/c^2, while that of an isolated neutron is $m_n \approx 939.57$ MeV/c^2. As will be shown in Section 1.2, protons and neutrons have slightly smaller masses when they are inside nuclei. If an extra several hundred MeV of energy is given to a nucleon, it can be converted into a more massive baryon such as a Δ, or its quarks can be sent into higher-energy internal orbits. This occurs at much higher energies than the nuclear phenomena that are covered in this summary; see the relativistic quantum field theory summary for more information.

If mesons were massless, the attractive potential between two nucleons would vary like $1/r_{12}$ with their separation distance r_{12}, just like the electrostatic Coulomb potential (which is mediated by the exchange of virtual massless photons). However, the number of virtual mesons decreases exponentially with distance, with the decay length found from Eq. (7). Thus the strong nuclear potential combines a $1/r_{12}$ dependence with exponential decay; this is called the **Yukawa potential**:

$$V(\mathbf{r_{12}}) \propto \frac{1}{r_{12}} \exp\left(-\frac{m_{\rm meson}c}{\hbar}\, r_{12}\right) . \qquad \textbf{Yukawa potential} \tag{9}$$

As expected, the Yukawa potential reduces to the Coulomb potential for $m_{\rm meson} = 0$.

The strong force between two nucleons also depends on the spin orientations of the nucleons, adding to Eq. (9) a factor involving Pauli spin matrices $\sigma_\mathbf{1}$ and $\sigma_\mathbf{2}$ for the nucleons. Using a constant g_π and the virtual pion range $r_\pi \equiv \hbar/(m_\pi c)$, the result is the **one-pion exchange potential** [1-4]:

$$V(\mathbf{r_{12}}) = \frac{g_\pi^2 (m_\pi c^2)^3}{3(m_p c^2)^2 \hbar^2} \left\{ \sigma_\mathbf{1} \cdot \sigma_\mathbf{2} + \left[\frac{3(\sigma_\mathbf{1} \cdot \mathbf{r_{12}})(\sigma_\mathbf{2} \cdot \mathbf{r_{12}})}{r_{12}^2} - (\sigma_\mathbf{1} \cdot \sigma_\mathbf{2}) \right] \left(1 + \frac{3r_\pi}{r} + \frac{3r_\pi^2}{r^2} \right) \right\} \frac{e^{-r_{12}/r_\pi}}{r_{12}/r_\pi} \tag{10}$$

Moreover, while single-pion exchange dominates the potential for $r_{12} > 2$ fm, for 1 fm$< r_{12} < 2$ fm exchanges of multiple pions or of more massive mesons become important. Reaching $r_{12} < 1$ fm requires a great deal of energy to promote some of the nucleons' quarks to higher energy levels, since as fermions they do not want to share the same state and location. Figure 2(b) qualitatively shows these effects. The large number of contributing processes and the complexities of QCD prevent a more quantitative calculation of the potential. Likewise, it is difficult to directly measure these virtual-meson effects, although experiments in which real mesons interact with nucleons provide some relevant data [1]. Fortunately, the nuclear models outlined in the coming sections do not require a detailed knowledge of the nucleon-nucleon potential to yield useful results.

The strong nuclear force among protons and neutrons overcomes the enormous electrostatic repulsion among the protons and holds a nucleus together (hence the name). However, the strong force decreases exponentially beyond the virtual meson range $\sim 1 - 2$ fm, which is comparable to the diameter of a nucleon, so nucleons typically only feel much strong force attraction from their nearest neighbors in a nucleus. Assuming that virtual mesons travel at nearly light speed $c = 3 \times 10^{23}$ fm/sec, the typical **nuclear interaction time** between adjacent nuclei is $\sim 10^{-23}$ sec.

The atomic number Z is the number of protons in an atomic nucleus; it is also the number of electrons orbiting around the nucleus when the atom is neutral. N is the number of neutrons in the nucleus. The atomic mass $A = N + Z$ is the total number of nucleons in the nucleus.

A particular type of nucleus is generally designated by the form ${}^{A}_{Z}\mathrm{X}_{N}$, using the values of Z, A, and N for the nucleus and the corresponding chemical abbreviation X for that element. For example, ${}^{235}_{92}\mathrm{U}_{143}$ is uranium with 92 protons, 143 neutrons, and 235 total nucleons. Because Z is uniquely specified for each element name and the number of neutrons may be obtained from $N = A - Z$, the designations are usually shortened to the form ${}^{A}\mathrm{X}$, such as ${}^{235}\mathrm{U}$.

Different nuclei having the same Z, N, or A are sometimes noteworthy. **Isotopes** are different nuclei having the same number of protons but different numbers of neutrons. For instance, ${}^{235}\mathrm{U}$ and ${}^{238}\mathrm{U}$ are important isotopes of uranium. **Isotones** have the same number of neutrons yet different numbers of protons. As an example, ${}^{3}\mathrm{H}$ (tritium) and ${}^{4}\mathrm{He}$ (helium-4) are isotones with two neutrons each. **Isobars** have the same A value but different Z and N values. For instance, ${}^{140}\mathrm{Xe}$ and ${}^{140}\mathrm{Cs}$ are isobars that can be produced by fission reactions.

The cross-sectional area of a nucleus is important for electromagnetic moments (Section 1.3) and nuclear reactions (Section 3). The customary unit of area in nuclear physics is the **barn** (as in hitting the side of a barn): 1 barn (b) $\equiv 10^{-28}$ m^2 $= 100$ fm^2. Note that the barn unit was chosen to correspond to the rough area of an average-sized nucleus of diameter ~ 10 fm.

1.3 Liquid Drop Model

The **liquid drop model** ignores individual nucleons and treats the nucleus essentially like a continuous drop of liquid. Although crude, this model accurately describes a variety of nuclear properties, including nuclear sizes, masses, and stable Z/A ratios (Fig. 3), as well as fission (Section 3.3).

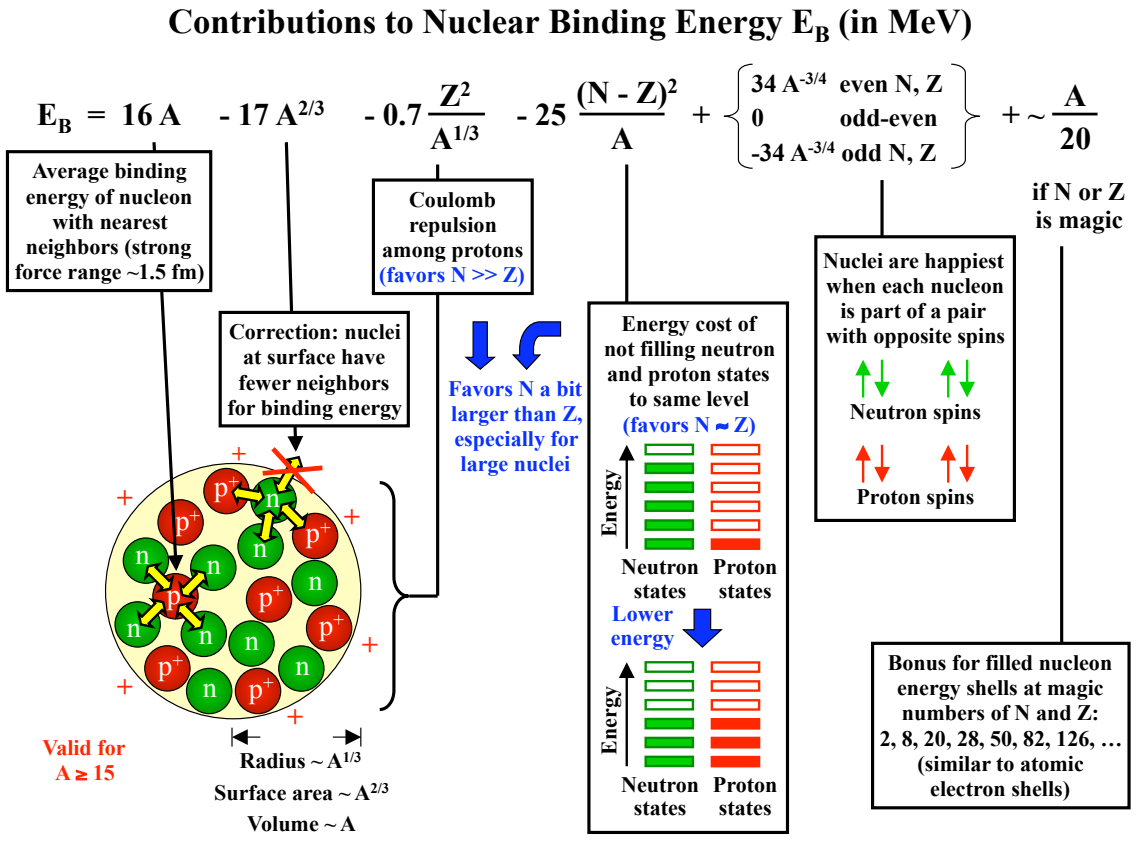

Figure 3. Contributions to the nuclear binding energy. The first term is simply the average binding energy per nucleon with its nearest neighbors. The second term is a surface-area correction, since nucleons at the surface of the nucleus have fewer neighbors to contribute to the binding energy. The third term, Coulomb repulsion among the protons, favors $N \gg Z$. The fourth term, the energy cost of not filling available neutron and proton states to the same level, favors $N \approx Z$. The net result of the third and fourth terms is to favor $N \approx Z$ for small nuclei and N a bit larger than Z for large nuclei. The fifth term accounts for the fact that nuclei are the happiest when each nucleon is part of a pair with opposite spins. Finally, the sixth term is a correction for shell effects that are not included in the liquid drop model; nuclei are more stable if their neutrons and/or protons have filled energy shells.

Assuming a constant density of matter in nuclei, the volume of a nucleus should be proportional to the number of nucleons A it contains. Noting that the radius of a sphere varies like the cube root of its volume, and using an experimentally determined constant, the radius of a nucleus is thus

$$R \;=\; 1.2\,A^{1/3}\;\text{fm} \tag{11}$$

The mass of an atom is basically the sum of the masses of its component protons, electrons, and neutrons. However, the atom has a certain binding energy E_B since its particles are happier being together than apart from each other. Because energy and mass are related by special relativity, $E = mc^2$, the binding energy lowers the total mass of the atom:

$$M \;\;=\;\; (m_p + m_e)Z \;+\; m_n(A-Z) \;-\; \frac{E_B}{c^2} \tag{12}$$

From quantum physics, atomic electrons have a binding energy on the order of several eV per electron due to their electrostatic attraction to the positive nucleus. This is much smaller than the nuclear binding energy of several MeV per nucleon and will be ignored here.

The nuclear binding energy arises from protons and neutrons glomming onto each other. If every pair of nucleons in the nucleus felt a mutual strong-force attraction, the binding energy would increase like A^2 with the number of possible pairs. Yet because the strong force has such a short range, each nucleon only feels an attractive potential from its nearest neighbors. Each nucleon has roughly the same number of nearest neighbors regardless of the size of the nucleus, so the strong-force binding energy is roughly constant per nucleon, or $\propto A$ for the whole nucleus. Empirically, the strong-force binding energy of a surrounded nucleon is approximately 16 MeV, giving a total

$$E_{\text{strong force}} \;\approx\; +16\,A\;\;\text{MeV} \tag{13}$$

However, this overestimates the binding energy, since nucleons at the surface of the nucleus don't have as many neighbors. Therefore we must subtract from the binding energy a correction term for the surface nucleons. These nucleons still have neighbors further inside the nucleus and around them on the surface, so we will only lop off $\sim$ 4 MeV of their binding energy. Assuming that nucleons are spaced $\sim$ 2 fm apart, each surface nucleon occupies $\sim$ 4 fm^2 of surface area. The surface area of a nucleus is $4\pi R^2$, with R from Eq. (11), so the net correction is

$$E_{\text{surface}} \;\approx\; -4\;\text{MeV}\;\times\left(\begin{array}{c}\text{No. of surface}\\ \text{nucleons}\end{array}\right) \approx\; -4\;\text{MeV}\;\times\;\frac{4\pi\left(1.2A^{1/3}\;\text{fm}\right)^2}{4\;\text{fm}^2}\;\approx\; -17\,A^{2/3}\;\text{MeV} \tag{14}$$

Because the nuclear volume is proportional to A, the surface area is proportional to $A^{2/3}$. This term E_{surface} is similar to the surface tension of a liquid drop.

Electrostatic repulsion among the protons in the nucleus further decreases the binding energy. This Coulomb repulsion energy may be estimated from the potential energy of a uniformly charged sphere with total charge Z (*Electromagnetism* ?.?) and radius R from Eq. (11):

$$E_{\text{Coulomb}} \;=\; -\,\frac{3}{5}\,\frac{(Ze)^2}{4\pi\epsilon_o R} \;\approx\; -0.7\,\frac{Z^2}{A^{1/3}}\;\;\text{MeV} \tag{15}$$

For a finite number of charges Z, there are only $Z(Z-1)$ pairs of charges to repel each other, so some authors use $Z(Z-1)$ instead of Z^2 in Eq. (15). However, there is very little difference between the two factors for nuclei large enough for these calculations to be valid ($Z > 7$ or so).

Protons and neutrons are fermions, so no proton can occupy the same state as any other proton in the nucleus, and no neutron can occupy the same state as any other neutron. As Sections 1.3 and 1.4 will show in more detail, protons successively fill up the lowest possible proton energy states in the nucleus, and neutrons fill up their own lowest energy states. If there are many more neutrons than protons, neutrons fill up the possible neutron states all the way to very high energies, while protons only fill low-energy proton states [Fig. 3 center]. This takes more energy than having roughly equal numbers of protons and neutrons, such that the filled proton and neutron states only extend up to moderate energies. The energy cost of having unequal numbers of protons and neutrons may be included by altering the binding energy by

$$E_{\text{symmetry}} \approx -25 \frac{(N-Z)^2}{A} \text{ MeV} = -25 \frac{(A-2Z)^2}{A} \text{ MeV} \tag{16}$$

This is called the **symmetry energy**, since it enforces a symmetry between the number of protons and the number of neutrons. The factor of $1/A$ is included because a given difference $N - Z$ is less significant when it represents only a small fraction of the total number of nucleons A. The numerical constant will be justified in Section 1.3.

Like atomic electrons, nucleons can have spin up or spin down. Identical fermions do not want to be in exactly the same state while they are at the same location. Two identical fermions with opposite spins are not in the same state and thus can be closer together than identical fermions that have the same spin. If the fermions are electrons, being closer together increases Coulomb repulsion, so atomic electrons prefer to be in different spin states (Hund's rules, *Nonrelativistic Quantum Physics* ?.?). Yet if the fermions are two neutrons or two protons, being closer together increases strong force attraction, so nuclei with the lowest energies have protons in pairs with opposite spins and neutrons in pairs with opposite spins. This pairing tendency means that nuclei are happier when Z and N are even than when they are odd. The binding energy increases by a **pairing energy** δ (which must be determined from experiments) for **even-even** nuclei with Z and N even, and decreases by δ for **odd-odd** nuclei with Z and N odd. For **even-odd** nuclei with even Z and odd N or vice versa, the even and odd effects cancel out and the binding energy need not be modified.

$$E_{\text{pairing}} \equiv \delta \approx \begin{cases} 34\, A^{-3/4} \text{ MeV} & \text{if even-even} \\ 0 \text{ MeV} & \text{if even-odd} \\ -34\, A^{-3/4} \text{ MeV} & \text{if odd-odd} \end{cases} \tag{17}$$

Collecting Eqs. (13)-(17), the net nuclear binding energy E_B is [Fig. 3]:

$$\begin{aligned} E_B &= E_{\text{strong force}} + E_{\text{surface}} + E_{\text{Coulomb}} + E_{\text{symmetry}} + E_{\text{pairing}} \\ &\approx 16\, A \text{ MeV} - 17\, A^{2/3} \text{ MeV} - 0.7 \frac{Z^2}{A^{1/3}} \text{ MeV} - 25 \frac{(A-2Z)^2}{A} \text{ MeV} \\ &\quad + \begin{cases} 34\, A^{-3/4} \text{ MeV} & \text{if even-even} \\ 0 \text{ MeV} & \text{if even-odd} \\ -34\, A^{-3/4} \text{ MeV} & \text{if odd-odd} \end{cases} \end{aligned} \tag{18}$$

E_B/A vs. N and Z is graphed in Fig. 4. Equation (18) used in conjuction with Eq. (12) is called the **Weizsäcker semiempirical mass formula**. It may be written more compactly as

$$Mc^2 \approx \left(\frac{100}{A} + \frac{0.7}{A^{1/3}}\right) Z^2 - 101Z + 949A + 17A^{2/3} - \delta \text{ MeV} \tag{19}$$

Because individual-particle effects in the nucleus have been mostly ignored, the Weizsäcker semiempirical mass formula is not valid for nuclei that contain only a few particles, $A < 15$. It also neglects shell effects which add $\sim A/20$ MeV to E_B at certain "magic" values of N and Z [Fig. 3 right side], as will be discussed in the next section.

For a given value of A, the most stable element has a value of Z that minimizes the mass M in Eq. (19). Setting $\partial M/\partial Z = 0$ yields the most stable ratio Z/A:

$$\frac{Z}{A} \approx \frac{1}{2}\,\frac{1}{1+7\times 10^{-3}A^{2/3}} \tag{20}$$

From Eq. (20), the most stable light elements have $N \approx Z$, due to the symmetry energy E_{symmetry}. However, heavy elements have somewhat more neutrons than protons, because of the large Coulomb repulsion E_{Coulomb} from the protons: $Z/A \sim 0.4$ for $A \sim 100$ and up. For example, the most abundant uranium isotope has $Z/A = 92/238 \approx 0.39$. Naturally occurring nuclei lie along this "valley of stability" given by Eq. (20) and shown as a valley in Fig. 4 and a line in Fig. 5(a).

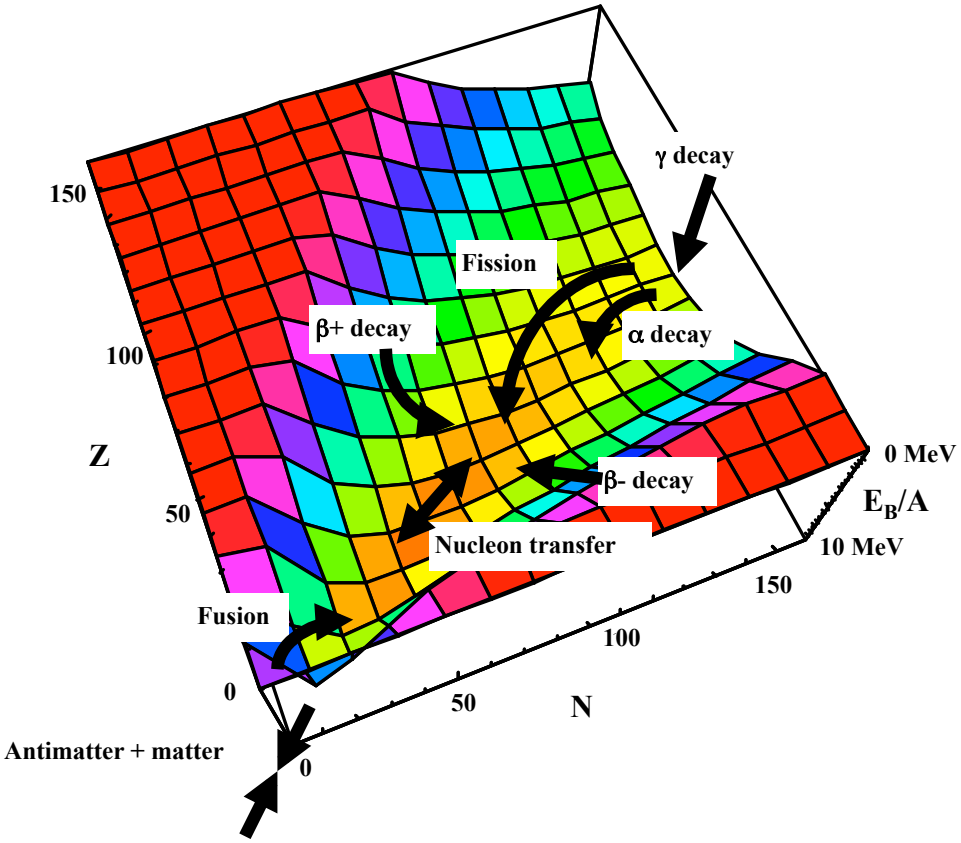

Figure 4. Binding energy per nucleon and methods of tapping into it. Nuclei lower on the vertical axis are more stable. Different types of decays and reactions (arrows) move nuclei lower, releasing energy and forming more stable nuclei, as will be discussed in Sections 2 and 3.

Figure 5(b) plots the binding energy per nucleon E_B/A versus A for nuclei along the line from Eq. (20). By convention this vertical axis is inverted relative to Fig. 4, so that in Fig. 5(b) higher nuclei are more stable. Note that the curve peaks at around iron, ^{56}Fe. Basically, nuclei are happiest when they are medium-sized, and they are less happy if they think they are too small or too large–sort of like people.

Sometimes nuclear masses are given in **unified atomic mass units** u instead of MeV/c^2 or kg. One u, defined as 1/12 the mass of a ^{12}C atom (electrons and all), is 931.5 MeV/c^2. Ignoring the electron contribution, this is essentially the average mass of a nucleon in ^{12}C, and it may be compared with the mass $\sim$ 939 MeV/c^2 of a free nucleon.

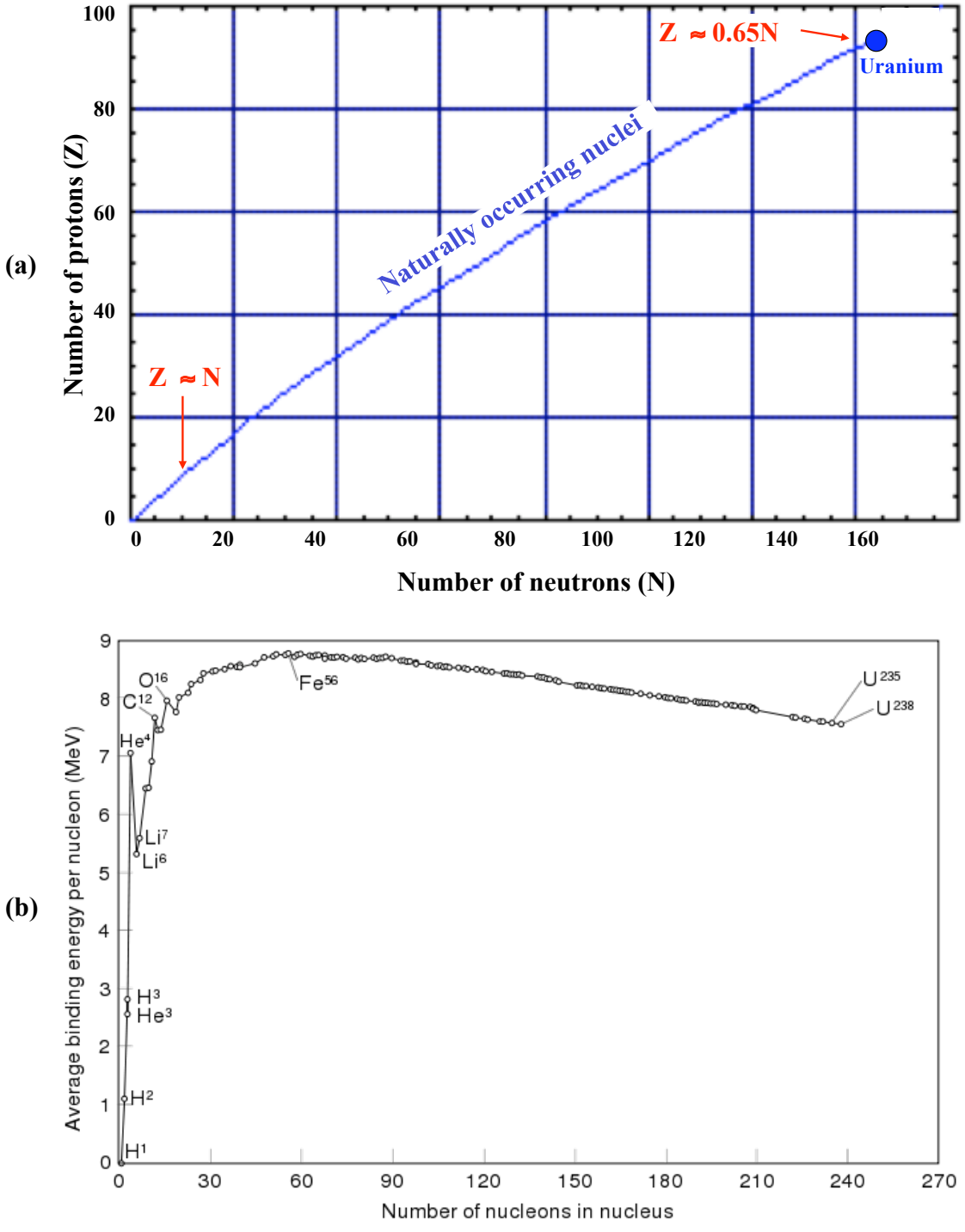

Figure 5. Effects of the nuclear binding energy. **(a)** This line of naturally occurring nuclei agrees with Eq. (20) and corresponds to the valley in Fig. 4. **(b)** Binding energy per nucleon in MeV, plotted along the line from (a) of the most beta-stable nucleus for each mass. This corresponds to the bottom along the length of the valley in Fig. 4, only plotted upside down (more stable nuclei are higher).

1.4 Fermi Gas Model

Whereas the liquid drop model treats the nucleus as a continuum of matter, the **Fermi gas model** treats the nucleus as a collection of individual nucleons. This model is particularly useful for estimating the energy levels in a nucleus and for defining the temperature of a nucleus.

Using $N \approx Z \approx A/2$ and Eq. (11), the density of identical fermions (neutrons or protons) within the volume $\frac{4}{3}\pi R^3$ of a nucleus is

$$n_{\text{fermions}} \;=\; \frac{N \text{ or } Z}{\frac{4}{3}\pi(1.2\text{ fm})^3 A} \;\approx\; \frac{3}{8\pi(1.2\text{ fm})^3} \tag{21}$$

From statistical physics, in the ground state a gas of fermions fills all available energy levels up to the **Fermi energy** E_F. Using Eq. (21), the Fermi energy for neutrons or protons in a nucleus is

$$E_F \;=\; \frac{\hbar^2}{2m}\left(3\pi^2 n_{\text{fermions}}\right)^{2/3} \;\approx\; 30\ \text{MeV} \tag{22}$$

The Fermi energy is independent of the size of the nucleus, since Eq. (11) assumes that the density of nuclear matter remains constant. The Fermi energy is the kinetic energy of the last bound neutron or proton. From statistical physics, the average kinetic energy per fermion is $\frac{3}{5}E_F \approx 18$ MeV. Using the strong force binding energy from Eq. (13), the nuclear potential well depth is

$$V_o \;\approx\; -16\text{ MeV} \;-\frac{3}{5}E_F \;\approx\; -34\text{ MeV} \tag{23}$$

By considering unequal numbers of neutrons and protons, the symmetry energy E_{sym} used in Eqs. (16) and (18) may be calculated. One begins by considering small asymmetries in the neutron and proton numbers and writing the number of neutrons as

$$N \;=\; \frac{A}{2}\left[1+\frac{(N-Z)}{A}\right] \qquad\qquad \frac{(N-Z)}{A} \ll 1 \tag{24}$$

Using Eqs. (21) and (22), the Fermi energy of the neutrons is

$$E_{FN} \;=\; \frac{\hbar^2}{2m}\left[3\pi^2\frac{N}{\frac{4}{3}\pi(1.2\text{ fm})^3 A}\right]^{2/3}, \tag{25}$$

and the total energy of all the neutrons is

$$\begin{aligned} E_N \;&=\; \frac{3}{5}NE_F \;=\; \frac{\hbar^2}{m_n}\,\frac{1}{(1.2\text{ fm})^2}\,\frac{3}{10}\left(\frac{9\pi}{4A}\right)^{2/3}N^{5/3} \\ &\approx\; \frac{\hbar^2}{m_n}\,\frac{1}{(1.2\text{ fm})^2}\,\frac{3}{10}\left(\frac{9\pi}{4A}\right)^{2/3}\left(\frac{A}{2}\right)^{5/3}\left[1+\frac{5}{3}\frac{(N-Z)}{A}+\frac{5}{3}\frac{2}{3}\frac{(N-Z)^2}{A^2}\right], \end{aligned} \tag{26}$$

where Eq. (24) and the binomial expansion were used in the last step. The total proton energy E_P is the same as Eq. (26) but with N and Z interchanged.

E_{sym} is the sum of the neutron and proton energies, relative to their values when $N = Z = \frac{A}{2}$:

$$\begin{aligned} E_{\text{sym}} \;&\equiv\; E_N \;+\; E_P \;-\; E_N\left(N=\frac{A}{2}\right) \;-\; E_P\left(Z=\frac{A}{2}\right) \\ &\approx\; \frac{(\hbar c)^2}{m_n c^2}\,\frac{1}{(1.2\text{ fm})^2}\,\frac{1}{3}\left(\frac{9\pi}{8}\right)^{2/3}\frac{(N-Z)^2}{A} \;\approx\; 22\,\frac{(N-Z)^2}{A}\ \text{MeV} \end{aligned} \tag{27}$$

The nuclear potential well shape (Section 1.4) modifies the constant in Eq. (27) from 22 to 25.

As will be shown in the next section, the energy levels of nucleons can be modeled as simple harmonic oscillator energy levels separated by a spacing $\hbar\omega_o$. The Fermi gas model can be used to estimate $\hbar\omega_o$. Drawing upon quantum physics, the number of identical fermions that can occupy level N of a three-dimensional harmonic oscillator is

$$(2\text{ spin states}) \times \left(\tfrac{N}{2}+1\text{ values of } l\right) \times (N+1\text{ values of } m_l) \;\approx\; N^2 \text{ for large } N \tag{28}$$

where the angular momentum of level N can be $l = N, N-1, N-2, ..., 0$ and the z component of the angular momentum can be $m_l = l, l-1, ..., 1, 0, -1, ..., -l$.

Accomodating $\sim A/2$ identical fermions requires N_{max} levels of the harmonic oscillator:

$$\frac{A}{2} \approx \sum_{N=0}^{N_{max}} N^2 \approx \int_{N=0}^{N_{max}} dN\, N^2 = \frac{1}{3} N_{max}^3$$
$$\implies N_{max} \approx A^{1/3} \tag{29}$$

With the assumption that N_{max} is large, the sum in Eq. (29) was approximated by an integral. The energy of the highest level is simply E_F, so the spacing between harmonic oscillator levels is

$$\hbar\omega_o \approx \frac{E_F}{N_{max}} \approx \frac{30 \text{ MeV}}{A^{1/3}} \tag{30}$$

Using the Sommerfeld approximation from solid state physics, adding an energy E beyond the ground state of a Fermi gas corresponds to a temperature T of the gas:

$$E = \frac{\pi^2}{4} A \frac{(k_B T)^2}{E_F} \equiv a(k_B T)^2 \tag{31}$$

where the constant a has been defined as

$$a \approx \frac{\pi^2}{4} \frac{A}{30 \text{ MeV}} \approx \frac{A}{12 \text{ MeV}} \tag{32}$$

Turning Eq. (31) around, a nucleus excited by an energy E may be said to have a temperature

$$k_B T \equiv \sqrt{\frac{E}{a}} = \sqrt{\frac{12 E_{\text{MeV}}}{A}} \text{ MeV} \tag{33}$$

In nuclear physics, it is common to express temperatures in terms of their equivalent energies in keV or MeV, where 1 keV=1.16×10^7 ^{o}K.

Differentiating Eq. (31) to obtain $dE = 2ak_B^2 T dT$ and using Eq. (33), the definition of entropy from statistical physics yields

$$S \equiv \int_0^T \frac{dE}{T} = \int_0^T \frac{2ak_B^2 T dT}{T} = 2ak_B^2 T = 2k_B\sqrt{aE}\,, \tag{34}$$

From *Statistical Physics* ?.?, the density of energy levels $\rho(E)$ around energy E (when the temperature is T) is related to the low-energy ($T = 0$) level density $\rho(0)$ by

$$\rho(E) = \rho(0) \exp\left[\frac{S(E)}{k_B}\right] = \rho(0) e^{2\sqrt{aE}} \tag{35}$$

Inverting the level density from Eq. (36), the average spacing D between energy levels is:

$$D(E) \approx D(0) e^{-2\sqrt{aE}} \tag{36}$$

Thus the spacing between adjacent energy levels decreases exponentially with increasing energy. Physically, the more energy there is, the more ways there are in which it might be distributed among all the nucleons, creating a greater variety of slightly different energy levels.

Equation (36) should only be used as a very rough guide, since it neglects many of the effects considered in Sections 1.2 and 1.4. Representative parameters are $D(0) \sim 1$ MeV and $a \sim 1/\text{MeV}$ for light nuclei, and $D(0) \sim 0.1$ MeV and $a \sim 5/\text{MeV}$ for heavy nuclei. For example, when a uranium or plutonium nucleus is excited by 6.5 MeV, its average level spacing is

$$D(E) \sim 10^5 \text{ eV } e^{-2\sqrt{5 \cdot 6.5}} \sim 1 \text{ eV} \tag{37}$$

1.5 Shell Model

The **shell model** extends the Fermi gas model by considering additional effects within the nucleus. It assumes that the nucleons collectively create an attractive strong-force potential well in the nucleus and that each nucleon orbits within this well, just as atomic electrons orbit within the electrostatic potential well. Like electrons in an atom, certain numbers of protons and neutrons in a nucleus form particularly stable closed orbital shells–hence the name of this model.

Just as atomic electrons act like blurry quantum mechanical waves that are spread over the volume of the atom, protons and neutrons act like waves described by a wavefunction spread over the nuclear volume. Like atomic electrons (see the nonrelativistic quantum physics summary), the nucleon wavefunctions are described by a few important quantum numbers:

$$\left.\begin{array}{lrcl} \text{Number of radial humps:} & n & = & 1,\ 2,\ 3, ... \\ \text{Orbital angular momentum:} & l & = & 0\ [s],\ 1\ [p],\ 2\ [d],\ 3\ [f],\ 4\ [g],\ 5\ [h], ... \\ \text{Component of } l \text{ in } z \text{ direction:} & m_l & = & l,\ l-1,\ l-2, ...,\ 0, ...\ -l+1,\ -l \end{array}\right\} \quad (38)$$

Angular momentum values l and m_l are expressed as multiples of $\hbar$. For nucleons, n stands for the number of radial humps in the wavefunction. In contrast, the convention for atomic electrons is that n means the number of radial humps plus l. Thus a nucleon with a certain value of n can have any value of l, but an electron with n can only have $l \leq n-1$.

A nucleon can have spin $s = +\frac{1}{2}$ ("up") or $-\frac{1}{2}$ ("down"), also in units of $\hbar$. The total angular momentum is $j = l \pm \frac{1}{2}$. As j is a magnitude, it cannot be negative, so it is restricted to $+\frac{1}{2}$ if $l = 0$. Nuclear physics borrows the spectroscopic notation used to describe atomic electrons, denoting the orbit of a nucleon by nl_j, where the numerical value of l is indicated by the corresponding letter. For example, $1\mathrm{d}_{3/2}$ means $n = 1$, $l = 2$, and $j = 3/2$; thus the spin must be $j - l = \frac{3}{2} - 2 = -\frac{1}{2}$. Each orbit with given values of n and l can contain up to $2(2l+1)$ protons and $2(2l+1)$ neutrons, because there are two available spin states and $2l+1$ possible values of m_l.

Since there is virtually no space between nucleons, how can nucleons freely orbit within a nucleus without continually tripping over each other? A collision would knock nucleons into a new state, and the lowest available energy states are already occupied by other nucleons. Climbing up to an unoccupied energy state would require too much energy, so collisions basically are not allowed.

The collective nuclear potential in which nucleons orbit resembles a three-dimensional simple harmonic oscillator. A harmonic oscillator potential can be written as $V(r) = -V_o + \frac{1}{2} m_{\text{nucleon}} \omega_o^2 r^2$ (*Nonrelativistic Quantum* ?.?) and produces discrete energy levels for nucleons trapped in it:

$$\begin{aligned} E &= -V_o + \hbar\omega_o \left(2n + l - \frac{1}{2}\right) = -V_o + \hbar\omega_o \left(N + \frac{3}{2}\right) \\ &\approx -34 \text{ MeV} + \frac{30}{A^{1/3}} \left(N + \frac{3}{2}\right) \text{ MeV}, \qquad (39) \\ &\text{where } N \equiv 2n + l - 2 = 0,\ 1,\ 2,\ 3, ... \qquad (40) \end{aligned}$$

Equation (39) used the results of Eqs. (23) and (30). The principal quantum number N was introduced to express the energy as multiples of $\hbar\omega_o$ above the zero-point energy $\frac{3}{2}\hbar\omega_o$. Many of the energy levels are degenerate–levels with different n and l but the same net value of N have the same energy. Figure 6(a) plots the simple harmonic oscillator energy levels, showing the number of available states in each level and the total number of states up to and including that level.

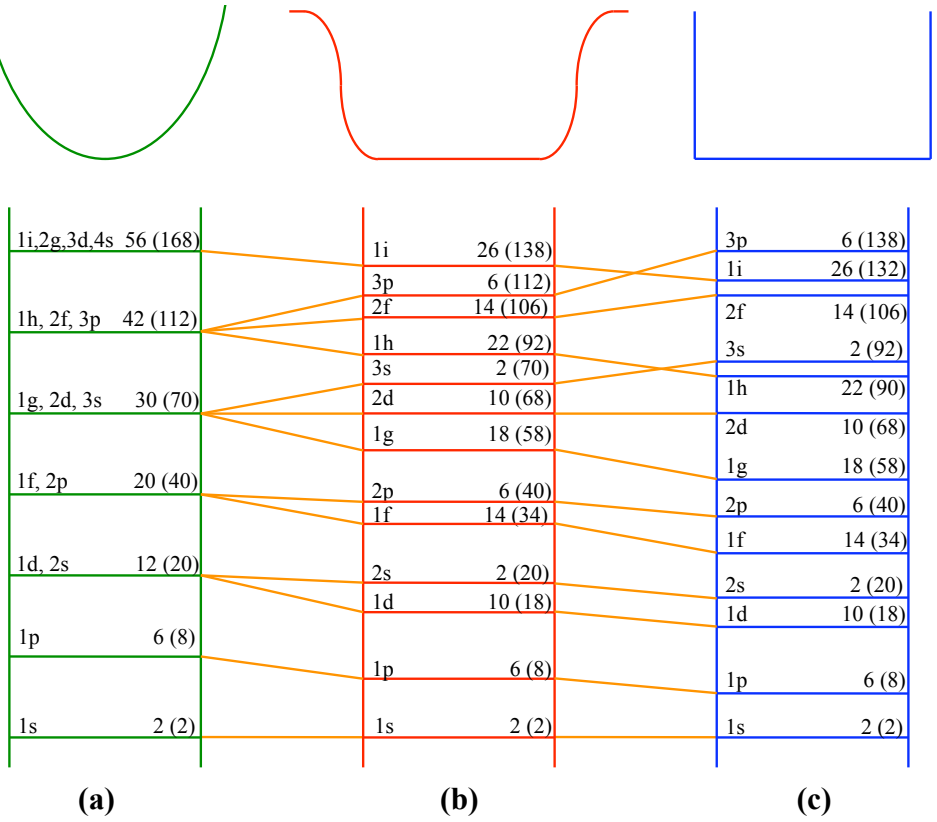

Figure 6. Potential well shape and energy levels for (a) simple harmonic oscillator, (b) realistic nuclear potential, and (c) infinite square well. Indicated for each level are its quantum numbers nl, its number of available states, and in parenthesis, the number of states up to and including that level.

By analogy with classical harmonic oscillators, ω_o may be regarded as the frequency at which nucleons oscillate back and forth in the potential. The corresponding period of the oscillations is

$$\tau_{\text{nucleon}} = \frac{2\pi}{\omega_o} = \frac{h\,A^{1/3}}{30\text{ MeV}} \approx 1.4\times10^{-22}\,A^{1/3}\text{ sec} \qquad \textbf{Nucleon oscillation time} \tag{41}$$

Actually, the bottom of the nuclear potential well is flatter than the simple harmonic oscillator potential. To demonstrate the effects of a flat-bottomed potential well, one can model the nucleus as a three-dimensional spherical square well with radius $R = 1.2A^{1/3}$ fm and infinitely high walls [Fig. 6(c) top]. From *Nonrelativistic Quantum Physics* ?.?, the energy levels of such a well are:

$$E = -V_o + \frac{\hbar^2}{2m_{\text{nucleon}}R^2}\left[\pi^2\left(n+\frac{l}{2}\right)^2 - l(l-1)\right] \tag{42}$$

$$= -34\text{ MeV} + \frac{14.4\text{ MeV}}{A^{2/3}}\left[9.87\left(n+\frac{l}{2}\right)^2 - l(l-1)\right]\text{ MeV} \tag{43}$$

Now n and l have distinctly different effects on the energy. This is shown at the bottom of Fig. 6(c), where numbers again indicate the number of states in each level as well as the total number of states up to and including that level. Thus flattening the bottom of the potential well eliminates the energy degeneracy found in simple harmonic oscillator levels.

In fact, the depth V_o of the nuclear potential well is finite, not infinite. From the quantum summary, inside the well the wavefunction oscillates like $\Psi \sim e^{ikr}$, where $k = \sqrt{2m(E-V_o)}/\hbar$. Outside the well, the wavefunction decays exponentially with distance, $\Psi \sim e^{-\kappa r}$, where $\kappa = \sqrt{2m(V_o-E)}/\hbar$. Ψ and $\partial\Psi/\partial r$ must be continuous at the boundary, but in general the exponential decay for $r > R$ can partially substitute for the outermost downward oscillation of the wavefunction for $r < R$.

For $E \ll V_o$, the walls are essentially infinitely high, so all n humps of the radial wavefunction must fit within the span $0 < r < R$. However, as E increases, the wavefunction begins to leak outside the well; this allows the wavefuction within the well to "decompress" a bit, lengthening its wavelength and decreasing its energy. For E just about equal to the well depth, only half of the last hump of the wavefunction occurs within the well. Since there are only $n - \frac{1}{2}$ humps within the well, the corresponding energy is lowered by substituting $n \to n - \frac{1}{2}$ in Eq. (43).

Realistic nuclear potential wells are intermediate between the harmonic oscillator and square well shapes; they are flat at the bottom and curve upward at the edges [Fig. 6(b) top]. Accordingly, their energy levels are intermediate between those in Eqs. (39) and (43) [Fig. 6(b) bottom].

Because the strong force is spin-dependent [Eq. (10)], the spin and orbital angular momentum of a nucleon interact. This interaction energy term modifies the energy levels we have already found, just as spin-orbit coupling modifies the energy levels of atomic electrons. The spin-orbit contribution to the level energies depends on the value $l \cdot s$, which must be calculated in a convoluted way to obtain the correct answer (see the quantum summary for more information):

$$\begin{aligned} \mathbf{j}^2 \quad &= \quad (\mathbf{l}+\mathbf{s})^2 \;=\; \mathbf{l}^2 + 2\mathbf{l}\cdot\mathbf{s} + \mathbf{s}^2 \\ &\Longrightarrow \quad \mathbf{l}\cdot\mathbf{s} \;=\; \frac{1}{2}\left[\mathbf{j}^2 - \mathbf{l}^2 - \mathbf{s}^2\right] \\ &\Longrightarrow \quad \langle \mathbf{l}\cdot\mathbf{s}\rangle \;=\; \frac{1}{2}\left[j(j+1) - l(l+1)^2 - s(s+1)^2\right] \end{aligned} \tag{44}$$

Using Eq. (44) and an empirical coefficient, the nuclear spin-orbit energy contribution is:

$$\begin{aligned} \Delta E \;&=\; -\frac{13\text{ MeV}}{A^{2/3}}\langle \mathbf{l}\cdot\mathbf{s}\rangle \;=\; -\frac{6.5\text{ MeV}}{A^{2/3}}[j(j+1) - l(l+1) - s(s+1)] \\ &= \begin{cases} -\frac{6.5\text{ MeV}}{A^{2/3}} l & \text{for } \; j = l + \frac{1}{2} \\ \\ +\frac{6.5\text{ MeV}}{A^{2/3}}(l+1) & \text{for } \; j = l - \frac{1}{2} \end{cases} \end{aligned} \tag{45}$$

The effect of the spin-orbit coupling on the nuclear energy levels in shown in Fig. 7(a) and (b). As shown, it profoundly modifies the groupings of energy levels. In contrast, spin-orbit coupling represents only a small perturbation to the energy levels of atomic electrons.

In Fig. 7(b), numbers once again indicate the number of available states in each energy level and the total number of states up to and including that level. Note that levels tend to occur in groups, with large energy gaps between different groups of levels. Each group of levels is called a **shell**. Shells are completely filled, or closed, when the number of neutrons or protons is a **magic number**:

$$2,\ 8,\ 20,\ 28,\ 50,\ 82,\ 126,\ 184, \ldots \qquad \textbf{Magic numbers} \tag{46}$$

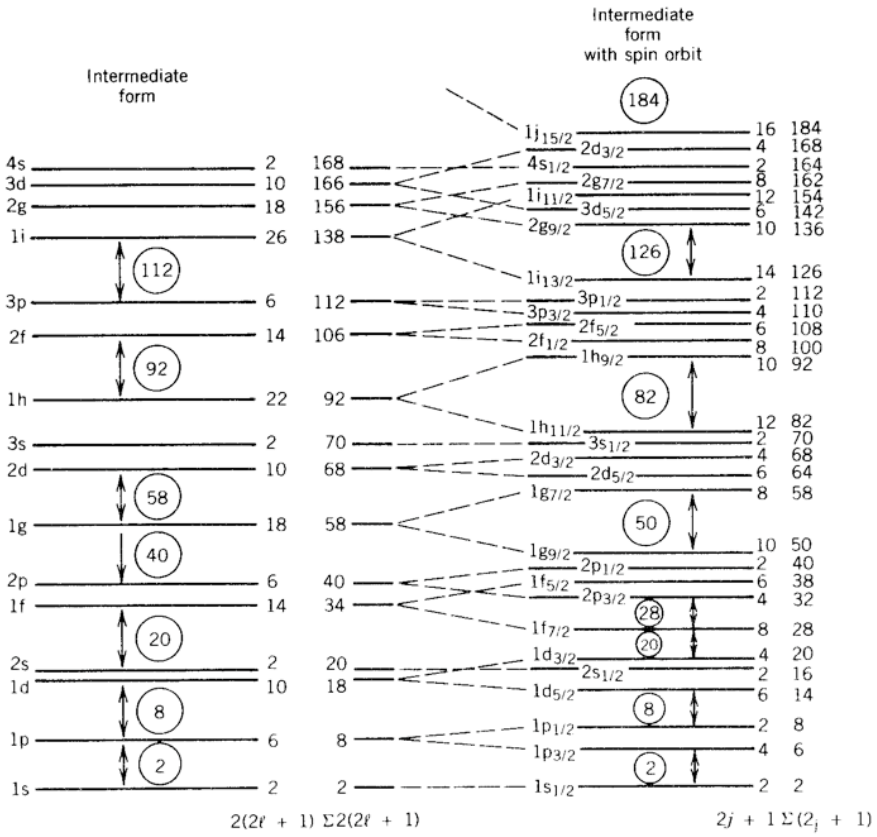

Figure 7. Nuclear energy levels (a) without and (b) with spin-orbit coupling.

Like atomic electrons, nuclei are happier when they have closed shells: the binding energy has an extra ~ 0.05 MeV/nucleon beyond what Eq. (18) predicts when N or Z is a magic number. Even nuclei within one or two nucleons of a magic number have an increased binding energy (Fig. 8).

The potential well and energy levels outlined thus far describe neutrons very well. However, protons feel an electrostatic repulsion as well as the strong nuclear force, so they experience a somewhat different potential well (Fig. 9). As a result, protons have slightly different energy levels, and their magic numbers are those in (46) plus the extra number 114. As Z increases beyond the largest value naturally found on earth, $Z = 92$, nuclei become increasingly unstable to α decay (Section 2.1) and spontaneous fission (Section 3.3). Yet because of the extra binding energy, there may be an **island of stability** around $Z = 114$, so folks keep trying to create such elements.

Nuclei with closed shells are spherical. Most nuclei without closed shells are slightly nonspherical, either prolate (somewhat cigar-shaped) or oblate (somewhat pancake-shaped). Generally the deviation from sphericity is small and is only significant for the electric quadrupole moment (Section 1.5). However, as Fig. 10 shows, nuclei with $150 < A < 190$ or $A > 220$ are far from magic numbers of both Z and N and hence are noticably deformed. Since their potential wells lack the spherical symmetry of the simple shell model, the energy levels in such nuclei must be described by a mathematically nasty **deformed shell model** that includes the asymmetry. Note that nonspherical nuclei can also have rotational energy levels, whereas spherical nuclei cannot.

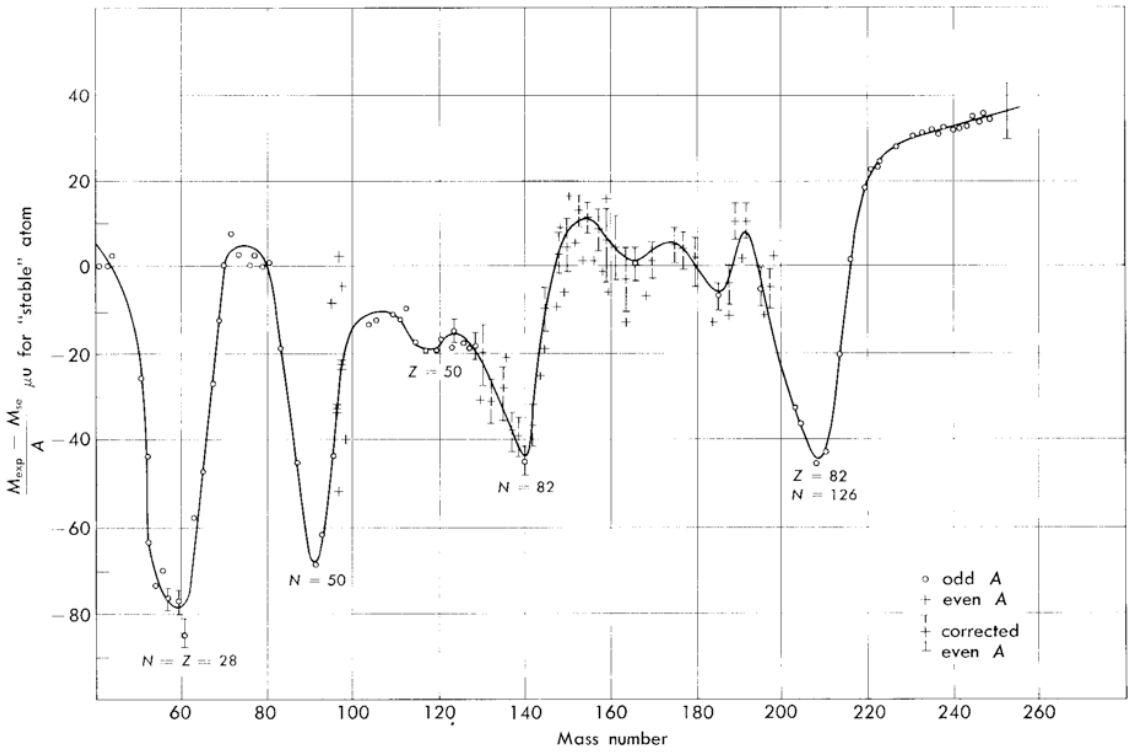

Figure 8. Difference between actual masses and those predicted by the Weizsacher mass formula (14), due to shell effects.

The deuteron is usually treated as a special case, since it only has one proton and one neutron instead of many nucleons as generally assumed in the liquid drop and shell models. The nuclear potential well depth estimated in Eq. (23) was ~ 34 MeV, yet experiments show that the deuteron is only weakly bound, with a binding energy of 2.22 MeV. For more insight, one can use a three-dimensional square well with radius R' and depth V_o as a simple model for the proton-neutron potential (Fig. 11). Assuming that the ground state binding energy is very small, $E_B \ll V_o$, the wavefunction expands so that only half of its hump is inside the well. One can therefore make the substitution $n \to n - \frac{1}{2} = \frac{1}{2}$ in Eq. (43), together with $E = -E_B$ and $l = 0$:

$$-2.22 \text{ MeV} \;=\; -V_o \;+\; \frac{\hbar^2 \pi^2}{8 m_r R'^{\,2}} \;=\; -V_o \;+\; \frac{103 \;\text{ MeV}}{R'^{\,2}_{\text{fm}}} \;, \tag{47}$$

where the reduced mass $m_r = m_p m_n (m_p + m_n) \approx 469.5 \text{ MeV}/c^2$ has been used. For $R' \approx 2$ fm, one finds $V_o \approx 28$ MeV, which is very close to the expected ~ 34 MeV, especially considering the approximations used for the well shape, wavefunction, and radius. Note that in these center-of-mass coordinates, one particle is assumed to remain at the center $r = 0$, while the other orbits around it. Thus R' is the separation between the proton and neutron, or in other words the diameter of the deuteron. The corresponding actual radius of the deuteron is $R = R'/2 \approx 1$ fm.

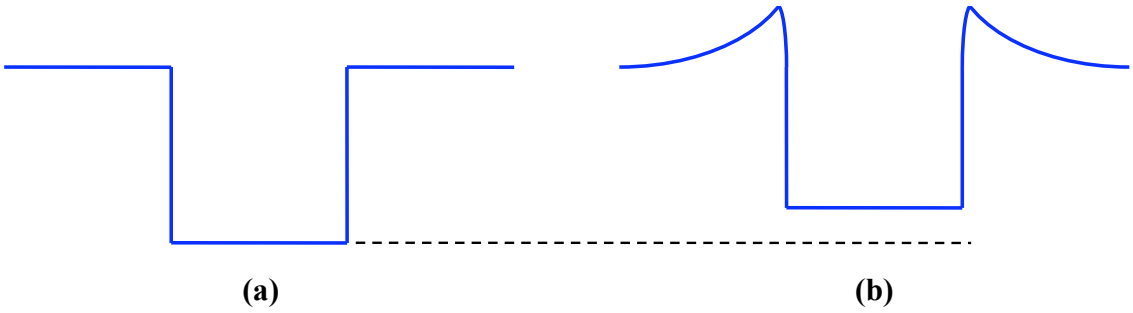

Figure 9. Nuclear potential wells for (a) neutrons and (b) protons. For the proton well, Coulomb repulsion adds a barrier at the edge of the well and makes the well a bit less deep.

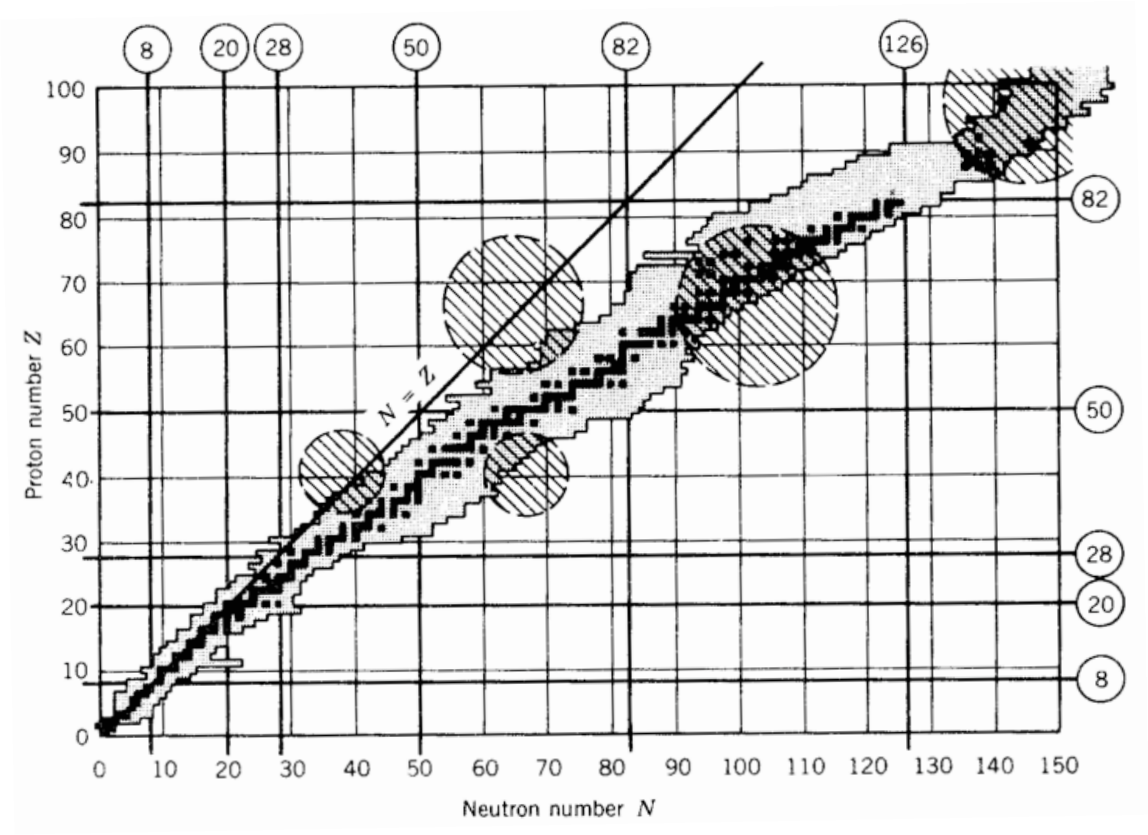

Figure 10. Plot of Z vs. N, where crosshatched circles show regions of asymmetric nuclei far from magic numbers. Stable nuclei are shown in black, while unstable but known nuclei are in grey.

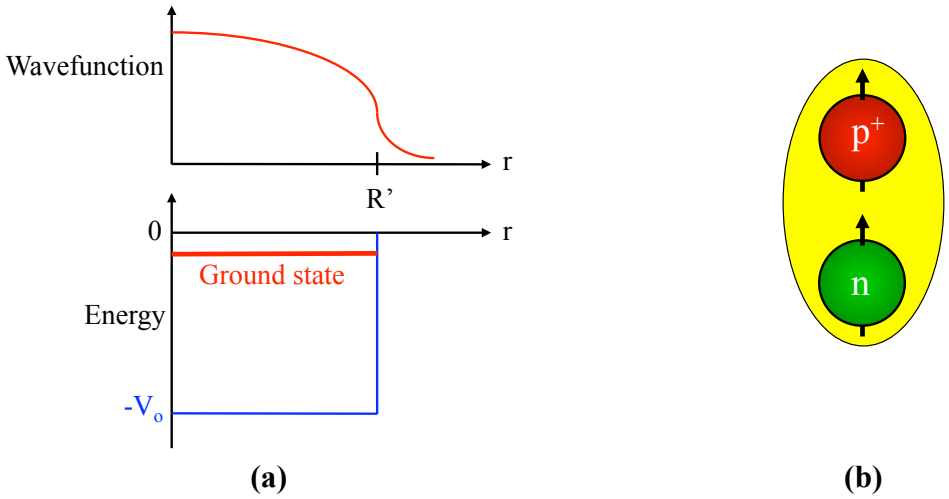

Figure 11. Deuteron. **(a)** This simple square well model for the proton-neutron potential shows the ground state energy near the top of the well and depicts the corresponding wavefunction. The actual potential resembles Fig. 2(b). **(b)** The deuteron is prolate, with the proton and neutron spins parallel.

Energy levels can be measured by exciting nuclei via collisions, then measuring the energies of gamma rays emitted as the nuclei decay from higher to lower energy levels (Section 2.3).

1.6 Spin and Other Things That Make You Dizzy

In addition to the energy levels, the shell model can be used to predict the spin, parity, magnetic moments, and electric moments of nuclei.

Nuclear Spin and Parity

The net spin **J** of a nucleus is the vector sum of the **j** values of its component nucleons. (To avoid confusion, uppercase designates total nuclear values of angular momentum, while lowercase is used for individual nucleons.) **J** can be measured by its effects on the nuclear magnetic dipole moment (this section) and on nuclear reactions (Section 3.1). As mentioned in Section 1.2, neutrons prefer to be in pairs with opposite spins, as do protons. Thus the ground state of an even-even nucleus has $J = 0$; the spins of the individual nucleons cancel each other out. Moreover, the ground-state spin of an even-odd nucleus is simply the j of the unpaired nucleon. Odd-odd nuclei have one unpaired proton with spin j_p and one unpaired neutron with spin j_n; the total nuclear spin in the ground state could be anywhere in the range $|j_p - j_n| \leq J \leq j_p + j_n$ but usually obeys the empirical **Nordheim rules** [1, 3, 4] (though there are many exceptions, especially among light nuclei):

$$J = \begin{cases} |j_p - j_n| & \text{for } s_p + s_n = j_p - l_p + j_n - l_n = 0 \quad \textbf{Nordheim rules} \\ |j_p - j_n| \text{ or } j_p + j_n & \text{for } s_p + s_n = j_p - l_p + j_n - l_n = \pm 1 \quad \textbf{for odd-odd nuclei} \end{cases} \tag{48}$$

Parity is an important principle from quantum physics. If a wavefunction changes sign when the spatial coordinates are reversed ($x \to -x$, $y \to -y$, $z \to -z$), it has odd (-1) parity. If the wavefunction does not change sign, it has even (+1) parity. As shown in the quantum summary, the parity P of an orbiting particle depends on the particle's orbital angular momentum l, $P = (-1)^l$. Intrinsic particle spin remains the same under coordinate reversal and need not be taken into account. Orbitals with $l = 0$ are spherically symmetric and hence have even parity, while orbitals with increasing angular momentum alternate between odd and even parity. The parity of a nucleus containing A nucleons is simply the product of the parities of all the nucleons:

$$P = (-1)^{\sum_{i=1}^{A} l_i} \tag{49}$$

Using Eq. (49), even-even nuclei in the ground state have even parity, $P = +1$, because nucleons with each value of orbital angular momentum occur in pairs. By extension, the ground-state parity of an even-odd nucleus is simply the parity of the extra nucleon, and the parity of an odd-odd nucleus is the product of the parities of the unpaired proton and unpaired neutron. Parity has important implications for transitions between different nuclear states in radioactive decays (Section 2), and indeed, such transitions are the best way to evaluate parity predictions.

Examples of spin and parity, written in the commonly used form J^P, are:

^{12}C :	$J^P = 0^+$	Even-even nucleus.
^{13}N :	$J^P = \frac{1}{2}^+$	One $1p_{1/2}$ proton outside ^{12}C core.
^{14}N :	$J^P = 1^+$	One $1p_{1/2}$ proton and one $1p_{1/2}$ neutron outside ^{12}C core.
^{16}O :	$J^P = 0^+$	Even-even nucleus.
^{17}O :	$J^P = \frac{5}{2}^+$	One $1d_{5/2}$ neutron outside ^{16}O core.

The deuteron is again considered as a special case. Its proton and neutron are both in the lowest state, $l = 0$, so the parity is definitely even. However, the proton and neutron spins could either be parallel, giving $J = 1$, or antiparallel, giving $J = 0$. Equation (10) indicates that nucleons are more attracted to each other when their spins are parallel, so $J = 1$ has the lowest energy. Thus the ground state of the deuteron has $J^P = 1^+$. In fact, the deuteron has no excited states, since the ground state is only weakly bound (recall that $E_B = 2.22$ MeV) and all states above that (even $J^P = 0^+$ with spins antiparallel) have too much energy to be bound.

Magnetic Moments of Nuclei

The interactions of nuclei with magnetic fields are governed by the nuclear magnetic moments. As there appear to be no magnetic monopoles to be had even for ready money, the lowest-order nuclear magnetic moment is the dipole moment, which arises from spinning or orbiting electric charges.

The magnetic dipole moment of a nucleus is the sum of the dipole moments of its component nucleons. As discussed in the nonrelativistic quantum summary, particles with charge e and mass m have a magnetic moment of order $\mu \sim e\hbar/2m$. With $m = m_e$, this quantity is called the **Bohr magneton** and is typical of the magnetic moments due to atomic electrons. With $m = m_p$, it is called the **nuclear magneton** and is typical of the magnetic moments in nuclei:

$$\mu_{\rm B} \equiv \frac{e\hbar}{2m_e} = 5.79 \times 10^{-5} \ \frac{\rm eV}{\rm T} \qquad \textbf{Bohr magneton for atomic electrons} \tag{50}$$

$$\mu_{\rm N} \equiv \frac{e\hbar}{2m_p} = 3.15 \times 10^{-8} \ \frac{\rm eV}{\rm T} \qquad \textbf{Nuclear magneton for nucleons} \tag{51}$$

Note that the nuclear magneton is smaller than the Bohr magneton by a factor of $m_p/m_e = 1836$, so an atom's nucleus interacts with magnetic fields much more weakly than its electrons do.

As shown in *Relativistic Quantum Physics* ?.?, isolated nucleons have a magnetic moment μ_s:

$$\mu_s = g_s \, s \, \mu_N \qquad g_s = \begin{cases} +5.59 & \text{for protons} \\ -3.83 & \text{for neutrons} \end{cases} \tag{52}$$

Because neutrons (like protons) are composed of charged quarks, they have an intrinsic magnetic dipole moment even though they have no net charge. Experimentally, it is found that the effective g_s of nucleons in a nucleus is ~ 0.6 of the values for free nucleons in Eq. (52), due to the effects of mesons and interactions with other nucleons.

From *Nonrelativistic Quantum Physics* ?.?, a charged particle with angular momentum l also has a magnetic dipole moment $\mu_l = e\hbar l/2m$ due to its orbital motion. The net electrical neutrality of neutrons makes their μ_l zero, but μ_l is nonzero for protons and in general may be written

$$\mu_l = g_l l \mu_N \qquad g_l = \begin{cases} 1 & \text{for protons} \\ 0 & \text{for neutrons} \end{cases} \tag{53}$$

Thus the contribution of each nucleon to the total magnetic dipole moment of a nucleus is:

$$\begin{aligned} \mu &= \mu_l + \mu_s = \mu_N(g_l l + g_s s) \\ &= \mu_N \left[g_l j + (g_s - g_l)s \right] = \mu_N j \left[g_l + (g_s - g_l) \frac{\langle \mathbf{j} \cdot \mathbf{s} \rangle}{\mathbf{j}^2} \right] \end{aligned} \tag{54}$$

In an even-even nucleus, all of the nucleons are in pairs with opposite spins, so their contributions cancel out and the nucleus has no net magnetic dipole moment. In an even-odd nucleus, the magnetic dipole moment of the nucleus is simply Eq. (54) evaluated for the unpaired nucleon.

The only part of s that really matters in Eq. (54) is the component that is parallel to j, $\mathbf{j} \cdot \mathbf{s}/j$. This is found via shenanigans similar to Eq. (44):

$$\begin{aligned} \mathbf{l}^2 = (\mathbf{j} - \mathbf{s})^2 &= \mathbf{j}^2 - 2\mathbf{j} \cdot \mathbf{s} + \mathbf{s}^2 \qquad \Longrightarrow \qquad \mathbf{j} \cdot \mathbf{s} = \frac{1}{2} \left[\mathbf{j}^2 + \mathbf{s}^2 - \mathbf{l}^2 \right] \\ \Longrightarrow \ \frac{\langle \mathbf{j} \cdot \mathbf{s} \rangle}{\mathbf{j}^2} &= \frac{j(j+1) + s(s+1)^2 - l(l+1)^2}{2j(j+1)} = \pm \frac{1}{2l+1} \qquad \text{for } j = l \pm \frac{1}{2} \end{aligned} \tag{55}$$

Inserting Eq. (55) into Eq. (54) yields the magnetic dipole moments of even-odd nuclei (Fig. 12):

$$\mu = \mu_N j \left(g_l \pm \frac{g_s - g_l}{2l+1} \right) = \begin{cases} \mu_N j \left(1 \pm \frac{g_s - 1}{2l+1} \right) & \text{for even } N \text{ and odd } Z \text{ with } j = l \pm \frac{1}{2} \\ \pm \mu_N j \frac{g_s}{2l+1} & \text{for even } Z \text{ and odd } N \text{ with } j = l \pm \frac{1}{2} \end{cases} \quad \textbf{Schmidt estimates} \tag{56}$$

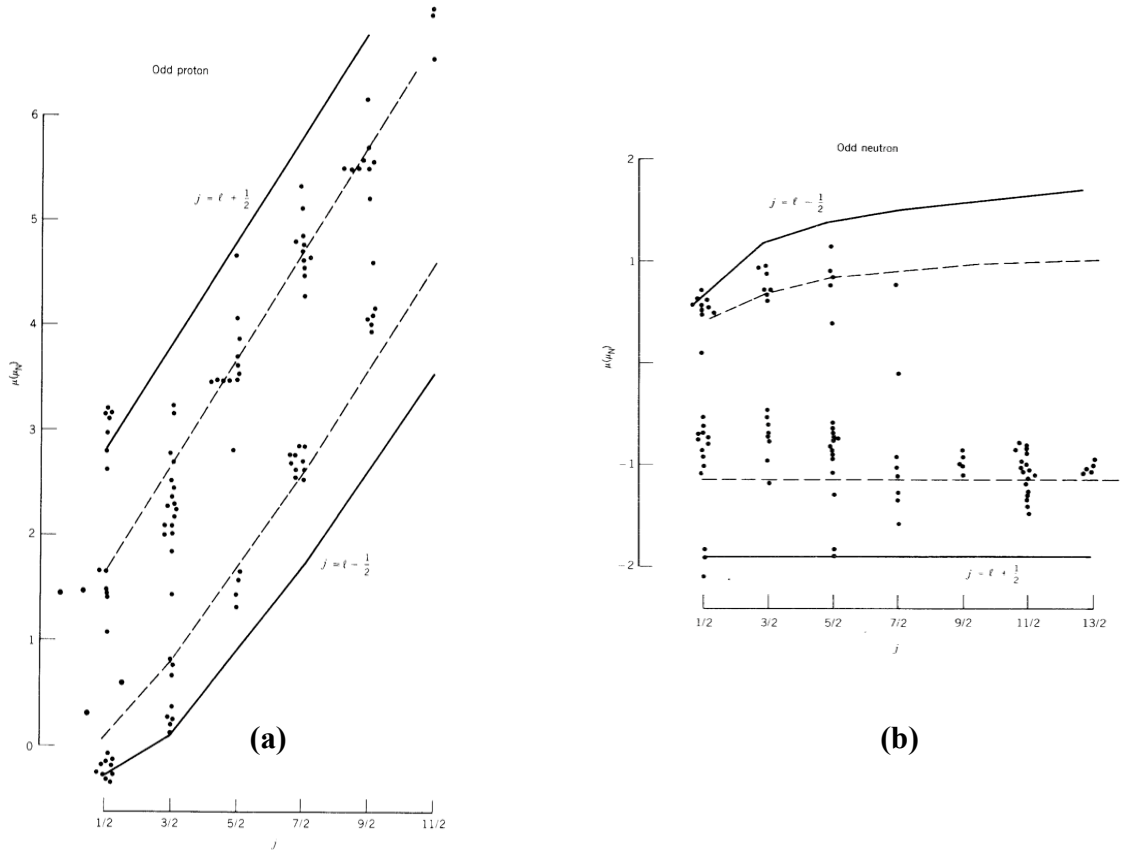

Figure 12. Measured magnetic dipole moments (points) compared with predicted values (lines) from Eq. (56) for odd-mass nuclei. Nuclei with **(a)** odd Z and even N or **(b)** even Z and odd N.

Like spin, the net magnetic dipole moment is much more difficult to predict for odd-odd nuclei.

The magnetic dipole moment of an atomic nucleus creates a weak magnetic field that interacts with that atom's electrons, leading to the **hyperfine splitting** of electron energy levels discussed in the nonrelativistic quantum summary. The dipole moment can also be directly measured via nuclear magnetic resonance (Section 6.2).

As usual, the deuteron is a special case. Since it has $L = 0$ and parallel proton and neutron spins, the deuteron's magnetic moment should simply be the sum of the proton and neutron moments, $\mu = \mu_{sp} + \mu_{sn} = 0.8798\mu_N$. Experiments indicate a deuteron magnetic moment of $\mu = 0.8574\mu_N$, which is close to but perversely not equal to our simple prediction.

To resolve this issue, consider the total orbital angular momentum L and total spin S of the proton and neutron. The deuteron has net spin $J = L + S = 1$. However, L can be 0 (s state, with $S = +1$: spins parallel) or 2 (d state, with $S = -1$: spins parallel). $L = 1$ (p state, with $S = 0$–spins antiparallel) would have odd parity and is not consistent with the observed even parity of the deuteron. If the nuclear attraction between the proton and neutron were a central force [Eq. (9)], L would have to assume a definite value. Yet because the attraction is actually a noncentral tensor force [Eq. (10)], different values of the orbital angular momentum get mixed together. In fact, the deuteron is a quantum superposition consisting mostly of the s state with a little of the d state, which is why the magnetic moment is nearly but not quite the simple s-state value.

The orbital angular momentum L is divided equally between the proton and neutron. Only the proton component $L/2$ contributes to the total magnetic momoment, which may be written as

$$\frac{\mu_{\text{deuteron}}}{\mu_N} \;=\; \frac{1}{2}S(g_{sp} + g_{sn}) + \frac{1}{2}L \;=\; \frac{1}{2}S(g_{sp} + g_{sn})J - \frac{1}{2}L(g_{sp} + g_{sn} - 1) \tag{57}$$

The magnetic moment is evaluated parallel to J, so in Eq. (57) one substitutes $J \to J_z = 1$ and

$$L \;\to\; L_z \;=\; \frac{\langle \mathbf{L}\cdot\mathbf{J}\rangle}{\mathbf{J}^2}J_z \;=\; \frac{J(J+1) - S(S+1) + L(L+1)}{2J(J+1)}J_z \;=\; \frac{L(L+1)}{4} \tag{58}$$

If the probabilities of being in the s or d states are P_s and P_d, the average value of Eq. (58) is

$$\langle L_z\rangle \;=\; \frac{\langle L(L+1)\rangle}{4} \;=\; \frac{0(0+1)P_s + 2(2+1)P_d}{4} \;=\; \frac{3}{2}P_d \tag{59}$$

Inserting $J = 1$ and $L = \langle L_z\rangle = \frac{3}{2}P_d$ into Eq. (57) yields

$$\frac{\mu_{\text{deuteron}}}{\mu_N} \;=\; \frac{1}{2}(g_{sp} + g_{sn}) - \frac{3}{4}P_d(g_{sp} + g_{sn} - 1) \;=\; 0.8798 - 0.5697P_d \tag{60}$$

Equation (60) gives the observed deuteron magnetic moment if $P_d \approx 0.04$, so $P_s = 0.96$. Since wavefunction amplitudes are the square roots of the probabilities, the deuteron wavefunction may be written as a superposition of the s- and d-state wavefunctions:

$$\Psi \;\approx\; \sqrt{0.96}\,\Psi_s \;+\; \sqrt{0.04}\,\Psi_d \tag{61}$$

Electric Moments of Nuclei

Electric moments, governing how nuclei interact with electric fields, are also important. The electric monopole moment is simply the nuclear charge, and the electric dipole moment is zero for nuclei in stationary states, since charge is not localized to one side of a nucleus. Nuclei in nonstationary states can have oscillating protons and hence an electric dipole moment–see Section 2.3.

The lowest-order nontrivial electric moment for a ground-state nucleus is thus the electric quadrupole moment. From the electromagnetism summary, the quadrupole moment Q of an orbiting charge e averaged over the orbital coordinates $\langle z^2 \rangle$ and $\langle r^2 \rangle$ is

$$eQ \;=\; e\left(3\left\langle z^2\right\rangle - \left\langle r^2\right\rangle\right) \;. \tag{62}$$

Now apply this to a proton orbiting in a nucleus. If the nucleus is spherical, as it is for closed shells, $\langle z^2 \rangle = \langle x^2 \rangle = \langle y^2 \rangle = \frac{1}{3}\langle z^2 \rangle$, so the electric quadrupole moment is zero. In fact $Q = 0$ for any even-even nucleus, since all nucleons are in pairs with opposite spin ($J = 0$) and their orbital motion cancels out. Moreover, even a nucleus with $J = \frac{1}{2}$ has no quadrupole moment, since such a nucleus may be regarded an even-even core plus one unpaired nucleon with $j = \frac{1}{2}$, $s = \frac{1}{2}$, and hence no orbital motion, $l = 0$.

If a nucleus is very oblate, $\langle z^2 \rangle \ll \langle r^2 \rangle \sim 1.2A^{1/3}$ fm, the quadrupole moment from Eq. (62) is

$$Q \;\sim\; -\left\langle r^2\right\rangle \sim -0.014A^{2/3} \text{ barn} \tag{63}$$

Equation (63) is typical of a nucleus that is starting a new shell, for example with one unpaired proton orbiting in the $x-y$ plane. An unpaired neutron produces a smaller but nonzero Q; although the neutron is uncharged, a nonspherical neutron orbit makes the proton orbits deviate slightly from spherical symmetry, yielding an electric quadrupole moment.

If the nucleus is very prolate, $\langle z^2 \rangle \sim \langle r^2 \rangle \sim 1.2A^{1/3}$ fm, the quadrupole moment from Eq. (62) is

$$Q \;\sim\; +2\left\langle r^2\right\rangle \sim 0.03A^{2/3} \text{ barn} \tag{64}$$

Equation (64) is typical of a nucleus with an almost-filled shell.

Figure 13 plots the measured electric quadrupole moment versus A for even-odd or odd-even nuclei. Q can be measured directly for beams of nuclei or indirectly by its small effect on atomic electrons' energy levels [1]. As expected from Eqs. (63) and (64), the electric quadrupole moment oscillates from negative to positive as shells fill up. Like spin and the magnetic dipole moment, Q is more difficult to predict for odd-odd nuclei. Most nuclei only deviate slightly from spherical symmetry, so actual quadrupole moments can be smaller than the values in Eqs. (63) and (64) for highly oblate or prolate nuclei. On the other hand, in the regions $150 < A < 190$ and $A > 220$ that are far from magic numbers (Fig. 10), even the paired core is nonspherical, and the contributions from many nucleons make Q several times larger than the single-nucleon estimates of Eqs. (63) and (64).

Using Eq. (61), the electric quadrupole moment of the deuteron is

$$Q = \int dV \Psi^* \left(3z^2 - r^2\right) \Psi = \int dV \left(\sqrt{0.96}\Psi_s^* + \sqrt{0.04}\Psi_d^*\right)\left(3z^2 - r^2\right)\left(\sqrt{0.96}\Psi_s + \sqrt{0.04}\Psi_d\right) \tag{65}$$

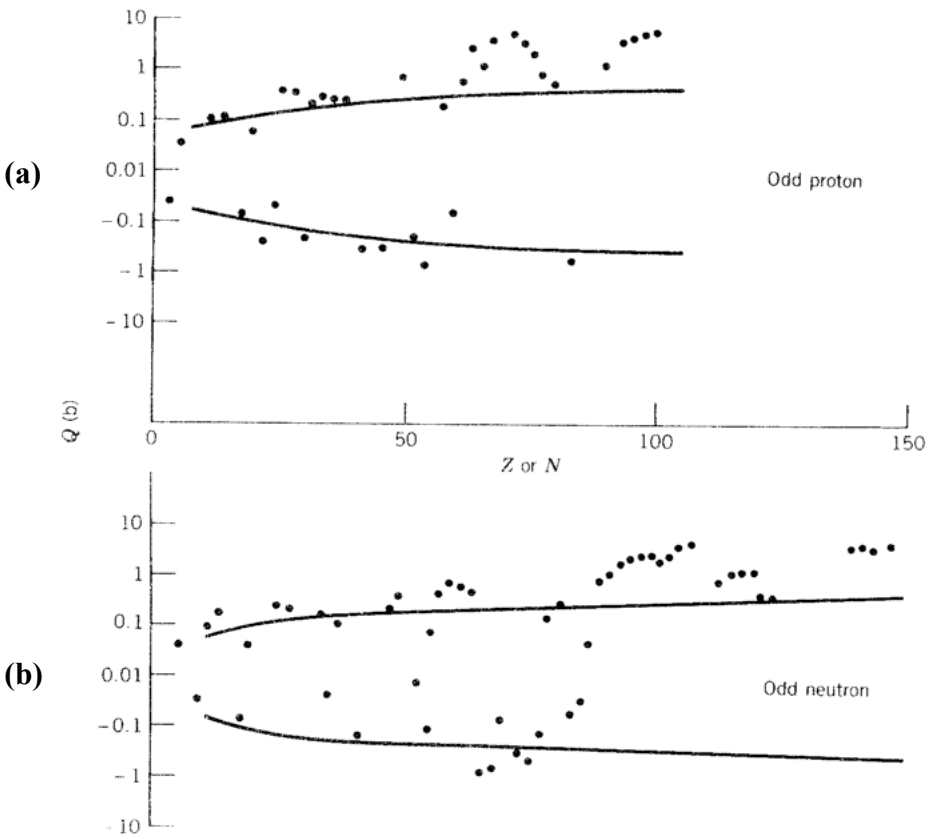

Figure 13. Measured electric quadrupole moments (points) compared with predicted values (lines) from Eqs. (63) and (64) for nuclei with (a) odd Z and even N or (b) even Z and odd N.

In Eq. (65), the purely s-state term containing $\Psi_s^*\Psi_s$ is spherically symmetric and thus does not contribute to the quadrupole moment. The purely d-state term containing $0.04\Psi_d^*\Psi_d$ only makes a small contribution to the quadrupole moment due to its small numerical coefficient. The dominant contribution is from the cross-term, which may be estimated as

$$Q = \int dV \Psi_s^* \left(3z^2 - r^2\right) \Psi_d + \int dV \Psi_d^* \left(3z^2 - r^2\right) \Psi_s \sim 2\sqrt{0.96} R^2 \sqrt{0.04} = 0.0039 R_{\rm fm}^2 \text{ barn} \quad (66)$$

Choosing $R \approx 1$ fm gives $Q \sim 0.0039$ barn. This is very close to the measured value of 0.00288 barn, especially considering the crude approximations made in evaluating the integrals in Eq. (66). Note that the measured electric quadrupole moment confirms that the deuteron has a small but nonzero amount of the d state. If the deuteron were purely in the s state, Q would be zero.

The tensor force makes the proton and neutron spins align along the major axis of the deuteron [Fig. 11(b)]. Of course, the neutron and proton wavefunctions are blurred out so that the proton is equally likely to be at each end, so the deuteron has no permanent electric dipole moment.

2 Nuclear Decay

In nuclear decays, nuclei spontaneously emit particles (Fig. 14). Decays are classified by what particles are emitted. This section will consider decays by emission of α particles (helium-4 nuclei), β particles (electrons or positrons), and γ rays (high-energy photons) [1-4]. Spontaneous decay of large nuclei by fission into two smaller nuclei will be considered along with induced fission in Section 3.2.

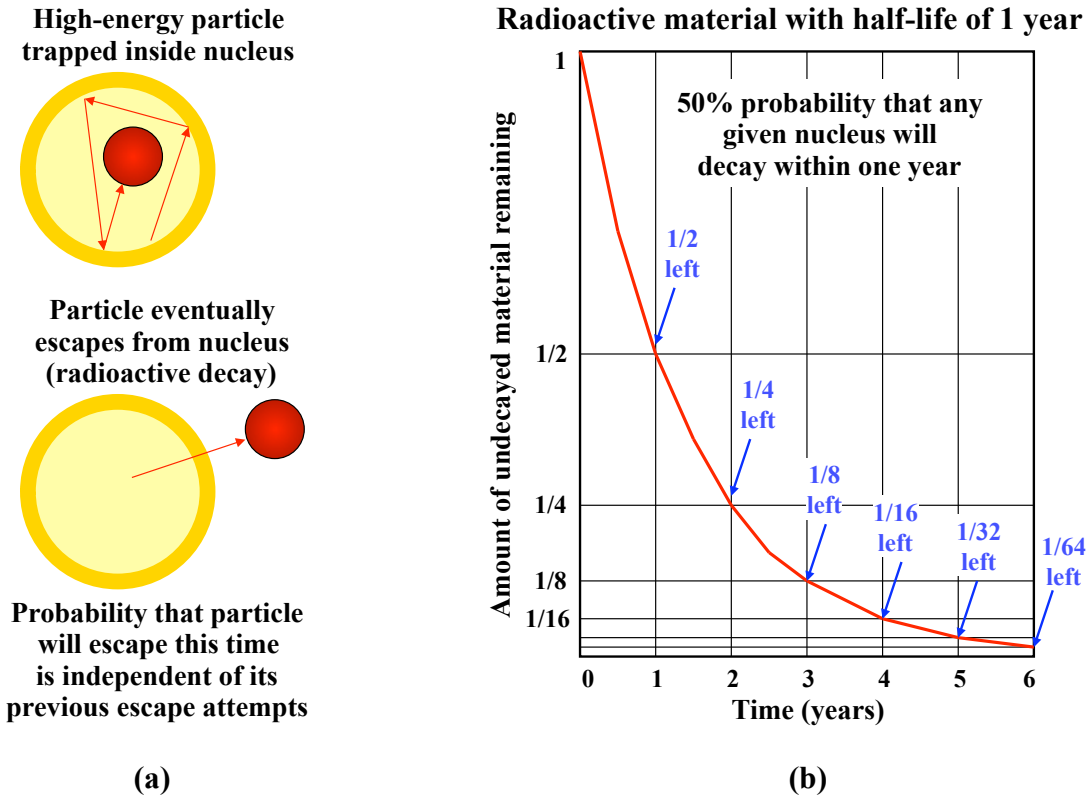

Figure 14. Radioactive decay. **(a)** A simple model of radioactive decay is that an energetic particle is rattling around inside the potential energy well of a nucleus. The particle has a small but nonzero probability of escaping each time it reaches the outer wall of the nucleus. The probability of escape each time is independent of the number of previous escape attempts. **(b)** The exponential decay half-life $\tau_{1/2}$ is the time required for half of the nuclei in a sample to decay, or to release their trapped energetic particle. After one half-life, 1/2 of the initial nuclei have decayed; after two half-lives, 3/4 of the of the initial nuclei have decayed; and so forth.

2.1 Alpha Decay

As Section 1.3 showed, medium-sized nuclei are happier (their nucleons are more tightly bound) than large nuclei. Emitting an α particle is a favorite way for large nuclei to lose weight and feel better about themselves (Fig. 15). The excess binding energy becomes particle kinetic energy; neglecting recoil of the nucleus, which is much more massive than the α particle, the α particle has energy

$$E_\alpha \;=\; [M(A,Z) - M(A-4,Z-2) - m_\alpha]c^2 \tag{67}$$

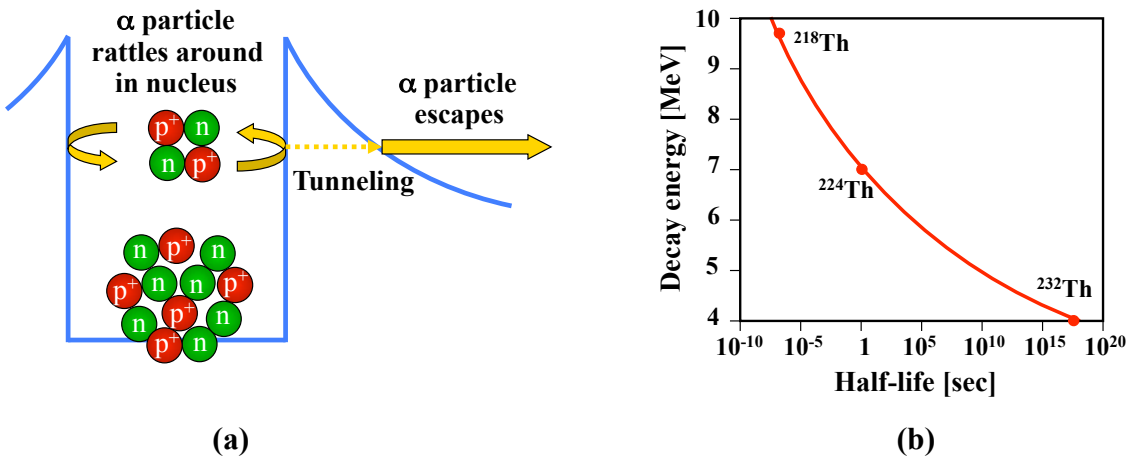

Figure 15. Alpha decay. **(a)** Potential energy V of an alpha particle vs. its distance r from a nucleus. **(b)** Energy E_α of the emitted alpha particle vs. the decay half life $\tau_{1/2}$.

Equation (67) may be evaluated using the α particle rest mass $m_\alpha c^2 = 3727.4$ MeV and Eq. (19). The results fall into different categories depending on the number of initial nucleons A:

$$A < 150 \implies E_\alpha < 0 \text{ MeV} \quad \text{Stable against } \alpha \text{ decay} \tag{68}$$

$$150 < A < 200 \implies 0 \text{ MeV} < E_\alpha < 4 \text{ MeV} \quad \text{Unstable but } \tau_{1/2} > 5 \text{ billion years} \tag{69}$$

$$200 < A < 260 \implies 4 \text{ MeV} < E_\alpha < 9 \text{ MeV} \quad 1\ \mu\text{sec} < \tau_{1/2} < 5 \text{ billion years} \tag{70}$$

$$260 < A \implies 9 \text{ MeV} < E_\alpha \quad \text{Very unstable–}\tau_{1/2} \text{ too short to care} \tag{71}$$

The above values for mass numbers and energies are approximate but illustrative. The half-lives $\tau_{1/2}$ are the times required for half of the nuclei in a sample to decay; they have been calculated using the methods below, where it is shown that a relatively small change in E_α corresponds to a change of many orders of magnitude in the half life. The short half-lives to α decay and spontaneous fission (Section 3.3) are why the periodic table of the elements ends where it does.

Figure 15(a) shows the potential energy V of an α particle as a function of its distance r from a nucleus. The α particle is effectively joined with the nucleus and subject to the attractive strong nuclear force if r is less than r_0, the sum of the nuclear radius [Eq. (11)] and the α radius ~ 1.4 fm:

$$r_0 \approx 1.2A^{1/3} + 1.4 \text{ fm} \tag{72}$$

Typical α-emitting nuclei, or α **emitters**, have $A \sim 200 - 260$ [Eq. (70)], so $r_0 \sim 9$ fm.

Outside the nucleus ($r > r_0$), the α particle feels the repulsive electrostatic potential

$$V(r) = \frac{Z_1 Z_2 e^2}{4\pi\epsilon_o r} = \frac{1.44 Z_1 Z_2}{r_{\text{fm}}} \text{ MeV} \tag{73}$$

The value $e^2/4\pi\epsilon_o \approx 1.44$ MeV·fm is often useful in evaluating nuclear physics expressions.

Using the α particle charge $Z_1 = 2$ and typical values $Z_2 \sim 90$ and $r_0 \sim 9$ fm, the maximum barrier height at $r = r_0$ is ~ 30 MeV, much larger than E_α from Eq. (70). Turning Eq. (73) around, the potential exceeds the actual α energy until the particle reaches a distance r_1 from the nucleus:

$$r_1 = \frac{Z_1 Z_2 e^2}{4\pi\epsilon_o E} = \frac{1.44 Z_1 Z_2}{E_{\text{MeV}}} \text{ fm} \tag{74}$$

For $r < r_0$, the α particle experiences the attractive strong force binding energy of ~ 15 MeV/nucleon from Eq. (18), which must be subtracted from the $\sim +30$ MeV electrostatic potential:

$$V(r < r_0) \;\approx\; 30 \text{ MeV} \;-\; 4 \times 15 \text{ MeV} \;\approx\; -30 \text{ MeV} \tag{75}$$

Classically an α particle does not have enough energy to travel over the barrier from $r = r_0$ to r_1. Yet thanks to quantum physics, it can tunnel through the barrier anyway. Using the WKB approximation (*Nonrelativistic Quantum Physics* ?.?), the transmission probability T that a particle of mass m and energy E can tunnel through the barrier is

$$T \;\approx\; \exp\left\{-\frac{2}{\hbar}\int_{r_0}^{r_1} dr\sqrt{2m[V(r)-E]}\right\} \;=\; e^{-2G} \tag{76}$$

The argument of the exponential in Eq. (76) is called the **Gamow factor** G when the potential barrier takes the form of Eq. (73) [sometimes the factor of 2 is absorbed into the definition of G]:

$$\begin{aligned} 2G \;&=\; 2\frac{\sqrt{2m}}{\hbar}\int_{r_0}^{r_1} dr\sqrt{\frac{Z_1 Z_2 e^2}{4\pi\epsilon_o r} - E} \;=\; 2\frac{\sqrt{2mE}}{\hbar}\int_{r_0}^{r_1} dr\sqrt{\frac{r_1}{r}-1} \\ &=\; 2\frac{\sqrt{2mE}}{\hbar} r_1\left[\cos^{-1}\sqrt{\frac{r_0}{r_1}} - \sqrt{\frac{r_0}{r_1}\left(1-\frac{r_0}{r_1}\right)}\right] \;\approx\; 2\frac{\sqrt{2mE}}{\hbar} r_1\left[\frac{\pi}{2} - 2\sqrt{\frac{r_0}{r_1}}\right] \qquad \text{for } r_0 \ll r_1 \\ &\approx\; \frac{0.99 Z_1 Z_2}{\sqrt{E_{\text{MeV}}}}\sqrt{\frac{m}{m_p}} - \frac{3.97}{\pi}\sqrt{\frac{m}{m_p}}\sqrt{Z_1 Z_2}\sqrt{1+0.83A^{1/3}}\,, \end{aligned} \tag{77}$$

in which Eq. (77) used Eqs. (72) and (74). Because of the strong dependence on r_0, α decay rates have been used to estimate nuclear radii. For α decay of a nucleus with initial atomic number Z ($Z_1 = 2$, $Z_2 = Z - 2$, $E = E_\alpha$, $m = m_\alpha \approx 4m_p$), the Gamow factor is

$$2G \;\approx\; \frac{3.97(Z-2)}{\sqrt{E_{\alpha,\text{ MeV}}}} \;-\; 3.57\sqrt{Z-2}\sqrt{1+0.83A^{1/3}} \tag{78}$$

An α particle rattling around inside the potential barrier has a probability $T = e^{-2G}$ of escaping each time it contacts the barrier. The frequency f_α of times that the α particle hits the barrier may be estimated from the particle's velocity v inside the nucleus and the diameter $2R$ of the nucleus:

$$f_\alpha \;=\; v\,\frac{1}{2R} \;=\; \sqrt{\frac{2(E_\alpha + 30\text{ MeV})}{m_\alpha}}\,\frac{1}{2\cdot 1.2A^{1/3}\text{ fm}} \;=\; 2.89\times 10^{21}\frac{\sqrt{E_{\alpha,\text{ MeV}}+30\text{ MeV}}}{A^{1/3}}\;\text{sec}^{-1} \tag{79}$$

Thus the typical timescale for nucleons rattling around inside a nucleus is $\tau_{\text{nucleon}} \sim 4\times 10^{-22}$ sec.

α decay also depends on the probability P_α that two neutrons and two protons inside a nucleus will associate to form an α-particle-like entity. For α-emitting nuclei, this probability is $P_\alpha \approx 0.1$. The exponential decay rate $1/\tau$ of a nucleus due to α decay is simply:

$$\frac{1}{\tau_\alpha} = \begin{pmatrix}\text{Probability of}\\ \alpha \text{ in nucleus}\end{pmatrix}\begin{pmatrix}\text{Frequency with which } \alpha\\ \text{hits potential barrier}\end{pmatrix}\begin{pmatrix}\text{Probability that } \alpha\\ \text{tunnels through barrier}\end{pmatrix} = P_\alpha f_\alpha e^{-2G} \tag{80}$$

The half-life is related to the exponential decay time from Eq. (80):

$$\begin{aligned} \tau_{1/2,\,\alpha} \;&=\; \ln 2\;\tau_\alpha \;=\; 0.693\tau_\alpha \;=\; \frac{0.693}{P_\alpha f_\alpha e^{-2G}} \\ &\approx\; \frac{2.4\times 10^{-21}\,A^{1/3}}{\sqrt{E_{\alpha,\text{ MeV}}+30\text{ MeV}}}\exp\left[+\frac{3.97(Z-2)}{\sqrt{E_{\alpha,\text{ MeV}}}} - 3.57\sqrt{Z-2}\sqrt{1+0.83A^{1/3}}\right]\;\text{sec} \end{aligned} \tag{81}$$

Equation (81) is a form of the **Geiger-Nuttall law** relating the decay time of the nucleus to the energy of the α particle that is produced. Sometimes the distance that the α particle can travel through air is given instead of the α energy. Figure 15(b) shows that Eq. (81) agrees fairly well with experimental data. More precise calculations take into account the angular momentum l, which adds a centrifugal force term to the potential barrier when $l \neq 0$ [1, 3]. They also consider nonspherical nuclei, in which α particles are most likely to escape from nuclear surface areas that are further from the center of the nucleus and hence where the Coulomb barrier is weaker.

Particles larger than α particles are generally not emitted by nuclei, because their larger mass drastically reduces the tunneling probability. (An exception is fission of certain large nuclei whose structural and energetic properties facilitate tunneling, as will be shown in Section 3.3) Moreover, the nucleons in α particles are tightly bound, so it is much more energetically preferable to emit an α particle than a proton or neutron or a less strongly bound small nucleus such as a deuteron.

2.2 Beta Decay

In **beta decay**, a neutron within a nucleus changes into a proton, or vice versa, emitting an energetic electron or positron (a beta particle) and an electron (anti)neutrino in the process [Fig. 16(a) and (b)]:

$$n \longrightarrow p^+ + e^- + \overline{\nu_e} \tag{82}$$

$$p^+ \longrightarrow n + e^+ + \nu_e \tag{83}$$

Thus beta decay keeps A constant but changes Z (and hence N). For constant A, the nuclear rest energy plotted versus Z is a parabola [Eq. (19), Fig. 16(c)]. Nuclei that are not at the bottom of the parabola undergo successive beta decays, adding one to their Z value and subtracting one from their N value (or vice versa) during each decay, until they reach the bottom of the parabola.

Actually, the pairing energy offset δ in Eq. (19) can assume any of three values, so there are three parabolas, the lowest one for even-even nuclei, a higher one for even-odd nuclei, and the highest one for odd-odd nuclei [Fig. 16(c) and (d)]. Odd-A nuclei remain on the middle even-odd/odd-even parabola (c) as they decay. In contrast, even-A nuclei alternate between the even-even and odd-odd parabolas (d) as they decay. As a result, there are very few stable odd-odd nuclei (only five light elements), since they can generally reach lower energy states by decaying to the even-even parabola. Typically only the single lowest energy state on the even-odd parabola is stable. Because of the exceptionally low energy of the even-even parabola, often the two lowest states are both stable.

The Feynman diagrams in Fig. 16(b) schematically illustrate beta decay. A neutron can turn into a proton, in the process emitting a virtual W weak nuclear force decay particle, which splits into a real electron and electron antineutrino. Turning things around, a proton can split into a neutron, positron, and neutrino. The quantum amplitude is the same for either process and may be estimated using the principles from *Relativistic Quantum Field Theory* 3.1. Each vertex of the diagram contributes a weak interaction coupling factor $g_w \approx 0.66$. The amplitude of the virtual W particle depends on the square of the ratio of the total energy ΔE released in the decay to the rest energy $m_w c^2$ that would be required to make the W particle real. Because typical beta decay energies $\Delta E \sim 1$ MeV are far smaller than $m_w c^2 \approx 82$ GeV, the chance of producing a virtual W particle is very small:

$$|A| \sim g_w^2 \left(\frac{\Delta E}{m_w c^2} \right)^2 \tag{84}$$

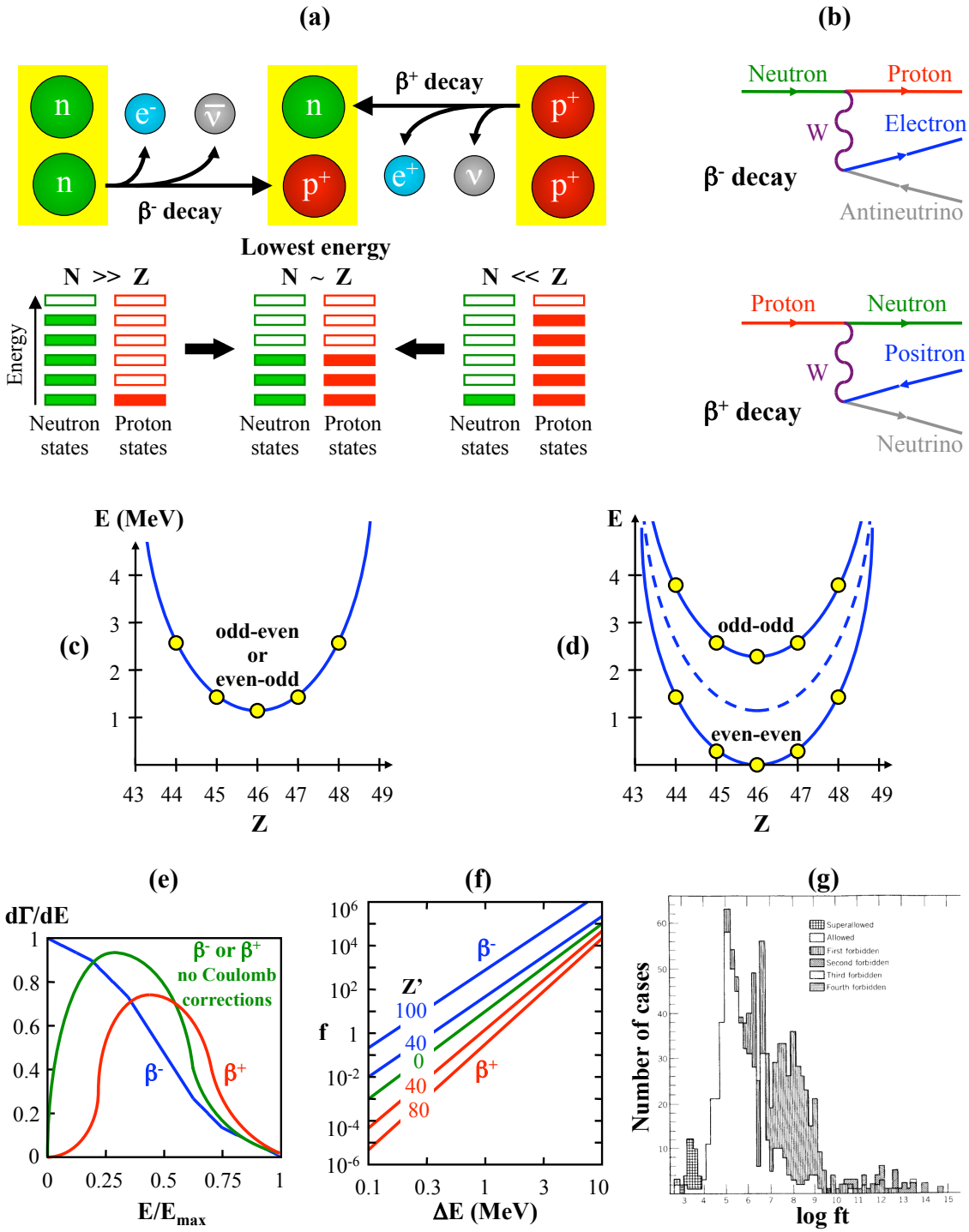

Figure 16. Beta decay. **(a)** Schematic and **(b)** Feynman diagrams for beta decay, showing conversion of a neutron into a proton or vice versa. **(c)** For odd-even or even-odd nuclei with constant A, the nuclear rest energy E vs. Z is a parabola. **(d)** Due to the pairing energy offset δ, there is a higher parabola for odd-odd nuclei and a lower one for even-even nuclei. **(e)** Normalized energy spectrum of emitted beta particles from Eq. (87), with and without the Coulomb correction function F from Eqs. (88) and (89). **(f)** The function $f(Z', \Delta E)$ from Eq. (90). **(g)** Measured ft values.

If a transition of energy ΔE is completely free to occur, its rate Γ is limited by the Heisenberg uncertainty principle, $\Gamma \equiv 1/\tau \sim \Delta E/\hbar$. For beta decay, the transition rate must also include the probability $|A|^2$ of the transition:

$$\Gamma \sim \frac{\Delta E}{\hbar} |A|^2 \sim \left(\frac{g_w}{m_w c^2}\right)^4 \frac{(\Delta E)^5}{\hbar} \tag{85}$$

Integrations over phase space and particle emission angles introduce factors of $\sim 4\pi$:

$$\Gamma \sim \frac{1}{(4\pi)^3} \left(\frac{g_w}{m_w c^2}\right)^4 \frac{(\Delta E)^5}{\hbar} \tag{86}$$

Relativistic Quantum Field Theory 3.2.2 derives a more accurate expression for beta decay of an isolated neutron. The weak force coupling constant is more complicated than assumed above. It includes a Cabibbo factor $\cos\theta_c \approx 0.974$ and separate coefficients for two types of coupling: vector ($c_V \approx 1$) and axial ($c_A \approx 1.26$). The variation of the decay rate with the emitted electron energy, $d\Gamma/dE_e$, is important because it gives the energy spectrum of the beta particles [Fig 16(e)]. The $d\Gamma/dE_e$ expression for decay of an isolated neutron can be extended to beta decay of a nucleon within a nucleus by including fudge factors, the **Fermi amplitude** A_F to modify vector coupling (beta particle and neutrino emitted with spins antiparallel) and the **Gamow-Teller amplitude** A_{GT} to modify axial coupling (beta and neutrino emitted with spins parallel):

$$\frac{d\Gamma}{dE_e} = \frac{\cos^2\theta_c}{(4\pi)^3\hbar} \left(\frac{g_w}{m_w c^2}\right)^4 \left(c_V^2 |A_F|^2 + c_A^2 |A_{GT}|^2\right) F(Z', E_e) E_e \sqrt{E_e^2 - m_e^2 c^4} \left(\Delta E + m_e c^2 - E_e\right)^2 \tag{87}$$

Equation (87) applies to either electrons or positrons emitted in beta decay. It reduces to the expression for isolated neutron decay for $|A_F|^2 = 1$, $|A_{GT}|^2 = 3$, and $\Delta E = (m_n - m_p - m_e)c^2$.

The function $F(Z', E_e)$ in Eq. (87) accounts for the effect of the final nuclear charge Z' on the probability of the emitted electron appearing at the nucleus ($r = 0$):

$$F(Z', E_e) = \left|\frac{\psi_e(Z', r=0)}{\psi_e(Z'=0, r=0)}\right|^2 \approx \frac{\frac{Z'e^2}{2\epsilon_o\hbar v}}{\left|1 - \exp\left(\mp\frac{Z'e^2}{2\epsilon_o\hbar v}\right)\right|} \tag{88}$$

where the approximate answer is a nonrelativistic result given by other authors [1, 3]. (The relativistic result is much nastier [3, 4].) The $\mp$ sign is negative for electrons and positive for positrons. In the limit of low energies or emission velocities $v \to 0$, Eq. (88) becomes

$$F(Z', E_e) \approx \begin{cases} \frac{Z'e^2}{2\epsilon_o\hbar v} & \text{for electrons} \\ \frac{Z'e^2}{2\epsilon_o\hbar v} \exp\left(-\frac{Z'e^2}{2\epsilon_o\hbar v}\right) & \text{for positrons} \end{cases} \tag{89}$$

The Coulomb field of the nucleus is attractive for escaping electrons and steals energy from them, or equivalently enhances electron emission at low energies, as shown by Eq. (89). In contrast, the field is repulsive for positrons and accelerates them, or suppresses positron emission at low energies. By analogy with alpha decay, Eq. (89) can also be viewed as a Gamow tunneling factor for positrons escaping from the nucleus.

The essence of Eq. (87) integrated over all energies is defined as the **Fermi integral** $f(Z', \Delta E)$:

$$\left(m_e c^2\right)^5 f(Z', \Delta E) \equiv \int_{m_e c^2}^{\Delta E} dE_e\, F(Z', E_e) E_e \sqrt{E_e^2 - m_e^2 c^4} \left(\Delta E + m_e c^2 - E_e\right)^2 \tag{90}$$

The factor $(m_e c^2)^5$ gives the correct units for the energy factors. For $Z' = 0$, the integral can be evaluated analytically, defining $\epsilon \equiv \Delta E / m_e c^2$:

$$f(Z'=0,\Delta E) = \sqrt{\epsilon^2-1}\left(\frac{1}{30}\epsilon^4 - \frac{3}{20}\epsilon^2 - \frac{2}{15}\right) + \frac{1}{4}\epsilon \ln\left(\epsilon + \sqrt{\epsilon^2-1}\right) \quad (91)$$

$$\approx \begin{cases} 0.2155\left(\frac{\Delta E}{m_e c^2} - 1\right)^{7/2} & \text{for } \Delta E - m_e c^2 \ll m_e c^2 \\ \frac{1}{30}\left(\frac{\Delta E}{m_e c^2}\right)^5 & \text{for } \Delta E \gg m_e c^2 \end{cases} \quad (92)$$

Coulomb effects ($Z' \neq 0$) necessitate numerical evaluation of $f(Z', \Delta E)$ [Fig. 16(f)]. However, they generally multiply $f(0, \Delta E)$ by $\sim \exp\left(\frac{2\pi Z'}{137}\frac{c}{v}\right)$ for electron emission and $\sim 0.1 - 0.3$ for positron emission with large Z'.

Using the Fermi integral, the total beta decay rate is

$$\Gamma = \frac{\cos^2\theta_c}{(4\pi)^3}\left(\frac{g_w}{m_w c^2}\right)^4 \frac{(m_e c^2)^5}{\hbar} f(Z', \Delta E)\left(c_V^2 |A_F|^2 + c_A^2 |A_{GT}|^2\right) \quad (93)$$

$$= \frac{G_F^2 m_e^5 c^4}{2\pi^3 \hbar^7} f(Z', \Delta E)\left(c_V^2 |A_F|^2 + c_A^2 |A_{GT}|^2\right) , \quad (94)$$

where by convention the **Fermi coupling constant** is defined as

$$G_F \equiv \cos^2\theta \left(\frac{g_w}{m_w c^2}\right)^2 \frac{(\hbar c)^3}{4\sqrt{2}} \approx 8.7 \times 10^{-5} \text{ MeV} \cdot \text{fm}^3 \quad (95)$$

As a sanity check, using $f(Z', \Delta E) \approx (\Delta E / m_e c^2)^5/30$, $|A_F|^2 = 1$, and $|A_{GT}|^2 = 3$, Eq. (93) agrees (within a factor of 5) with the crude estimate of Eq. (86):

$$\Gamma \approx 0.2 \frac{1}{(4\pi)^3}\left(\frac{g_w}{m_w c^2}\right)^4 \frac{(\Delta E)^5}{\hbar} \quad (96)$$

The half-life for beta decay is

$$\tau_{1/2} = \frac{\ln 2}{\Gamma} = \frac{\ln 2\ 2\pi^3\hbar^7}{G_F^2 m_e^5 c^4} \frac{1}{f(Z', \Delta E)} \frac{1}{c_V^2 |A_F|^2 + c_A^2 |A_{GT}|^2} \quad (97)$$

The ft value is the half-life adjusted with the $f(Z', \Delta E)$ dependence removed, so it is only a function of the Fermi and Gamow-Teller amplitudes:

$$ft \equiv f(Z', \Delta E)\tau_{1/2} = \frac{\ln 2\ 2\pi^3\hbar^7}{G_F^2 m_e^5 c^4} \frac{1}{c_V^2 |A_F|^2 + 3c_A^2 |A_{GT}|^2} \approx \frac{6140 \text{ sec}}{|A_F|^2 + 1.59 |A_{GT}|^2} \quad (98)$$

A centrifugal barrier impedes the emission of beta particles and neutrinos with angular momentum $l \neq 0$ (just as it does for alpha particles), making beta decays with larger and larger values of emitted l increasingly unlikely. Or viewed in a different way, a high-energy electron with momentum $p \sim m_e c$ emitted from a typical nuclear radius $R \sim 5$ fm has an angular momentum (in units of $\hbar$) $l \sim p \cdot R/\hbar \sim 10^{-2}$. Since angular momentum must be quantized, emission of $l = 0$ is therefore much more probable than emission of $l = 1$. This is a direct result of the nucleus being practically a point source. More mathematically, the beta particle wavefunction may be Taylor-expanded in terms representing successive values of $l = 0$, $l = 1$, $l = 2$, etc.:

$$\psi_e \sim \exp\left(\frac{i\mathbf{p}\cdot\mathbf{r}}{\hbar}\right) \approx 1 + \frac{i\mathbf{p}\cdot\mathbf{r}}{\hbar} + \frac{1}{2}\left(\frac{i\mathbf{p}\cdot\mathbf{r}}{\hbar}\right)^2 + \ldots \quad (99)$$

As calculated above, each term is $\sim 10^{-2}$ smaller than the previous term. When the wavefunction is squared to get the probability, each term is $\sim 10^{-4}$ smaller. Equations (97) and (98) describe the most probable case, $l = 0$. Beta decay with emission of $l = 1$ has a half-life that is $\sim 10^4$ longer than that, and each higher value of l introduces an additional factor of $\sim 10^4$.

If the initial and final nucleons are in similar orbits, the squared amplitudes $|A_F|^2$ and $|A_{GT}|^2$ are of order unity [4], as they are for neutron decay. If the initial and final orbits are rather different, the amplitudes are much smaller, typically increasing the half-life by a factor of $\sim 10^1 - 10^4$.

Since parity varies like $(-1)^l$, the parity of the nucleus changes during odd-l but not even-l emission.

In Fermi decay, the electron and neutrino have antiparallel spins and hence carry off no net spin, $s = 0$. In contrast, they have parallel spins in Gamow-Teller decay and thus carry off $s = 1$. The nuclear spin can change by as much as the sum of the emitted l and s values. If $l = 0$, Fermi decay cannot change the nuclear spin, $\Delta J = 0$, since the emitted particles have no net spin. Gamow-Teller decay with $l = 0$ must change the component m_J of nuclear spin by the one unit carried by the emitted particles, so ΔJ could be -1, 0, or +1. An exception is that Gamow-Teller decay cannot mediate a transition from one $J = 0$ nuclear state to another, as $m_J = 0$ could not change in that case.

Putting all of this information together, beta decays may be divided into the following categories based on their ft lifetime [Fig. 16(g)]. Since a nucleus generally decays via the most probable (fastest) allowed route, these categories may be regarded as **selection rules** to predict the most probable type of beta decay for given initial and final nuclear states:

1. **Superallowed decays** are the fastest, occuring when the emitted l is 0 (thus the nuclear parity cannot change) and $|A_F|^2$ and/or $|A_{GT}|^2$ are of order unity (the initial and final nucleon states are similar). From Eq. (98), such decays have $ft \approx 3000$ sec ~ 1 hour. The nuclear spin can change by $\Delta J = 0$ (Fermi or Gamow-Teller modes) or ± 1 (Gamow-Teller only).

2. **Allowed decays** are the next fastest. They have $l = 0$ but rather different initial and final nucleon states, so their comparitive half-lives are $ft \sim 10^4 - 10^7$ sec $\sim 1 - 100$ days. As with superallowed decays, the nuclear spin changes by $\Delta J = 0$ or ± 1.

3. **First forbidden decays** are not actually forbidden, just less probable. They have an emitted $l = 1$ and thus involve a nuclear parity change and $\Delta J = 0$, ± 1, or ± 2. Their comparative half-lives are in the range $ft \sim 10^6 - 10^9$ sec, depending on how similar or different the initial and final nucleon states are.

4. **Second forbidden decays** have $l = 2$. They do not alter the nuclear parity but change the nuclear spin by $\Delta J = \pm 2$ or ± 3. (While second forbidden decays with $\Delta J = 0$ or ± 1 are theoretically possible, they are overwhelmed by the much faster allowed or superallowed decays that also satisfy those ΔJ and parity conditions.) The comparitive half-lives of second forbidden decays are in the range $ft \sim 10^{10} - 10^{13}$ sec.

5. **Third forbidden decays** have $l = 3$ and $ft \sim 10^{14} - 10^{20}$ sec $\sim 3 \times 10^6 - 3 \times 10^{12}$ years. They involve a nuclear parity change and $\Delta J = \pm 3$ or ± 4. (Transitions with a parity change but smaller ΔJ are dominated by first forbidden decays.) There are only four known cases of third forbidden decay.

6. **Fourth forbidden decays** have $l = 4$ and extraordinarily long comparative half-lives, $ft \sim 10^{23}$ sec $\sim 3 \times 10^{15}$ years. They involve $\Delta J = 4$ or 5 and no nuclear parity change, and there are only two known cases.

As an example, beta decay of tritium to helium-3 releases 18.6 keV, or $\epsilon = 1 + 18.6/511 \approx 1.0364$. The initial and final nuclear states are very similar (mirror images with neutrons↔protons) and the nuclear spin remains $J = 1/2$, so the decay is superallowed with $ft \sim 3000$ sec. Using $f(2, 1.0364) \approx 5 \times 10^{-6}$ yields $\tau_{1/2} = ft/f \sim 19$ years, relatively close to the actual half-life of 12.3 years.

Instead of emitting a positron, a nucleus undergoing beta decay can sometimes absorb one of the orbiting atomic electrons, a process called **electron capture**:

$$p^+ \ + \ e^- \ \longrightarrow \ n \ + \ \nu_e \tag{100}$$

Calculations of electron capture are very similar to those of positron-emission beta decay, except the density of states for a free emitted positron with momentum p_e, $4\pi p_e^2 dp_e/\hbar^3 \sim (\Delta E)^3/(\hbar c)^3$, must be replaced by the density of an atomic electron in orbital shell n at the nucleus, $\sim |\psi_n(r=0)|^2 \sim \left(\frac{Z}{n} \, \frac{e^2}{4\pi\epsilon_o} \, \frac{m_e}{\hbar^2}\right)^3$, using atomic electron wavefunctions from the nonrelativistic quantum summary evaluated at $r = 0$. Thus the ratio of electron capture to positron emission is

$$\frac{\Gamma_{\text{capture}}}{\Gamma_{e^+}} \approx \begin{matrix}\text{numerical} \\ \text{constant}\end{matrix} \times \frac{\left(\frac{Z}{n} \, \frac{e^2}{4\pi\epsilon_o} \, \frac{m_e}{\hbar^2}\right)^3}{\left(\frac{\Delta E}{\hbar c}\right)^3} \approx 60\pi \left(\frac{Z}{n} \, \frac{e^2}{4\pi\epsilon_o \hbar c} \, \frac{m_e c^2}{\Delta E}\right)^3 \approx 1 \times 10^{-5} \left(\frac{Z}{n \, \Delta E_{\text{MeV}}}\right)^3, \tag{101}$$

where the numerical constant 60π comes from more detailed calculations [4]. While Eq. (101) does not extend down to low transition energies ΔE or include relativistic effects that occur at high Z [3, 4], it nonetheless illustrates the general behavior of electron capture. Because of the cube of the **fine structure constant** $\alpha_{fs} \equiv e^2/4\pi\epsilon_o\hbar c \approx 1/137$, electron capture is generally less likely than positron emission. Due to the factor of $1/n^3$, $n = 1$ (also known as 1s or K-shell) electrons are most likely to be captured, since they orbit closer to the nucleus and have a much higher probability of entering the nucleus. The Z^3 dependence means that electron capture is most significant for heavy elements. Finally, electron capture is most important for low transition energies ΔE.

The only particle emitted directly in electron capture is a neutrino, which is virtually impossible to detect. However, X-rays are emitted soon after the decay, when an electron in a higher shell drops down to replace the captured electron in the lower orbital.

Electron capture is covered by the same selection rule as the corresponding type of positron-emission beta decay, but a crucial difference is the energies involved. In positron emission, part of the transition energy $\Delta E = [M(Z-1, N+1) - M(Z, N)]c^2$ must be converted into the rest energy $m_e c^2$ of the created positron. In contrast, electron capture reactions can *consume* the rest energy $m_e c^2$ of the captured electron (neglecting the atomic binding energy of that electron), adding it to the nuclear transition energy. Thus positron emission requires a minimum nuclear transition energy $\Delta E \geq m_e c^2$, whereas electron capture reactions can occur even for nuclear transition energies that are slightly negative, down to almost $\Delta E \approx -m_e c^2$.

2.3 Gamma Decay

In **gamma decay**, a nucleus in an excited state decays to a lower state, emitting a gamma ray photon in the process (Fig. 17). This decay process is in contrast to alpha and beta decay, in which the composition of the nucleus changes during the decay.

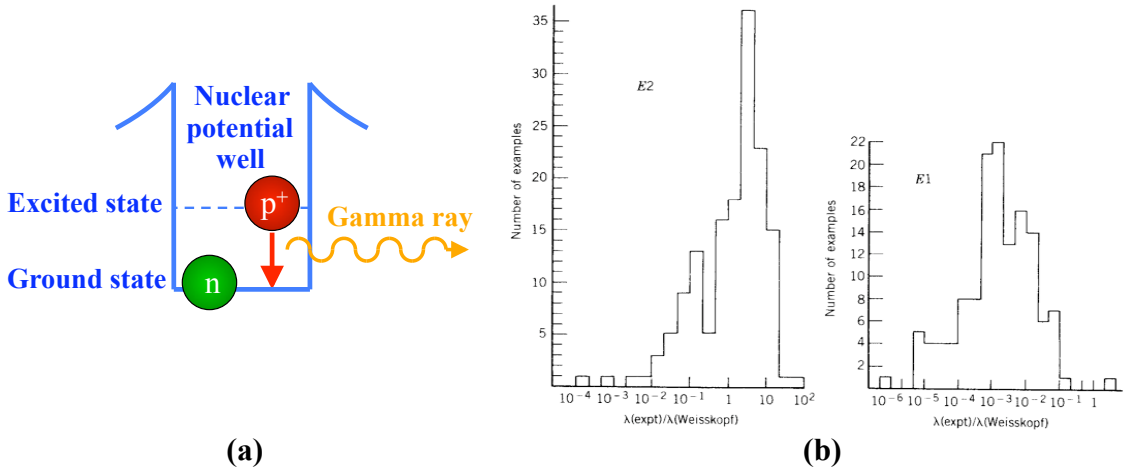

Figure 17. Gamma decay. (a) In gamma decay, one or more nucleons in the nucleus decay from an excited state to a lower energy state, releasing excess energy as a gamma ray. **(b)** Comparison of experimental data with Weisskopf estimates for gamma decay rates. From S. J. Skorka *et al., Nucl. Data* **2**, 347 (1966).

Gamma decay rates may be estimated by treating the nucleus as an electric or magnetic multipole that radiates photons. From *Electromagnetism* ?.?, the power radiated by an electric or magnetic multipole of order L ($L = 1$ for a dipole, 2 for a quadrupole, 3 for an octupole, etc.) is

$$P(XL) = \frac{2(L+1)}{L[(2L+1)!!]^2}\frac{c}{\epsilon_o}\left(\frac{\omega}{c}\right)^{2L+2}[M(XL)]^2 \tag{102}$$

in which X is E for electric or M for magnetic multipoles. The double factorial used in Eq. (102) is defined as $(2L+1)!! \equiv 1\cdot 3\cdot 5\cdot ...(2L+1)$. M is the generalized multipole moment; for an electric dipole, it can be expressed in terms of the more familiar dipole moment d, $M(E1) = \sqrt{\frac{3}{16\pi}}d$.

Equation (102) can be extended to cover a quantum system like a nucleus by letting the multipole moment become an operator $\hat{M}$ evaluated between the wavefunctions of the excited and ground states of the nucleus, the initial state i and final state f. L then indicates not only the multipole order but also the angular momentum emitted by the nucleus during the decay. The lifetime of the excited state is simply the time required for a photon of energy $\Delta E = \hbar\omega$ to be emitted:

$$\Gamma(XL) \equiv \frac{1}{\tau(XL)} = \frac{P(XL)}{\hbar\omega} = \frac{2(L+1)}{L[(2L+1)!!]^2}\frac{1}{\epsilon_o\hbar}\left(\frac{\omega}{c}\right)^{2L+1}\left|\left\langle f\left|\hat{M}(XL)\right|i\right\rangle\right|^2 \tag{103}$$

The electric multipole operator is $\hat{M} = er^L Y_{LM}$. Assuming that the wavefunction and angular factors are ~ 1, the electric multipole moment can be evaluated approximately:

$$\left\langle f\left|\hat{M}(EL)\right|i\right\rangle = \frac{\int d\Omega\int_0^R dr\, r^2\,\psi_f\, er^L Y_{LM}\,\psi_i}{\int d\Omega\int_0^R dr\, r^2} \sim \frac{3}{L+3}eR^L \tag{104}$$

Inserting Eq. (104) into Eq. (103), the electric multipole decay rate is

$$\Gamma(EL) \sim \frac{2(L+1)}{L[(2L+1)!!]^2}\,\frac{e^2}{\epsilon_o\hbar}\left(\frac{\Delta E}{\hbar c}\right)^{2L+1}\left(\frac{3}{L+3}\right)^2 R^{2L} \tag{105}$$

Using Eq. (11), Eq. (105) gives the **Weisskopf estimates** for electric multipole decay rates:

$$\Gamma(E1) \sim 1.0\times10^{14}\,A^{2/3}\,(\Delta E_{\rm MeV})^3\ \ {\rm sec}^{-1} \tag{106}$$
$$\Gamma(E2) \sim 7.3\times10^{7}\,A^{4/3}\,(\Delta E_{\rm MeV})^5\ \ {\rm sec}^{-1} \tag{107}$$
$$\Gamma(E3) \sim 34\,A^{2}\,(\Delta E_{\rm MeV})^7\ \ {\rm sec}^{-1} \tag{108}$$
$$\Gamma(E4) \sim 1.1\times10^{-5}\,A^{8/3}\,(\Delta E_{\rm MeV})^9\ \ {\rm sec}^{-1} \tag{109}$$

The Weisskopf estimates are only ballpark values since they omit nuclear wavefunction and angular factors, yet they illustrate the functional dependence and relative magnitudes of the decay rates.

Because the electric multipole operator assumed only a single charge, decay rates can be considerably larger if many oscillating nucleons contribute to the process. On the other hand, decay rates can be significantly smaller than the Weisskopf estimates if the initial and final nuclear wavefunctions do not match up well. Figure 17(b) compares experimental data with the Weisskopf estimates.

Using the magnetic multipole operator $\hat{M} \approx (\mu_p - \frac{1}{L+1})\frac{e\hbar}{m_pc}r^{L-1}Y_{LM}$ and assuming the wavefunction and angular factors are ~ 1, the magnetic multipole moment is roughly:

$$\begin{aligned}\left\langle f\left|\hat{M}(XL)\right|i\right\rangle &\approx \frac{\int d\Omega\int_0^R dr\,r^2\psi_f\,\left(\mu_p-\frac{1}{L+1}\right)\frac{e\hbar}{m_pc}r^{L-1}Y_{LM}\,\psi_i}{\int d\Omega\int_0^R dr\,r^2}\\ &\sim \left(\mu_p-\frac{1}{L+1}\right)\frac{3}{L+2}\,\frac{e\hbar}{m_pc}\,R^{L-1} \sim \sqrt{10}\,\frac{3}{L+2}\,\frac{e\hbar}{m_pc}\,R^{L-1}\end{aligned} \tag{110}$$

in which the nuclear physicists' convention of estimating $\mu_p - \frac{1}{L+1} \sim \sqrt{10}$ has been used.

From Eqs. (110) and (103), the magnetic multipole decay rate is

$$\Gamma(ML) \sim 10\,\frac{2(L+1)}{L[(2L+1)!!]^2}\,\frac{e^2}{\epsilon_o\hbar}\left(\frac{\hbar}{m_pc}\right)^2\left(\frac{\Delta E}{\hbar c}\right)^{2L+1}\left(\frac{3}{L+2}\right)^2 R^{2L-2} \tag{111}$$

Using Eq. (11) in Eq. (111), the Weisskopf estimates for magnetic multipole decay rates are:

$$\Gamma(M1) \sim 5.6\times10^{13}\,(\Delta E_{\rm MeV})^3\ \ {\rm sec}^{-1} \tag{112}$$
$$\Gamma(M2) \sim 3.5\times10^{7}\,A^{2/3}\,(\Delta E_{\rm MeV})^5\ \ {\rm sec}^{-1} \tag{113}$$
$$\Gamma(M3) \sim 16\,A^{4/3}\,(\Delta E_{\rm MeV})^7\ \ {\rm sec}^{-1} \tag{114}$$
$$\Gamma(M4) \sim 4.5\times10^{-6}\,A^{2}\,(\Delta E_{\rm MeV})^9\ \ {\rm sec}^{-1} \tag{115}$$

As with the electric multipole decay rates, the actual magnetic multipole decay rates can be higher than the Weisskopf estimates if many nucleons contribute to the process or lower if the initial and final nuclear wavefunctions are poorly matched.

For multipoles of the same order L, the ratio of the magnetic and electric decay times is:

$$\frac{\tau(ML)}{\tau(EL)} \sim \frac{1}{10}\left(\frac{Rm_pc}{\hbar}\right)^2 \sim \frac{1}{10}\left(\frac{1.2\ {\rm fm}\ A^{1/3}m_pc}{\hbar}\right)^2 \sim 3\,A^{2/3} \tag{116}$$

Selection rules indicate which multipole is predominant for a given nuclear transition:

1. The emitted angular momentum L must lie between the difference and the sum of the initial J_i and final J_f nuclear angular momentum, $|J_i - J_f| \leq L \leq J_i + J_f$, but L cannot be zero because a photon has an intrinsic spin of 1.

2. If the nuclear state has the same parity before and after the transition, the decay must be an even electric or odd magnetic multipole transition, in order to keep the product of the nuclear parity and radiation parity constant.

3. If the nuclear parity changes, the decay must be an odd electric or even magnetic multipole.

4. Using Eqs. (106)-(109) to compare electric multipoles or Eqs. (112)-(115) to compare magnetic multipoles, decay of order $L+1$ is typically $4.5 \times 10^{-7} A^{2/3} (\Delta E_{\rm MeV})^2 \sim 10^5$ less probable than decay of order L for medium or heavy nuclei with $\Delta E \sim 1$ MeV. Therefore the multipole emission with the smallest allowed L is generally dominant.

5. For the same L, Eq. (116) shows that EL is typically $\sim$ 100x more probable than ML for medium or heavy nuclei. (However, note that Rules 2 and 3 forbid electric and magnetic multipoles of the same order from competing with each other in the same case.)

6. From Rules 4 and 5, generally $\frac{\tau(E\,L+1)}{\tau(ML)} = \frac{\tau(E\,L+1)}{\tau(EL)} \frac{\tau(EL)}{\tau(ML)} \sim 10^5 \times 10^{-2} \approx 1000$, so depending on the details of the nuclear wavefunctions, the $E2$ decay rate may approach that of $M1$, $E3$ may approach $M2$, and so forth.

7. Similarly, combining Rules 4 and 5 shows that $\frac{\tau(M\,L+1)}{\tau(EL)} = \frac{\tau(M\,L+1)}{\tau(ML)} \frac{\tau(ML)}{\tau(EL)} \sim 10^5 \times 100 \approx 10^7$, so generally $M2$ cannot compete with $E1$, $M3$ cannot compete with $E2$, etc.

A nucleus can decay from an excited state by emitting a virtual photon instead of a real photon. In **internal conversion**, such a virtual photon is absorbed by an electron orbiting the nucleus, with the net result that the atom emits a high-energy electron instead of a gamma ray. The **internal conversion coefficient** α_n is the ratio of the decay rate due to internal conversion involving an atomic electron from the nth shell and the gamma decay rate. The internal conversion coefficient depends on the probability that an atomic electron will be found within the nucleus, so it has the same $\left(\frac{Z}{n} \frac{e^2}{4\pi\epsilon_o \hbar c} \frac{m_e c^2}{\Delta E}\right)^3$ dependence as the electron capture ratio in Eq. (101). However, the virtual-photon-to-electron conversion process introduces an extra factor of $e^2/4\pi\epsilon_o\hbar c$:

$$\alpha_n \equiv \frac{\Gamma_{e,\,n}}{\Gamma_\gamma} \sim \left(\frac{e^2}{4\pi\epsilon_o \hbar c}\right)^4 \left(\frac{Z}{n}\right)^3 \left(\frac{2m_e c^2}{\Delta E}\right)^3 \tag{117}$$

More detailed calculations [1, 3] show the energy exponent depends on L for electric multipoles EL:

$$\alpha_n(EL) \equiv \frac{\Gamma_{e,\,n}(EL)}{\Gamma_\gamma(EL)} \sim \left(\frac{e^2}{4\pi\epsilon_o \hbar c}\right)^4 \left(\frac{Z}{n}\right)^3 \left(\frac{2m_e c^2}{\Delta E}\right)^{L+\frac{5}{2}} \approx \frac{1}{(137)^4} \left(\frac{Z}{n}\right)^3 \left(\frac{2m_e c^2}{\Delta E}\right)^{L+\frac{5}{2}} , \tag{118}$$

Likewise, the internal conversion coefficient for magnetic multipoles ML is [1, 3]:

$$\alpha_n(ML) \equiv \frac{\Gamma_{e,\,n}(ML)}{\Gamma_\gamma(ML)} \sim \frac{1}{(137)^4}\left(\frac{Z}{n}\right)^3\left(\frac{2m_ec^2}{\Delta E}\right)^{L+\frac{3}{2}} \tag{119}$$

The results in Eqs. (118) and (119) are only order-of-magnitude estimates, since they do not include relativistic effects or details of the wavefunctions. Nonetheless, they reveal important aspects of internal conversion coefficients. Like the electron capture ratio from Eq. (101), the internal conversion coefficient is generally quite small but is most significant for $n = 1$ electrons, high-Z elements, and low transition energies ΔE. Large changes in angular momentum L also make internal conversion more important.

Internal conversion is particularly important when the selection rules hinder gamma emission. For example, 0-0 transitions simply cannot decay via gamma emission, so they decay instead via internal conversion. The internal conversion coefficient for such transitions is thus meaningless, and the decay rate must be calculated from first principles [3].

Isomers, nuclei in especially long-lived excited or **metastable** states, are often denoted by an "m" with the atomic number, for example ^{99m}Tc. There are over 100 isomers with lifetimes of minutes or longer; they generally have $\Delta E \leq 300$ keV, reducing the incentive to decay, and $\Delta J \geq 3$, greatly hindering the decay. Due to these characteristics, isomers generally decay via internal conversion. One important isomer is an excited state of ^{60}Co, which decays via emission of a 58.6 keV gamma ray with a half-life of 10.7 minutes and is used for medical applications.

An even rarer process than internal conversion is **internal pair creation**, in which the virtual photon emitted by a nucleus splits into a real electron-positron pair [3,4]. Since the rest and kinetic energies of the electron and positron must come from the decay energy ΔE, internal pair creation can only happen when $\Delta E \geq 2m_ec^2$.

3 Nuclear Reactions

Nuclei can react with each other or with other particles. This section introduces general methods for analyzing nuclear reactions, then specifically applies those methods to fusion and fission reactions.

3.1 General Principles

In a typical nuclear reaction, a nucleus X and particle a combine and react to produce a different nucleus Y and particle b. Such a reaction can be written as

$$X + a \longrightarrow Y + b \qquad \text{Straightforward notation for a nuclear reaction} \tag{120}$$

$$\text{or} \quad X\,(\,a\,,\,b\,)\,Y \qquad \text{Intimidating nuclear physicist's notation for a reaction} \tag{121}$$

Particles a and b could be nuclei, gamma rays, nucleons, electrons, or anything else. When using the intimidating notation, the smaller initial and smaller final particle/nucleus go inside the parentheses. Moreover, expressions of the form (a, b) refer to reactions involving the absorption of a and emission of b which could happen to a number of possible initial X and final Y nuclei.

For simplicity, relativistic effects are ignored in this section. Indeed, common nuclear reactions such as fusion and fission occur at nonrelativistic collision velocities, $v \ll c$. For reactions at relativistic velocities, see *Relativistic Quantum Field Theory*, [1], or [4].

Two frames of reference are commonly used. The frame in which particle a is moving and nucleus X is initially at rest is called the **lab frame**; it describes the point of view of many laboratory experiments, in which a beam of a particles bombards a target containing initially stationary X nuclei. In contrast, in the **center-of-mass (CM) frame**, the initial particles X and a have equal but opposite momenta and the final particles Y and b have equal but opposite momenta. As shown in *Classical Mechanics* ?.?, this CM frame is equivalent to one particle remaining at rest and the other particle moving as if it has a reduced mass m_{red} or reduced mass number A_{red}:

$$m_{\text{red}} = \frac{m_X m_a}{m_X + m_a} \qquad \text{or} \qquad A_{\text{red}} = \frac{A_X A_a}{A_X + A_a} \tag{122}$$

In either frame, the velocity of one particle relative to the other is v. If the kinetic energy of the bombarding particle a in the lab frame is $E_{a,\,\text{lab}}$, the total kinetic energy E_{CM} in the CM frame is

$$E_{CM} = \frac{1}{2} m_{\text{red}} v^2 = \frac{m_X}{m_X + m_a} \frac{1}{2} m_a v^2 = \frac{A_X}{A_X + A_a} E_{a,\,\text{lab}} \tag{123}$$

Because $E_{CM} < E_{a,\,\text{lab}}$ in Eq. (123), not all of the initial kinetic energy $E_{a,\,\text{lab}}$ of the bombarding a particles can be used to trigger the reactions. An amount E_{CM} of that energy goes into the reaction, and the rest remains kinetic energy after the particles collide, due to conservation of momentum.

The rate of a reaction in a population of nuclei is usually described in terms of the **reaction cross section** σ, the equivalent cross-sectional area that bombarding particles must hit to trigger the reaction. For a general introduction to cross sections, see *Classical Mechanics* ?.?. In nuclear physics, cross sections are usually measured in units of barns (b, as in hitting the side of a barn), where $1\ \text{b} \equiv 10^{-28}\ \text{m}^2$. Note that the barn unit was chosen to correspond to the rough area of an average-sized nucleus of diameter $\sim 10^{-14}$ m.

Nuclear reaction cross sections can be calculated by a variety of methods, some of which are more appropriate for certain types of reactions than others [1-4]. However, the most broadly applicable method is the compound nucleus/Breit-Wigner approach, in which the initial particles form a compound nucleus C as an intermediate state before disintegrating into the final products:

$$X + a \longrightarrow C \longrightarrow Y + b \qquad \text{Compound nucleus treatment of reactions} \tag{124}$$

From quantum physics, colliding particles behave like blurry waves with de Broglie wavelength λ or wavevector $k = 2\pi/\lambda = p/\hbar = m_{\rm red}v/\hbar$. Colliding particles cannot be localized within a distance smaller than $\sim \lambda/\pi = 2/k$ or equivalently an area $\sim \pi/k^2$, so the reaction cross section varies like

$$\sigma \sim \frac{\pi}{k^2} = \frac{\pi\hbar^2}{2m_{\rm red}\,E_{CM}} = \frac{6.5\times10^5 \text{ barn}}{A_{\rm red}\,E_{CM,\,\rm eV}} \tag{125}$$

At high energies, the wavelength becomes smaller than the classical radius R of the colliding particles, so they stop acting like blurry waves and act more like hard spheres with a reaction cross section $\sigma \sim \pi R^2$.

From conservation of angular momentum, the compound nucleus must have spin $J = J_X + J_a + l$, where J_X and J_a are the spins of the initial particles and l is the relative angular momentum between them if they do not collide head-on. Usually the spin orientations are not known, so the cross section is averaged over the $(2J_X+1)(2J_a+1)$ possible initial particle spin orientations and summed over the $2J+1$ spin orientations of the compound nucleus, introducing a factor G_s in σ:

$$G_s = \frac{2J+1}{(2J_X+1)(2J_a+1)} \tag{126}$$

For spinless particles, Eq. (126) reduces to $G_s = 2l+1$. Physically, particles with momentum p and angular momentum between $l\hbar$ and $(l+1)\hbar$ have an impact parameter between $b_l = l\hbar/p = l/k$ and $b_{l+1} = (l+1)\hbar/p = (l+1)/k$ [1]. Thus these particles strike an area [Fig. 18(a)]

$$\pi b_{l+1}^2 - \pi b_l^2 = \frac{\pi}{k^2}\left[(l+1)^2 - l^2\right] = \frac{\pi}{k^2}(2l+1) = \frac{\pi}{k^2}G_s \tag{127}$$

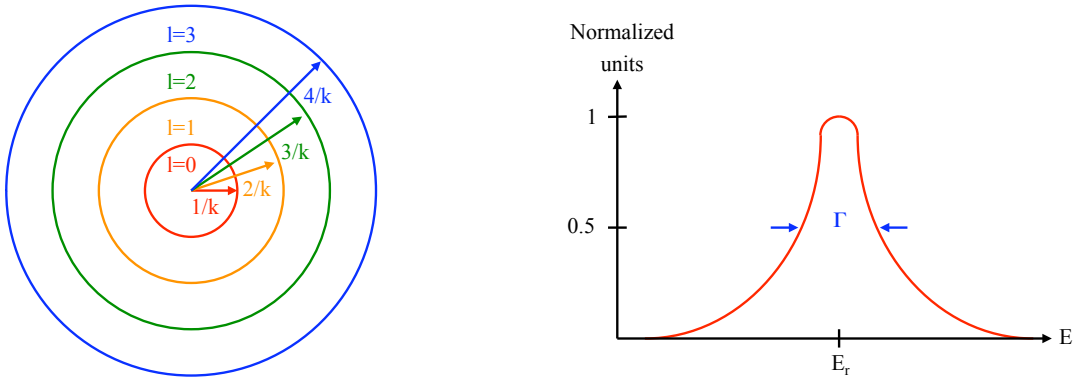

(a) **(b)**

Figure 18. Factors in nuclear reaction rates. **(a)** The area in which a particle can strike depends on its impact parameter b, which in turn depends on the particle's angular momentum l as shown in Eq. (127). **(b)** The energy spectrum of the excited state of the compound nucleus introduces the Lorentzian shape from Eq. (132).

Due to the energy of the initial particles, the compound nucleus is generally created in an excited state, which decays after a certain period of time into a lower-energy state, for instance by disintegration into final particles Y and b or back into the original particles X and a. Because excited states do not last forever, their energies are not exact but rather get blurred out a bit, thanks to the Heisenberg uncertainty principle. If an excited state decays by process i with an exponential decay time τ_i, the energy of the excited state is spread out by a **width** Γ_i according to

$$\tau_i \approx \frac{\hbar}{\Gamma_i} \tag{128}$$

Treating excited states of the compound nucleus as harmonic oscillator states separated by an energy spacing $D = \hbar\omega_o$, nucleons slosh back and forth and hit the potential barrier surrounding the nucleus at a frequency $f = \omega_o/2\pi$. If T_i is the transmission probability that the nucleons will escape through the barrier via decay process i, the corresponding width of an excited state is

$$\Gamma_i \;=\; \frac{\hbar}{\tau_i} \;=\; T_i\,\hbar f \;=\; T_i\,\frac{\hbar\omega_o}{2\pi} \;=\; T_i\,\frac{D}{2\pi} \tag{129}$$

The transmission probability depends on whether the escaping particles are charged, have angular momentum l, and have an energy E above or below the potential barrier V_B surrounding the nucleus. For charged particles with no angular momentum, T is given by Eqs. (76) and (77) for $E \ll V_B$, while T approaches 1 for $E \gg V_B$.

For a neutron with no angular momentum, T may be found by applying quantum physics to a particle exiting a square well. The transmission coefficient depends on the neutron's wavevector or energy inside and outside the nuclear potential well (*Nonrelativistic Quantum Physics* ?.?),

$$T \;=\; \frac{4\,k_{\text{inside}}\,k_{\text{outside}}}{(k_{\text{inside}} \;+\; k_{\text{outside}})^2} \;=\; \frac{4\,\sqrt{E_{\text{inside}}\,E_{\text{outside}}}}{(\sqrt{E_{\text{inside}}} \;+\; \sqrt{E_{\text{outside}}})^2} \tag{130}$$

If an escaping particle has angular momentum, it must pass through an additional potential barrier caused by centrifugal force. This greatly complicates the transmission coefficients for both charged and uncharged particles [3]. Fortunately, nuclear reactions are generally dominated by particles without angular momentum due to the lower potential barriers.

The total width of an excited state is the sum of the decay mode widths, $\Gamma = \sum_i \Gamma_i$. In the reaction in Eq. (124), the compound nucleus C can disintegrate back into $X + a$ with width Γ_a or it can go on and disintegrate into $Y + b$ with width Γ_b, so the total decay width of state C is $\Gamma = \Gamma_a + \Gamma_b$. An excited state's wavefunction oscillates due to the state's mean energy E_r and decays due to Γ:

$$\Psi(t) \;=\; \Psi_o\,\exp\left(-\,\frac{iE_r t}{\hbar}\right)\exp\left(-\,\frac{\Gamma t}{2\hbar}\right) \;=\; \Psi_o\,\exp\left[-\left(iE_r + \frac{\Gamma}{2}\right)\,\frac{t}{\hbar}\right] \tag{131}$$

Equation (131) uses $\Gamma/2$ because it is actually the measured probability $|\Psi(t)|^2$ that decays like Γ. Fourier-transforming Ψ from a function of t to a function of energy E and squaring to obtain the probability density, the energy spectrum of the excited state is a Lorentzian shape [Fig. 18(b)]:

$$|\Psi(E)|^2 \;=\; \frac{1}{(E - E_r)^2 + \frac{1}{4}\Gamma^2} \tag{132}$$

A nuclear reaction is far more likely if the initial particles have the right energy to produce a specific state of the compound nucleus, a condition which is called a **resonance**. To account for this effect, the probability density of the excited state can be multiplied by the energy widths of the incoming process a and final process b:

$$\frac{\Gamma_a\Gamma_b}{(E - E_r)^2 + \frac{1}{4}\Gamma^2} \tag{133}$$

Because the step $X + a \leftrightarrow C$ is reciprocal, the decay width Γ_a figures even in the forward reaction.

Combining Eqs. (125), (126), and (133) yields the complete **Breit-Wigner cross section formula** for reactions involving an isolated resonance of a compound nucleus:

$$\sigma_{ab} \;=\; \frac{\pi}{k^2}G_s\frac{\Gamma_a\Gamma_b}{(E - E_r)^2 + \frac{1}{4}\Gamma^2} \qquad\qquad \textbf{Breit-Wigner formula} \tag{134}$$

If there are many closely spaced resonances, Eq. (134) must be averaged over the typical spacing $\langle D \rangle$ between the resonances:

$$\sigma_{ab} = \frac{\pi}{k^2} \left\langle G_s \frac{\Gamma_a \Gamma_b}{\Gamma} \right\rangle \frac{2\pi}{\langle D \rangle} \tag{135}$$

Unlike in compound nucleus reactions, in **direct reactions** only a few nucleons of the colliding nuclei actually interact. Direct reactions generally occur at energies above $\sim$ 20 MeV. At these energies, the de Broglie-wavelength-limited cross section for an incident nucleon ($A_{red} = 1$) in Eq. (125) is < 3 fm^2 or < 2 fm wide, small enough to strike individual nucleons instead of an entire nucleus. Because the nucleons in a deuteron are more weakly bound and more widely spaced than nucleons in other nuclei, deuterons can undergo direct reactions at even lower energies, $\sim$ 10 MeV. A common example is the (d,p) reaction, in which a deuteron strikes a nucleus and becomes just a free proton, leaving its neutron behind in the target nucleus. This process is illustrated in Fig. 19(a) and is called a **stripping reaction**. The opposite process, shown in Fig. 19(b), is a **pickup reaction** (p,d) in which a proton steals a neutron from a target nucleus to become a deuteron. Whereas compound nuclear reactions can take up to $\sim 10^{-15}$ sec for the compound nucleus to sort itself out (see Section 3.3), direct reactions only require a few nuclear interaction times, say 10^{-22} sec, for their nucleon-nucleon interactions. Because direct reactions require high energies and only occur in certain situations, they will not be considered further here; see [1-3] for more information.

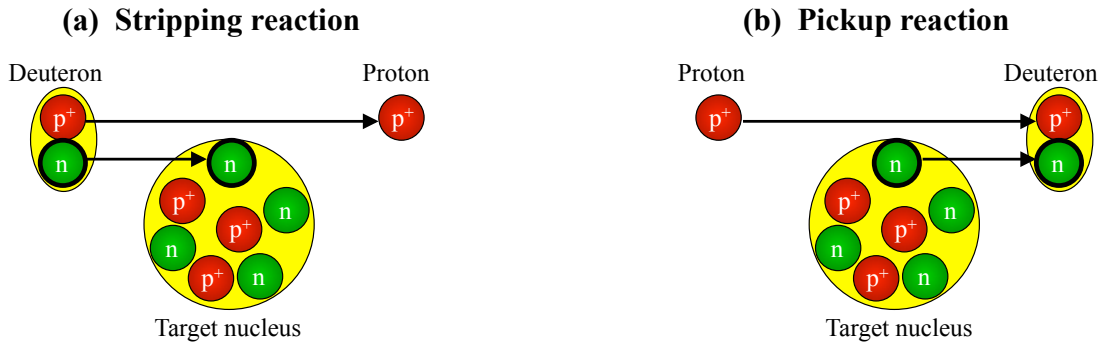

Figure 19. Direct reactions. (a) In a stripping reaction, an energetic nucleus loses one of its neutrons to a target nucleus in a collision. **(b)** In a pickup reaction, an energetic nucleus acquires an extra neutron from a target nucleus in a collision.

The **optical model** is useful for analyzing scattering events, $X + a \rightarrow X + a$. It assumes that incident particles interact with a nucleus in a fashion similar to light waves striking a refracting and slightly absorptive glass sphere. For this reason, the optical model is sometimes called the cloudy crystal ball model. The optical model is explained in more detail in *Nonrelativistic Quantum Physics* ?.? and [1-3]. Because this model is not particularly useful for analyzing reactions in which nuclei undergo changes, it will not be considered further here.

3.2 Fusion Reactions

In **fusion**, two small nuclei react to form a larger nucleus, generally releasing several MeV of energy in the process. This is the energy source in stars and hydrogen or H-bombs, and someday it may power fusion reactors. (See *Plasma Physics and Fusion* and [5].)

Fusion Reaction Cross Sections

The most readily achieved fusion reactions involve deuterons (D) and/or tritium nuclei (T) [Fig. 20]:

$$\mathrm{D} + \mathrm{T} \rightarrow {}^4\mathrm{He}\ (3.5\ \mathrm{MeV}) + \mathrm{n}\ (14.1\ \mathrm{MeV}) \tag{136}$$

$$\mathrm{D} + {}^3\mathrm{He} \rightarrow {}^4\mathrm{He}\ (3.6\ \mathrm{MeV}) + \mathrm{p}\ (14.7\ \mathrm{MeV}) \tag{137}$$

$$\mathrm{D} + \mathrm{D} \rightarrow \begin{cases} \mathrm{T}\ (1.01\ \mathrm{MeV}) + \mathrm{p}\ (3.02\ \mathrm{MeV}) & [50\%] \\ {}^3\mathrm{He}\ (0.82\ \mathrm{MeV}) + \mathrm{n}\ (2.45\ \mathrm{MeV}) & [50\%] \end{cases} \tag{138}$$

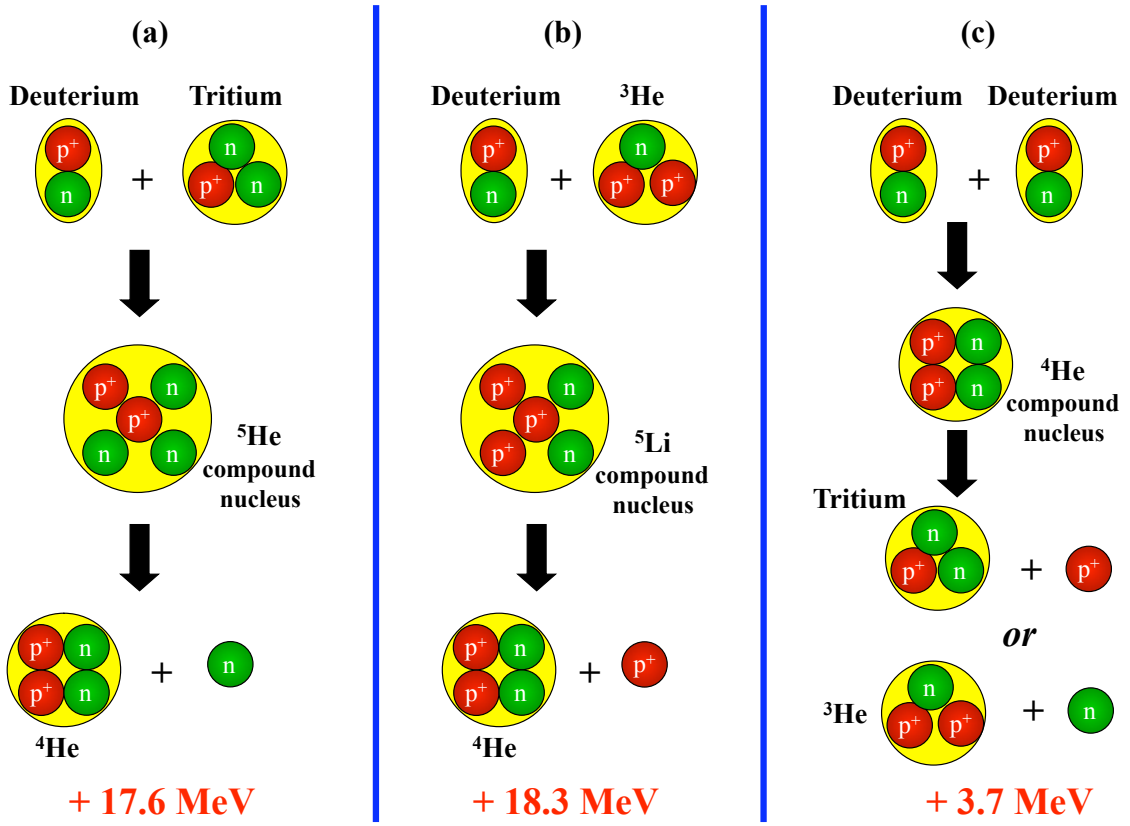

Figure 20. Most readily achieved fusion reactions. **(a)** Deuterium + tritium reaction. **(b)** Deuterium + helium-3 reaction. **(c)** Deuterium + deuterium reaction.

Fusion energy appears as kinetic energy $p^2/2m$ of the products. When the fragments separate with equal but opposite momenta p, the ratio of their kinetic energies agrees with Reactions (136)-(138):

$$\frac{E_1}{E_2} = \frac{p^2/2m_1}{p^2/2m_2} = \frac{A_2}{A_1} \tag{139}$$

Fusion cross sections are a product of four factors (Fig. 21), which will be calculated below.

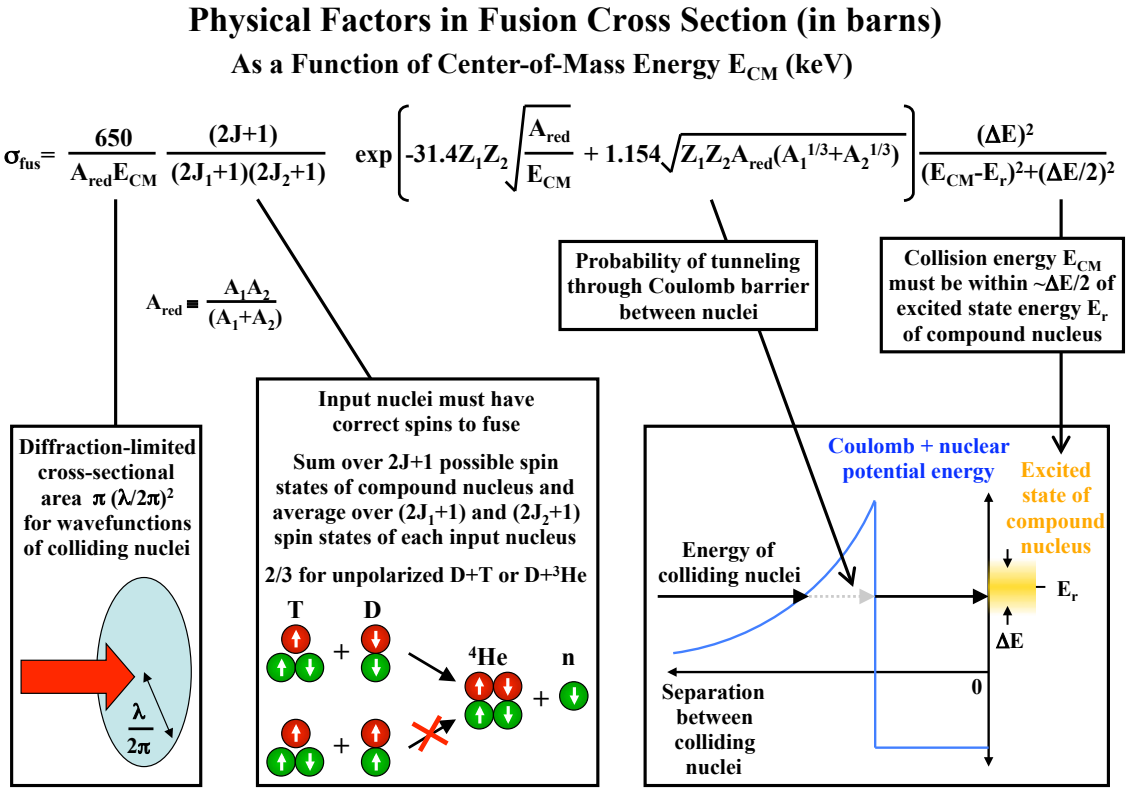

Figure 21. Physical origin of the four factors in fusion cross sections.

When two nuclei collide, they must tunnel through the Coulomb barrier between them in order to fuse. Adapting Eqs. (76) and (77), the tunneling transmission probability is

$$T \;=\; e^{-2G} \;\approx\; \exp\left(-\frac{31.4 Z_1 Z_2 \sqrt{A_1}}{\sqrt{E_{1\text{ lab, keV}}}}\right) \exp\left[1.154\sqrt{Z_1 Z_2 A_{\rm red}\left(A_1^{1/3}+A_2^{1/3}\right)}\right] \tag{140}$$

The ratio A/E in the first factor in Eq. (140) may be expressed in either the CM or the lab frame:

$$\frac{A_{\rm red}}{E_{CM}} \;=\; \frac{A_1 A_2}{A_1+A_2}\,\frac{A_1+A_2}{A_2}\,\frac{1}{E_{1\text{ lab}}} \;=\; \frac{A_1}{E_{1\text{ lab}}} \tag{141}$$

Using Eq. (129), the incoming Γ_a and outgoing Γ_b widths for a fusion reaction are

$$\Gamma_a \;=\; e^{-2G}\frac{D}{2\pi} \qquad \Gamma_b \;=\; \frac{D}{2\pi} \gg \Gamma_a \qquad \Gamma \;=\; \Gamma_a + \Gamma_b \;\approx\; \frac{D}{2\pi} \tag{142}$$

It has been assumed that $T \approx 1$ for the outgoing fusion reaction products, since they gain enough energy to go well over the top of the Coulomb barrier.

From Eqs. (134) and (125), the cross section for a fusion reaction is

$$\sigma \approx 4\,\frac{\pi}{k^2}\,\frac{G_s}{1+16\pi^2\left(\frac{E-E_r}{D}\right)^2}\,e^{-2G} = \frac{S(E)}{E_{1\text{ lab, keV}}}\exp\left(-\frac{31.4Z_1Z_2\sqrt{A_1}}{\sqrt{E_{1\text{ lab, keV}}}}\right)\text{ barn} \quad (143)$$

$$\text{where}\quad S(E) \equiv \frac{(A_1+A_2)^2}{A_1A_2^2}\,\frac{2600\,G_s}{1+16\pi^2\left(\frac{E-E_r}{D}\right)^2}\exp\left[1.154\sqrt{Z_1Z_2A_{\text{red}}\left(A_1^{1/3}+A_2^{1/3}\right)}\right] \quad (144)$$

S and E may be expressed in either the lab or CM frame by using Eq. (141).

G_s depends on the particles' spins [Eq. (126)]. For a deuteron, $J_1 = 1$ from Section 1.5. A triton or ^{3}He nucleus has one unpaired nucleon, giving $J_2 = 1/2$. In the compound nucleus formed in a D+T or D+^{3}He reaction, the odd nucleon must have $l = 1$ (two nucleons already occupy $l = 0$) and $s = +1/2$ (the energy is lower if s and l are parallel instead of antiparallel), so $J = 3/2$. Thus the spin-dependent factor is $G_s = 2/3$ for D+T and D+^{3}He reactions.

For $l = 0$, the spin factor G_s is the fraction of nuclei that have the correct spins to fuse out of a population with randomly oriented spins. If the spins are all oriented correctly, G_s is replaced by 1. This boosts the cross section by 50% for D+T and D+^{3}He and thus could significantly improve the performance of fusion reactors. Nuclear polarization can also greatly suppress neutron-producing D+D side reactions relative to cleaner D+^{3}He reactions in a D+^{3}He plasma, thereby reducing the radioactivity in a fusion reactor. Nuclei in a fusion plasma can be initially polarized by strong magnetic or electromagnetic fields, and the nuclear polarization is approximately conserved during two-nucleon collisional scattering events because the nuclei cannot exert much torque on each other [6]. However, the polarization is affected by three-body long-range Coulomb scattering, interactions with plasma waves, and interactions with the walls of the plasma confinement system. It is unclear whether these effects would randomize the nuclear polarizations before most of the nuclei can fuse.

For energies near the resonance energy E_r, the factor $S(E)$ varies rapidly, reaching a peak value at $E = E_r$ that does not depend on the parameters E_r and D. For D+T, the resonance peak occurs at $E_{1\text{ lab, r}} = 128$ keV. This yields $S(E_r)$ =19,200 in Eq. (144) and hence $\sigma = 3$ barns in Eq. (143), compared with the actual peak $\sigma \approx 5$ barns [Fig. 22(a)]. Similarly, using $E_{1\text{ lab, r}} = 450$ keV for D+^{3}He yields $S(E_r)$ =45,500 and $\sigma \approx 1.5$ barns, whereas the actual peak is $\sigma \approx 0.9$ barns. One should note that the WKB approximation underlying the Gamow factor e^{-2G} is only an order-of-magnitude estimate, that the results depend exponentially on the precise values of nuclear radii, and that more than one resonance may actually contribute to the measured value. In view of these limitations, the agreement between the calculated and measured cross sections is quite satisfactory.

From Section 1.3, the average spacing between low-lying energy levels of light nuclei is $D(0) \sim 1$ MeV in the CM frame, or ~ 2 MeV as judged from its effect on energies in the lab frame. This is in general agreement with the values that make Eqs. (143) and (144) give the best experimental agreement, $D \approx 2$ MeV for D+T and $D \approx 5.5$ MeV for D+^{3}He.

At low energies, $E \ll E_r$, the factor S is approximately constant, $S(E) \approx S(0) = S(E_r)[1 + 16\pi^2(E_r/D)^2]^{-1}$, and the fusion cross section becomes

$$\sigma \approx \frac{S(E_r)}{1+16\pi^2\left(\frac{E_r}{D}\right)^2}\,\frac{\exp\left(-31.4Z_1Z_2\sqrt{A_1/E_{1\text{ lab, keV}}}\right)}{E_{1\text{ lab, keV}}}\text{ barn} \quad (145)$$

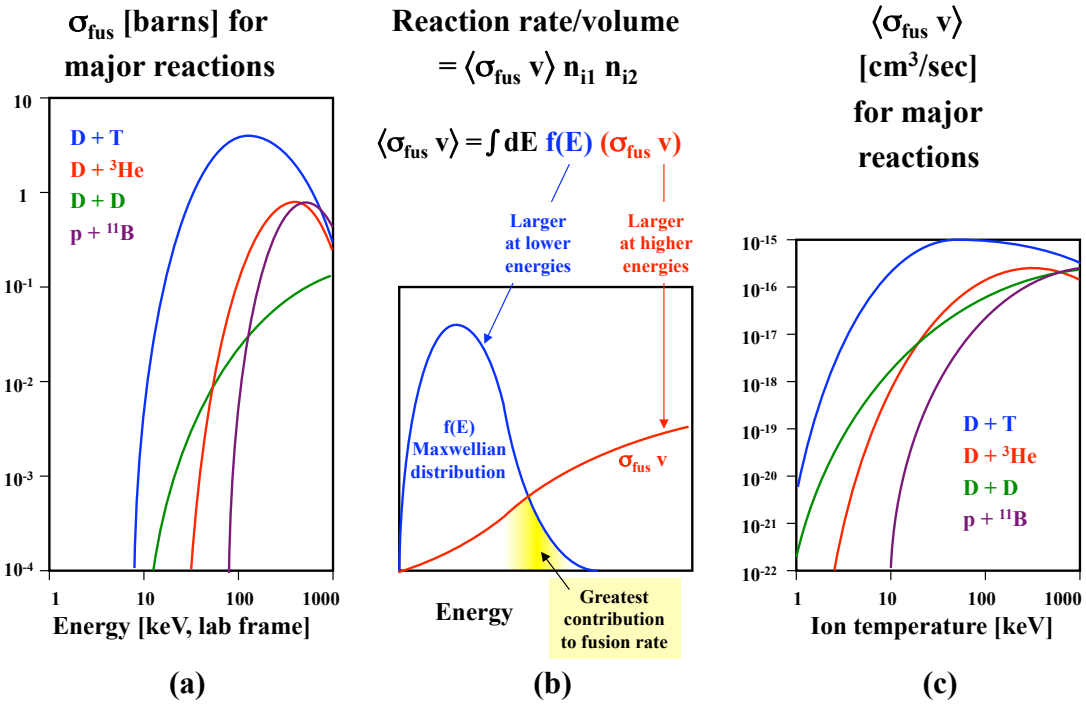

Figure 22. Fusion cross sections. **(a)** Cross section $\sigma(E)$ for key reactions. **(b)** For a Maxwellian distribution of particle energies, the overlap between $\langle\sigma v\rangle$ and the number of particles $dn(E)/dE$ with a given energy determines the reactivity $\langle\sigma v\rangle$. **(c)** The reactivity $\langle\sigma v\rangle$ vs. T for selected reactions.

Adjusting $S(E_r)$ to match the measured peak cross sections and inserting the other necessary parameters, one finds for energies far below resonance:

$$\sigma_{\mathrm{D+T}} \approx 20{,}000\,\frac{\exp\left(-44.4/\sqrt{E_{1\text{ lab, keV}}}\right)}{E_{1\text{ lab, keV}}}\ \text{barn} \approx 12{,}000\,\frac{\exp\left(-34.4/\sqrt{E_{\text{CM, keV}}}\right)}{E_{\text{CM, keV}}}\ \text{barn} \quad (146)$$

$$\sigma_{\mathrm{D+^3He}} \approx 10{,}000\,\frac{\exp\left(-88.8/\sqrt{E_{1\text{ lab, keV}}}\right)}{E_{1\text{ lab, keV}}}\ \text{barn} \approx 6000\,\frac{\exp\left(-68.8/\sqrt{E_{\text{CM, keV}}}\right)}{E_{\text{CM, keV}}}\ \text{barn} \quad (147)$$

Reaction (138) is more difficult to achieve at similarly low energies. Because these energies are too low for direct reactions, (138) must proceed via formation of a ^{4}He compound nucleus. Yet ^{4}He is exceptionally stable and its excited states are at very high energies, so it does not make a good intermediate. Empirically, this lowers the total cross section for both branches to

$$\sigma_{\mathrm{D+D}} \approx 350\,\frac{\exp\left(-44.4/\sqrt{E_{1\text{ lab, keV}}}\right)}{E_{1\text{ lab, keV}}}\ \text{barn} \approx 175\,\frac{\exp\left(-31.4/\sqrt{E_{\text{CM, keV}}}\right)}{E_{\text{CM, keV}}}\ \text{barn} \quad (148)$$

The first step that occurs in most fusion reactions in the sun is

$$\mathrm{p} + \mathrm{p} \rightarrow \mathrm{D} + \mathrm{e}^+ + \nu_e \quad (149)$$

This reaction requires one of the protons to beta decay into a neutron *during* the fusion process. Fusion occurs within roughly a nuclear interaction time 10^{-23} sec [Section 1.2], whereas beta decay of isolated nucleons requires ~ 900 sec [Section 2.2]. If the probability of simple fusion has $S(0) \sim 20{,}000$ comparable to the value for hydrogen isotopes in Eq. (146), this value must be modified to account for the probability that a beta decay will occur during the fusion process: $S(0) \sim (10^{-23}$ sec$/900$ sec$) \times 20{,}000 \sim 2 \times 10^{-22}$. This agrees with the measured cross section:

$$\sigma_{\text{p+p}} \approx 6 \times 10^{-22} \frac{\exp\left(-31.4/\sqrt{E_{\text{1 lab, keV}}}\right)}{E_{\text{1 lab, keV}}} \text{ barn} \approx 3 \times 10^{-22} \frac{\exp\left(-22.2/\sqrt{E_{\text{CM, keV}}}\right)}{E_{\text{CM, keV}}} \text{ barn} \quad (150)$$

As shown in Fig. 23, the easiest fusion reactions to achieve are (136)-(138). Of other reactions with hydrogen isotopes, p+T involves a ^{4}He intermediate, p+D has too few neutrons to proceed efficiently, and T+T has too many neutrons. ^{4}He, the only other available helium fuel, is already so happy with respect to its binding energy that it makes a very poor partner for fusion. All other elements have a higher charge, which increases the Coulomb barrier, and a higher mass, which reduces the probability of tunneling through that barrier, as may be seen from Eq. (145). p+^{12}C and higher reactions can occur, but the high Coulomb barrier makes the cross section so low that only stars have enough nuclei to produce a significant number of these reactions (*Plasma Physics and Fusion* 5.3).

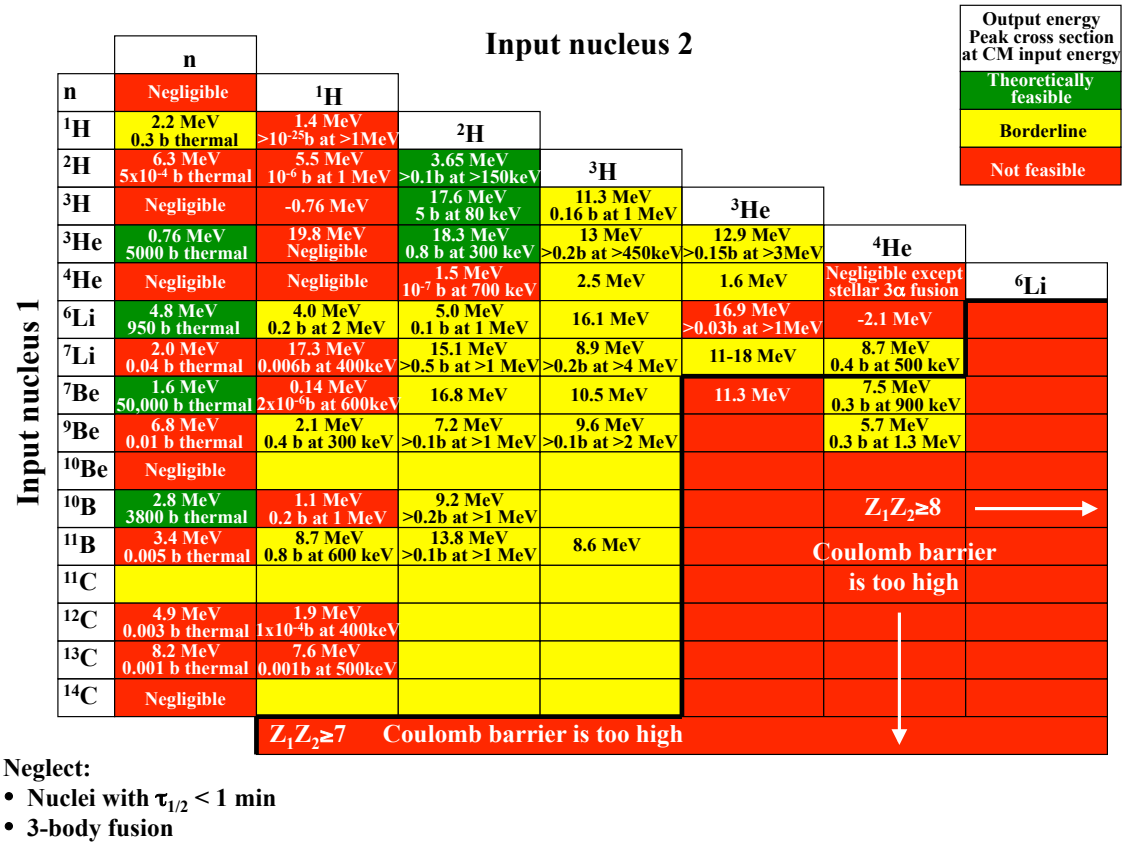

Figure 23. Possible fusion reactions. Reactions which are theoretically feasible for power production in controlled fusion reactors are green, those which are borderline are yellow, and those that are not feasible are red. Because of their size, stars can produce power from a greater number of reactions than are feasible in controlled fusion reactors. For more information, see *Plasma Physics and Fusion*.

Fusion Reactivity $\langle\sigma v\rangle$ for Maxwellian Velocity Distributions

In a population of nuclei with densities n_1 and n_2, the fusion reaction 1+2 occurs at a rate

$$\frac{\text{fusion reactions/sec}}{\text{volume}} \;=\; n_1 n_2 \,\langle\sigma v\rangle \tag{151}$$

in which the **reactivity** $\langle\sigma v\rangle$ is the product of the cross section and the relative collision velocity, averaged over all possible collision velocities in the population. If like nuclei fuse, 1+1, $n_1 n_2$ in Eq. (151) should be replaced by $\frac{1}{2}n_1^2$; the $\frac{1}{2}$ prevents double-counting of reacting pairs of nuclei.

Coulomb scattering makes nuclei rapidly assume a Maxwellian distribution of velocities (*Plasma Physics and Fusion* 2.1). Thus $\langle\sigma v\rangle$ is usually averaged over Maxwellian distributions of nuclei. This calculation uses the center-of-mass energy $E \equiv E_{\rm CM}$ and proceeds as follows:

$$\langle\sigma v\rangle \;=\; \int_0^\infty \Big(4\pi v^2 dv\Big)\,(\sigma v)\left(\frac{m_{\rm red}}{2\pi k_B T}\right)^{3/2}\exp\left(\frac{-m_{\rm red}v^2}{2k_BT}\right) = \sqrt{\frac{8}{\pi m_{\rm red}}}\int_0^\infty dE\,E\,\sigma\,\frac{e^{-E/k_BT}}{(k_BT)^{3/2}} \tag{152}$$

$$\approx\; \sqrt{\frac{8}{\pi m_{\rm red}}}\,\frac{S(0)}{(k_BT)^{3/2}}\int_0^\infty dE\,e^{-f(E)} \qquad \text{where } f(E) \equiv \frac{E}{k_BT} + \frac{\sqrt{E_G}}{E} \tag{153}$$

The integral in Eq. (153) involves σ, which drops off rapidly at low energies due to the Gamow barrier penetration factor, and the number of particles at a given energy, which falls exponentially at high energies for a Maxwellian distribution. The function $e^{-f(E)}$ describes the overlap between these factors [Fig. 22(b)]. Setting the derivative $f'(E_o) \equiv df/dE|_{E_o} = 0$, one finds the energy E_o with the peak value of $e^{-f(E)}$, the best combination of penetration probability and particle number:

$$E_o \;\approx\; \left(\frac{1}{2}\,k_BT\,\sqrt{E_G}\right)^{2/3} \;\approx\; 6.27\left(Z_1Z_2\sqrt{A_{\rm red}}\,T_{\rm keV}\right)^{2/3}\ \text{keV} \tag{154}$$

For example, for D+T at $T = 20$ keV, nuclei with $E_o = 49$ keV contribute most to the fusion rate.

A Taylor expansion of $f(E)$ about $E = E_o$ [where $f'(E_o) = 0$] simplifies the integral in Eq. (153):

$$f(E) \;\approx\; f(E_o) + \frac{1}{2}(E-E_o)^2 f''(E_o) \tag{155}$$

$$\text{in which}\quad f(E_o) = 3\left(\frac{E_G}{4k_BT}\right)^{1/3} = 18.76\left[\frac{Z_1^2Z_2^2A_{\rm red}}{(k_BT)_{\rm keV}}\right]^{1/3} \quad\text{and}\quad f''(E_o) = \frac{3}{\left[2E_G(k_BT)^5\right]^{1/3}} \tag{156}$$

The integral in Eq. (153) may be evaluated analytically by extending its lower limit to $E = -\infty$ (with negligible error) and using Eqs. (155)-(156) and the relation $\int_{-\infty}^{\infty} e^{-ax^2} = \sqrt{\pi/a}$:

$$\langle\sigma v\rangle \;\approx\; \frac{8}{9}S(0)\sqrt{\frac{2}{3m_{\rm red}E_G}}\,[f(E_o)]^2\,e^{-f(E_o)}$$

$$\approx\; \frac{2.54\times10^{-16}}{T_{\rm keV}^{2/3}}[S(0)]_{\rm CM,\ keV\cdot b}\left(\frac{Z_1Z_2}{A_{\rm red}}\right)^{1/3}\exp\left[-\frac{18.76(Z_1Z_2)^{2/3}A_{\rm red}^{1/3}}{T_{\rm keV}^{1/3}}\right]\ \frac{\rm cm^3}{\rm sec} \tag{157}$$

For reactions of interest, Eq. (157) yields:

$$\langle \sigma v \rangle_{\rm D+T} \sim \frac{5\times10^{-12}}{T_{\rm keV}^{2/3}} \exp\left(-\frac{19.94}{T_{\rm keV}^{1/3}}\right) \frac{\rm cm^3}{\rm sec} \qquad \text{for } T < 30 \text{ keV} \tag{158}$$

$$\langle \sigma v \rangle_{\rm D+^3He} \sim \frac{3\times10^{-12}}{T_{\rm keV}^{2/3}} \exp\left(-\frac{31.65}{T_{\rm keV}^{1/3}}\right) \frac{\rm cm^3}{\rm sec} \qquad \text{for } T < 150 \text{ keV} \tag{159}$$

$$\langle \sigma v \rangle_{\rm D+D} \sim \frac{4\times10^{-14}}{T_{\rm keV}^{2/3}} \exp\left(-\frac{18.76}{T_{\rm keV}^{1/3}}\right) \frac{\rm cm^3}{\rm sec} \qquad \text{for } T < 50 \text{ keV} \tag{160}$$

$$\langle \sigma v \rangle_{\rm p+p} \sim \frac{8\times10^{-38}}{T_{\rm keV}^{2/3}} \exp\left(-\frac{14.89}{T_{\rm keV}^{1/3}}\right) \frac{\rm cm^3}{\rm sec} \qquad \text{for } T < 50 \text{ keV} \tag{161}$$

Equations (157)-(161) used several approximations: (1) The low-energy cross section (145) neglects resonance effects included in the full cross section, Eqs. (143) and (144). (2) The Taylor series in Eq. (155) only approximates the actual $f(E)$. (3) The Gamow factor e^{-2G} neglects nuclei with enough energy to go over the Coulomb barrier instead of tunneling through it. These approximations limit the accuracy of Eqs. (157)-(161) to within $\sim 20\%$ and constrain their range of validity to the temperatures indicated. Much more accurate results [Fig. 22(c)] can be obtained via numerical integration using Eqs. (152), (143), and (144) with the substitution $e^{-2G} \to 1/(e^{2G}+1)$ so that the transmission probability approaches the correct value of 1 for energies far above the barrier.

Muon-Catalyzed Fusion

Instead of using high thermal energies to bash nuclei together until they fuse, an alternative is to use muons (μ^-) to catalyze fusion between low-temperature nuclei (Fig. 24) [6]. A muon is basically an overweight electron with a mass $m_\mu \approx 106$ MeV/c^2, or ~ 207x larger than the usual electron mass m_e (*Relativistic Quantum Field Theory* 1.4 and 3.2.1). Muons undergo a form of beta decay:

$$\mu^- \quad \stackrel{2.2\,\mu\rm sec}{\longrightarrow} \quad {\rm e}^- + \overline{\nu_e} + \nu_\mu \tag{162}$$

As will be shown, the muon half-life is long enough for a muon to catalyze many fusion reactions by temporarily imitating an electron in hydrogen molecules. *Nonrelativistic Quantum Physics* ?.? gives the Bohr energy of a particle with charge $-e$ and mass m bound to a hydrogen nucleus:

$$E_{\rm Bohr} = -\left(\frac{e^2}{4\pi\epsilon_o}\right)^2 \frac{m}{2\hbar^2}\,, \tag{163}$$

which is $E_e \approx -13.6$ eV for an electron but $E_\mu = (m_\mu/m_e)E_e \approx -2.81$ keV for a muon. Thus it is energetically very favorable for a muon to displace an electron orbiting a hydrogen nucleus.

Likewise, the Bohr orbital radius for a negative particle circling a hydrogen nucleus is

$$r_{\rm Bohr} = \frac{4\pi\epsilon_o}{e^2}\frac{\hbar^2}{m} \tag{164}$$

The Bohr radius is $r_{\rm Bohr,\,e} \approx 5.3\times10^{-11}$ m for an electron but only $r_{\rm Bohr,\,\mu} = (m_e/m_\mu) r_{\rm Bohr,\,e} \approx 256$ fm for a muon. The separation between a deuteron and triton bound together by a muon (a DT^+ molecule, analogous to the molecule H_2^+) is $r_o \approx 2r_{\rm Bohr,\,\mu} \approx 500$ fm. In the CM frame, this molecular binding may be represented by a simple harmonic oscillator potential with $m_{\rm red} = m_{_D} m_{_T}/(m_{_D}+m_{_T})$, plus the usual Coulomb repulsion between the deuteron and triton:

$$V(r) = \frac{e^2}{4\pi\epsilon_o r} + \frac{1}{2}\, m_{\rm red}\, \omega_o^2\, r^2 \tag{165}$$

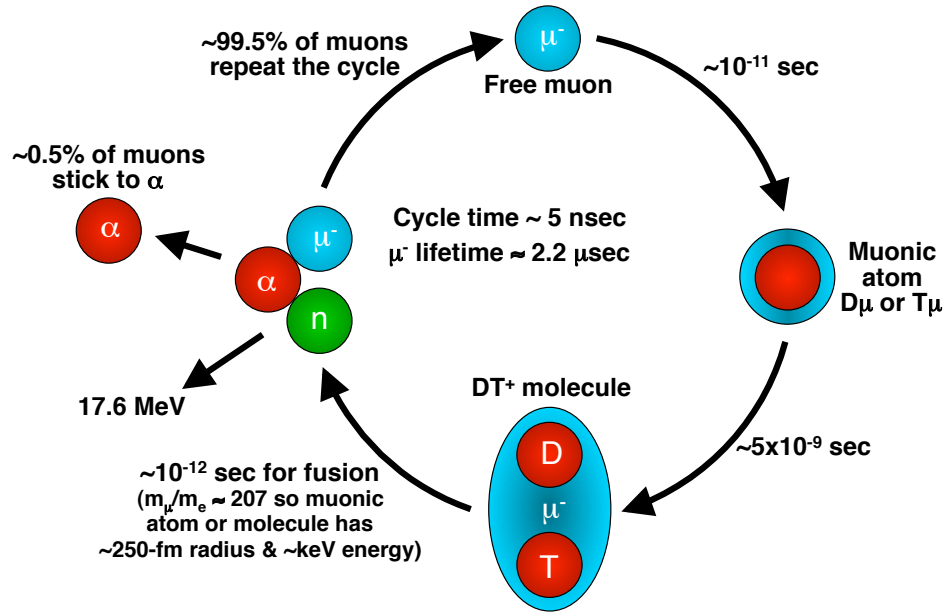

Figure 24. Muon-catalyzed fusion cycle. A free muon injected into a liquid mixture of deuterium and tritium displaces an electron to form a very tightly bound DT^+ molecule. The D and T rapidly fuse, emitting an α particle, a neutron, and the muon. Approximately 0.5% of the muons permanently stick to the α particle, but the remaining 99.5% repeat the fusion cycle.

The minimum of the potential occurs at the separation distance r_o:

$$V'(r_o) \;=\; 0 \qquad \Longrightarrow \qquad m_{\rm red}\,\omega_o^2 \;=\; \frac{e^2}{4\pi\epsilon_o r_o^3} \qquad \Longrightarrow \qquad \omega_o \;=\; \sqrt{\frac{1}{m_{\rm red}\,r_o^3}\,\frac{e^2}{4\pi\epsilon_o}} \tag{166}$$

The potential and its second derivative can also be calculated at that equilibrium separation:

$$V(r_o) \;=\; \frac{e^2}{4\pi\epsilon_o r_o} \;+\; \frac{1}{2}\,m_{\rm red}\,\omega_o^2 r_o^2 \;=\; \frac{3}{2}\,\frac{e^2}{4\pi\epsilon_o r_o} \;\approx\; 4.32\;\;{\rm keV} \tag{167}$$

$$V''(r_o) \;=\; 2\,\frac{e^2}{4\pi\epsilon_o r_o} \;+\; m_{\rm red}\,\omega_o^2 \;=\; 3m_{\rm red}\,\omega_o^2 \tag{168}$$

$V(r)$ may then be approximated as a Taylor series about $r = r_o$:

$$V(r) \;\approx\; V(r_o) \;+\; \frac{1}{2}\,V''(r_o)(r-r_o)^2 \;\approx\; V(r_o) \;+\; \frac{1}{2}\,m_{\rm red}\left(\sqrt{3}\omega_o\right)^2 (r-r_o)^2 \tag{169}$$

From Eq. (169), the DT^+ molecule vibrates at an angular frequency $\omega_{\rm vibr}$:

$$\omega_{\rm vibr} \;=\; \sqrt{3}\omega_o \;=\; \sqrt{\frac{3}{m_{\rm red}\,r_o^3}\,\frac{e^2}{4\pi\epsilon_o}} \;\approx\; 1.66\times10^{18}\;\;{\rm sec}^{-1} \qquad {\rm or} \qquad \hbar\omega_{\rm vibr} \;\approx\; 1.09\;\;{\rm keV} \tag{170}$$

Including $V(r_o)$ and the zero point energy $\frac{1}{2}\hbar\omega_{\rm vibr}$, a DT^+ molecule has a 4.87 keV ground state energy. Using this CM energy and $A_{\rm red} = 6/5$, Eq. (140) gives a transmission probability $T \approx 1.36\times10^{-6}$ upon each encounter with the Coulomb barrier between the D and T. These encounters occur with frequency $f_{\rm vibr} = \omega_{\rm vibr}/2\pi$, yielding a decay rate $f_{\rm vibr}T$ due to fusion, or a half-life

$$\tau_{1/2} \;=\; \frac{\ln 2}{T}\,\frac{2\pi}{\omega_{\rm vibr}} \;\approx\; 2\times10^{-12}\;\;{\rm sec} \tag{171}$$

Muons are produced via an indirect route. When high-energy neutrons collide, a neutron can turn into a proton. To conserve charge, it emits a negative pion, converting some of the initial kinetic energy into the mass of the new π^-. Negative pions convert to muons $\sim$ 85x faster than the muons decay, resulting in a population of useful muons:

$$\mathrm{n} + \mathrm{n} \longrightarrow \mathrm{n} + \mathrm{p} + \pi^- \tag{172}$$

$$\pi^- \overset{26\ \mathrm{nsec}}{\longrightarrow} \mu^- + \overline{\nu_\mu} \tag{173}$$

Plain neutrons are uncharged and therefore difficult to accelerate and control. The next best approach is collisions of neutron-rich nuclei, particularly triton-triton collisions.

In the CM frame, at least the pion rest energy 139 MeV must be supplied to achieve reaction (172). Yet there are several competing processes that consume much of the supplied energy, such as n+n$\rightarrow$n+n+π^0 and collisions involving the proton in T. This raises the net energy required to produce a negative pion in the CM frame by roughly an order of magnitude to at least 1.5 GeV.

Because it is difficult to achieve high densities and hence large reaction rates with colliding T beams, usually a T beam and dense stationary T target are used. From Eq. (123), this lab frame method needs $m_1/m_{\mathrm{red}} = 2$ times as much energy as the CM frame, or > 3 GeV. At typical accelerator efficiencies, producing a muon therefore requires $\sim$ 5 GeV, or $\sim$ 50x more than the muon rest energy of 106 MeV. It would be useful to find ways to lower the required energy, perhaps by exploiting a resonance that greatly promotes reaction (172) over the competing reactions or by somehow making muons directly.

With charge $Z = 2$, α particles bind muons more tightly than D or T do. The measured probability that a μ^- will permanently stick to the α particle after D+T fusion is $P_{\mathrm{stick}} \approx 0.005$. Thus one muon can catalyze $1/P_{\mathrm{stick}} \approx 200$ fusion reactions before binding to an α, where it remains until it decays. With 17.6 MeV of fusion energy produced per reaction, the 200 reactions catalyzed by one muon generate 3.5 GeV total, or $\sim$ 1 GeV after Carnot-limited conversion of the thermal energy to electricity. This is significantly less than the $\sim$ 5 GeV of input energy required to create the muon initially. Operating at temperatures $T > 1$ keV eliminates μ^- sticking to α particles but unfortunately also to deuterons and tritons. Clever ways to selectively unstick muons from α particles, such as electromagnetic waves that resonantly impart just the right energy, are needed.

An initially free muon leads to a desired composite molecule in an experimentally measured time $\tau_{\mathrm{mol}} \sim 5 \times 10^{-9}$ sec for a liquid mixture of equal parts D and T. This is far longer than the actual fusion time calculated in Eq. (171) and limits the rate at which consecutive fusion reactions can be catalyzed (Fig. 24). The time to form a composite molecule can be reduced a few-fold if the initial muon has just the right energy, but this can only be controlled for the first fusion when the muon is injected, not succeeding fusion reactions. Note that if sticking of muons to α particles could be entirely overcome, a muon could produce $\tau_\mu/\tau_{\mathrm{mol}} \approx 440$ fusion reactions before it decayed, only about twice as many as the current limit.

Improvements on the fundamental approach of muon-catalyzed fusion are difficult to find. Reactions other than D+T are considerably more difficult to catalyze. Moreover, massive negative particles other than muons are even harder to produce and generally have shorter lifetimes than muons.

3.3 Fission Reactions

Fission is the separation of a large nucleus into two smaller nuclei, and it can be either spontaneous or induced by neutron absorption [7]. Examples of each type are:

$$\text{Spontaneous:} \quad {}^{254}\text{Fm} \longrightarrow {}^{139}\text{Ba} + {}^{112}\text{Ru} + 3\,\text{n} + \sim 230\ \text{MeV} \tag{174}$$

$$\text{Neutron-induced:} \quad \text{n} + {}^{235}\text{U} \longrightarrow {}^{236}\text{U} \longrightarrow {}^{140}\text{Xe} + {}^{94}\text{Sr} + 2\,\text{n} + \sim 200\ \text{MeV} \tag{175}$$

Figure 25 shows a timescale for the fission process. This section will explain the characteristics of fission, starting with the reaction products and energies. Then it will analyze the potential energy barrier that a nucleus must overcome to fission. Finally it will explain the different ways in which spontaneous and neutron-induced fission overcome this barrier. To accomplish these tasks, we will rely heavily on the liquid drop model of the nucleus, only introducing shell corrections as necessary.

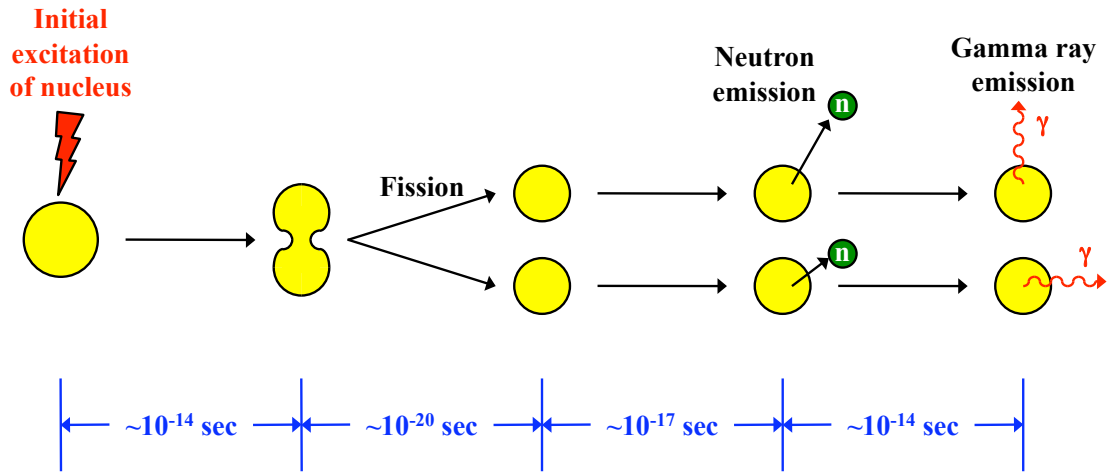

Figure 25. Time scale for events occuring in the fission process.

Fission Energy and Products

Equation (18) shows that as nuclei become larger and larger, the Coulomb repulsion among the protons increases rapidly, $E_{\text{Coulomb}} \propto Z^2/A^{1/3} \propto A^{5/3}$ (recall that $Z \sim 0.4A$ for large nuclei). This is the fundamental cause of fission, since division of a large nucleus into two smaller nuclei greatly lowers this energy and hence its contribution to the total mass. On the other hand, fission increases the nuclear surface area and thus the mass contribution of the surface term E_{surface} from Eq. (18). The relative values of these competing effects determine whether fission can occur; the other terms in the mass formula are relatively unaffected by fission. The energy ΔE released by a nucleus with given values of A and Z which fissions into two equal fragments with $A/2$ and $Z/2$ is

$$\begin{aligned} \Delta E &= \left[M(A,Z) - 2M\left(\frac{A}{2},\frac{Z}{2}\right)\right]c^2 = 0.7\frac{Z^2}{A^{1/3}}\left(1-\frac{1}{2^{2/3}}\right) + 17A^{2/3}\left(1-2^{1/3}\right)\ \text{MeV} \\ &= 0.26A^{2/3}\left(\frac{Z^2}{A}-17\right)\ \text{MeV} \end{aligned} \tag{176}$$

The parameter Z^2/A, arising from the ratio between the Coulomb and surface contributions to nuclear mass, is very important for fission. It increases roughly linearly with atomic number ($Z^2/A \sim 0.4Z$ for $Z/A \sim 0.4$). From Eq. (176), elements with $Z^2/A > 17$, or equivalently $Z \geq 42$, can undergo fission with a net release of energy. For uranium with $A = 236$ and $Z^2/A \approx 36$, Eq. (176) predicts an energy release $\Delta E \approx 190$ MeV. This is very close to the actual value in Eq. (175), even though the two fission fragments do not have equal sizes as assumed in Eq. (176).

Uranium actually fissions into a light fragment with mass number $A_1 \sim 95$ and a heavy fragment with $A_2 \sim 140$. The sizes of the resulting light and heavy fragments vary somewhat, creating a double-peaked mass distribution [Fig. 26(a)] which is difficult to fully explain even with complex computer models. However, an important key is that the doubly magic nucleus with $Z = 50$ and $N = 82$ occurs at the lower edge of the heavy fragment mass range. During fission, it is energetically preferable to form this doubly magic nucleus, or this nucleus with a few extra nucleons added on. The remainder of the original nucleus becomes the light fragment. As further proof of this principle, Fig. 26(b) shows that for different masses of the fissioning nucleus, the heavy fragment mass peak remains essentially fixed (especially at its lower end near the doubly magic numbers). The light peak is left to shift with the changes in total mass. If there is very little energy initially put into the fission reaction, the trough between the light and heavy mass peaks is quite deep. Yet as the input energy increases, the trough becomes less and less deep [Fig 26(c)]; the fissioning nucleus becomes able to fall into almost any final state, not just the energetically lowest ones.

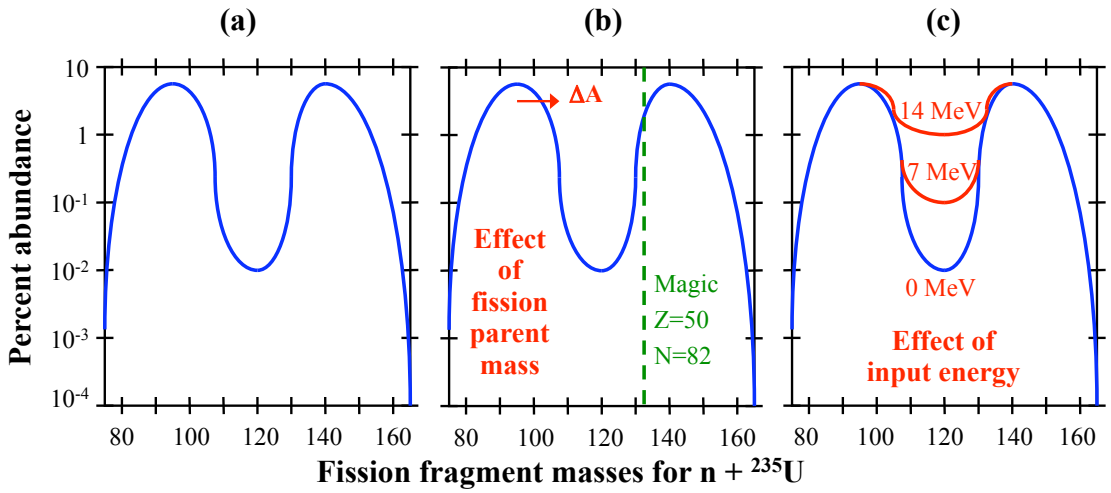

Figure 26. Mass distributions of nuclear fragments resulting from fission. **(a)** Low-energy neutron-induced fission of ^{235}U. **(b)** Effect of increasing the initial mass of the nucleus undergoing fission by ΔA. **(c)** Effect of input energy on neutron-induced ^{235}U fission.

Most of the energy released by fission appears as kinetic energy of the light and heavy fragments. For fission of ^{235}U, approximately 168 MeV is released as kinetic energy of the fission fragments. Using Eq. (139), the light fragment thus has an average energy $(140/235) \times 168$ MeV $=$ 100 MeV, while the heavy fragment has an average energy $(95/235) \times 168$ MeV $=$ 68 MeV. Of course, the observed energies vary about these mean values just as the observed atomic masses vary about the values 95 and 140.

Immediately after fission, each fragment has a great deal of residual energy $E_{\rm res}$. From Eq. (33), this is equivalent to a nuclear temperature $k_B T_{\rm nuc} = \sqrt{E_{\rm res}/a}$, where $a \sim 5/\text{MeV}$ for relatively large nuclei. Roughly half of this residual energy is imparted to neutrons, which then escape from the nuclear potentials of the fragments. This process is analogous to evaporation, in which particles from a hot liquid are ejected into the gaseous state, thereby cooling the remaining liquid. The ejected neutrons are called **prompt neutrons**, because they are emitted very soon after the fission event. For ^{235}U, the prompt neutrons have an average energy $\langle E_n \rangle \approx 2$ MeV. Extending the thermodynamic analogy, the energy spectrum $f(E_n)$ of the emitted neutrons may be approximated as that of a Maxwellian gas (see *Statistical Physics* ?.?),

$$f(E_n) \;=\; \frac{2}{(k_B T_n)^{3/2}} \sqrt{\frac{E_n}{\pi}} \exp\left(-\frac{E_n}{k_B T_n}\right) , \tag{177}$$

where the relation $\langle E_n \rangle = \frac{3}{2} k_B T_n$ gives a neutron temperature of $k_B T_n \approx 1.3$ MeV, which must also be the initial temperature $T_{\rm nuc}$ of the fission fragments that emit the neutrons. More precise expressions for the neutron energy distribution take into account the moving frame of the fission fragments during neutron emission, but Eq. (177) still gives a good idea of the energy distribution. On average roughly 2.5 prompt neutrons are emitted per fission event for uranium or plutonium, making chain reactions possible: one neutron-induced fission produces ~ 2 neutrons and hence two neutron-induced fissions, which cause ~ 4 more fissions, and so forth.

The other half of the energy of the excited fission fragments (~ 7 MeV) is radiated away as gamma rays with an average energy 1 MeV each. Most of the gamma rays are emitted after the prompt neutrons when there is not enough residual energy to liberate another neutron.

As shown by Eq. (20), the most stable heavy isotopes have a lower value of Z/A than the most stable light isotopes. Even after emitting approximately one prompt neutron each, the fission fragments have almost the same Z/A ratio as their parent nucleus [Fig. 27(a)]. Thus the fragments have too many neutrons and too few protons to be stable against β decay at their new mass values. The fragments undergo a series of beta decays, emitting energetic electrons and neutrinos until they arrive at stable Z/A ratios. As the fragments approach the stable values, the half-lives of the decays generally become longer and longer. Examples of these decay chains are:

$$A = 93: \qquad {}_{37}\text{Rb} \xrightarrow{6\ \text{sec}} {}_{38}\text{Sr} \xrightarrow{7\ \text{min}} {}_{39}\text{Y} \xrightarrow{10\ \text{hr}} {}_{40}\text{Zr} \xrightarrow{10^6\ \text{yr}} {}_{41}\text{Nb}\ \text{(stable)} \tag{178}$$

$$A = 140: \qquad {}_{54}\text{Xe} \xrightarrow{16\ \text{sec}} {}_{55}\text{Cs} \xrightarrow{66\ \text{sec}} {}_{56}\text{Ba} \xrightarrow{12.8\ \text{days}} {}_{57}\text{La} \xrightarrow{40\ \text{hr}} {}_{58}\text{Ce}\ \text{(stable)} \tag{179}$$

After a β decay, a fission fragment may be in an excited state of an element in which one of the neutrons has enough energy to escape. Such **delayed neutrons** are emitted long after the fission event, only after one or more β decays. Although there are only $\sim 1/100$ as many delayed neutrons as prompt neutrons, they can be quite significant. As discussed in the fission power summary, balancing a fission reactor so that it needs the delayed neutrons to sustain its chain reaction makes the reactor easier to control, since the reaction rate cannot change very quickly.

Neutron activation within the fission fuel also produces a variety of radioactive actinides. As shown in Fig. 27(b), there are few choices for fissile fuel to control the products. Eliminating non-fuel actinides from fresh fuel would reduce the resulting actinide waste, but at the price of making the fuel a proliferation and criticality hazard and also preventing breeding of new fuel species.

Table 1 lists the average energy breakdowns for neutron-induced fission of ^{235}U and ^{239}Pu, the two nuclei of greatest applied interest.

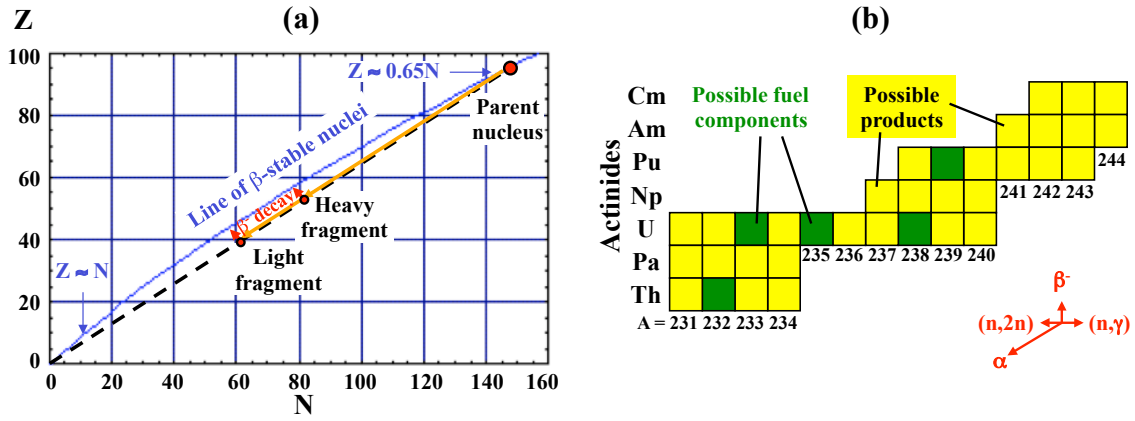

Figure 27. Products of fission reactions are inherently radioactive. **(a)** Fission fragments must be β^- emitters. **(b)** Neutron activation within the fission fuel produces a variety of actinides. Red arrows indicate the direction in which one nucleus is transmuted into another via (n,γ) neutron capture, (n,2n) neutron loss, β^- decay, and α decay.

Product	^{235}**U**	^{239}**Pu**
Light fragment	99.8	101.8
Heavy fragment	68.4	73.2
Prompt neutrons	4.8	5.8
Prompt gamma	7.5	7
β from fragments	7.8	8
γ from fragments	6.8	6.2
Neutrinos	12	12
Total	207 MeV	214 MeV

Table 1. Average energy breakdowns (in MeV) for neutron-induced fission of ^{235}U and ^{239}Pu.

Fission Barrier

The potential energy of a nucleus varies during the fission process, primarily because of changes in the Coulomb and surface energy contributions. For a typical heavy nucleus [Fig. 28], the potential has a local minimum for the undeformed nucleus, increases as the nucleus stretches and divides into two nuclei, and then decreases greatly as the daughter nuclei separate due to their mutual Coulomb repulsion. In spontaneous and neutron-induced fission, this potential energy **fission barrier** is overcome in different ways. Calculating the rates of either type of fission requires information about the precise shape of the barrier, which fortunately can be obtained from simple models.

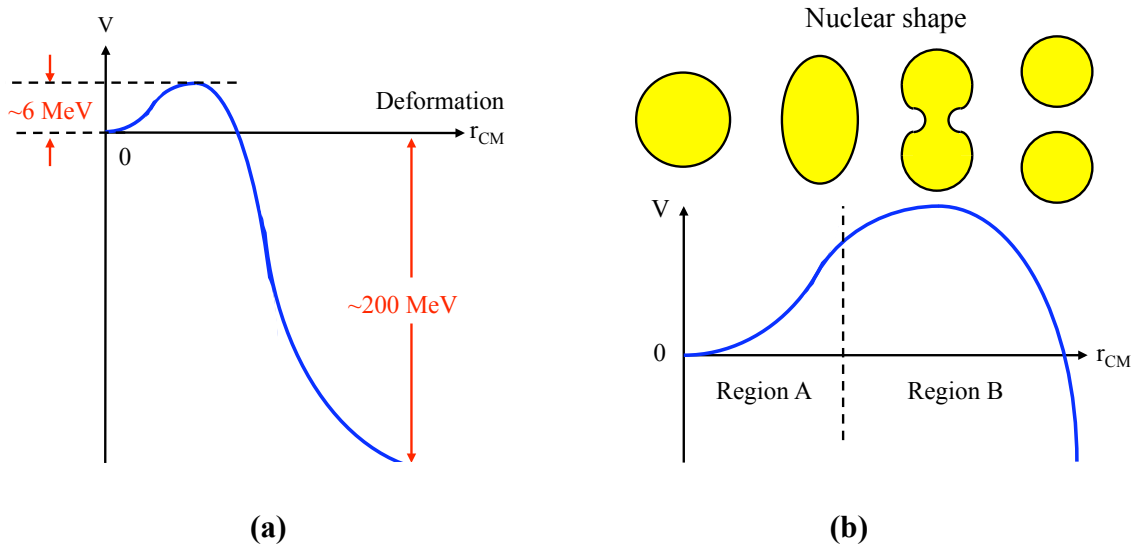

Figure 28. Potential energy V of a nucleus fissioning into two fragments as a function of the separation rCM between the fission fragments. (a) The complete function $V(r_{CM})$ shows the local energy minimum of the intact nucleus, the potential barrier to fission, and the large energy release that accompanies fission. **(b)** The fission barrier is shown in more detail.

Region A of the potential in Fig. 28(b) covers the nucleus in its undeformed state and as it stretches to initiate fission. To account for elongation, one models the nucleus as an ellipsoid with eccentricity

$$\epsilon \equiv \frac{\Delta R}{R} = \frac{(\Delta R)_{\text{fm}}}{1.2A^{1/3}} \tag{180}$$

where ΔR is the departure of the radius from that of a spherical nucleus of comparable volume, as measured in the direction of elongation. In other words, the ellipsoidal nucleus has a semimajor axis $a = R(1+\epsilon)$. To preserve the same volume, the cross-sectional area perpendicular to the semimajor axis must decrease by this same factor $(1+\epsilon)$. Thus the semiminor axis is $b = R/\sqrt{1+\epsilon}$.

Changing a spherical nucleus to an ellipsoidal one generally alters only the surface and Colomb contributions to the nuclear binding energy. Taking the terms of lowest order in ϵ, one finds [1]:

$$E_s \approx 17A^{2/3}\left(1+\frac{2}{5}\epsilon^2\right) \text{ MeV} \qquad E_c \approx 0.7\frac{Z^2}{A^{1/3}}\left(1-\frac{1}{5}\epsilon^2\right) \text{ MeV} \tag{181}$$

Using Eqs. (181) and (180), the net potential energy change upon elongation of the nucleus is

$$\Delta V \;=\; \Delta E_s + \Delta E_c \;=\; \epsilon^2 \left(\frac{2}{5} 17 A^{2/3} - \frac{1}{5} 0.7 \frac{Z^2}{A^{1/3}} \right) \text{ MeV} \;=\; 6.8 \epsilon^2 A^{2/3} \left(1 - \frac{Z^2/A}{49} \right) \text{ MeV} \quad (182)$$

$$= \; 4.72 \left(1 - \frac{Z^2/A}{49} \right) (\Delta R)^2_{\text{fm}} \text{ MeV} \quad (183)$$

The parameter Z^2/A appears again. For $Z^2/A < 49$, elongation increases the potential energy of the nucleus, erecting a barrier on the path to fission. Yet for $Z^2/A > 49$, elongation is energetically favorable and there is no barrier to fission. Using $Z/A \approx 0.39$, this means elements with $Z \approx 125$ or greater would immediately undergo spontaneous fission. Together with instability to α decay (Section 2.1), this explains why the periodic table of the elements does not extend into this region.

It is useful to use center-of-mass coordinates to describe the two separating fission fragments. In such coordinates, one fragment remains fixed at the origin and hence may be regarded as infinitely massive. The other fragment behaves as if it has a reduced mass m_r. Assuming for simplicity that a nucleus with A nucleons is separating into two equal fission fragments, the reduced mass is

$$m_r \;\equiv\; \frac{\left(\frac{1}{2}A\right)\left(\frac{1}{2}A\right)}{\frac{1}{2}A + \frac{1}{2}A} \, 931.5 \;\; \frac{\text{MeV}}{c^2} \;=\; \frac{1}{4} \, A \, 931.5 \;\; \frac{\text{MeV}}{c^2} \quad (184)$$

The asymmetric sizes of fragments actually obtained from uranium and plutonium only affect the reduced mass by a few percent and will be ignored here.

In center-of-mass coordinates, the radial distance from the center of the fragment at the origin to the center of the other fragment is approximately

$$r_{CM} \;\approx\; 2 \, \Delta R \;=\; 2.4 A^{1/3} \epsilon \text{ fm} \quad (185)$$

The energy change due to elongation of the nucleus may be written in the form of a simple harmonic oscillator potential in the center-of-mass frame:

$$\Delta V \;=\; \frac{1}{2} \, m_r \, \frac{(\hbar \omega_{\text{vibr}})^2}{\hbar^2} \, r^2_{CM} \;=\; \frac{931.5}{2} \, A \, \frac{(\hbar \omega_{\text{vibr}})^2_{\text{MeV}}}{(\hbar c)^2_{\text{MeV·fm}}} \, (\Delta R)^2_{\text{fm}} \text{ MeV} \quad (186)$$

where the nucleus vibrates about the equilibrium spherical shape with angular frequency ω_{vibr}, repeatedly going from prolate to spherical to oblate and back again like a vibrating drop of liquid.

Setting Eq. (186) equal to Eq. (183), using $\hbar c \approx 197.3$ MeV·fm, and solving for $\hbar \omega_{\text{vibr}}$ yields

$$\hbar \omega_{\text{vibr}} \;\approx\; 20 \sqrt{\frac{1}{A} \left(1 - \frac{Z^2/A}{49} \right)} \text{ MeV} \quad (187)$$

For uranium and plutonium isotopes, this value is $\hbar \omega_{\text{vibr}} \approx 0.7$ MeV. Of course, treating a continuously connected, vibrating nucleus like two oscillating fragments is a crude approximation. More accurate calculations have the same functional dependence as Eq. (187) but give approximately 1 MeV as the vibrational energy of heavy elements [3, 7]. The corresponding vibration time is

$$\tau_{\text{vibr}} \;=\; \frac{2\pi}{\omega_{\text{vibr}}} \;\approx\; 4 \times 10^{-21} \text{ sec} \qquad \text{for heavy nuclei} \quad (188)$$

Even a nucleus in the ground state is slightly above the bottom of the well in region A because it has a harmonic oscillator zero point energy $\frac{1}{2}\hbar\omega_{\text{vibr}} \approx 0.5$ MeV. This energy is generally much smaller than the barrier energy and can simply be absorbed into the definition of the barrier height.

In region B of Fig. 28(b), the potential reaches a maximum and then declines sharply due to terms of higher order in ϵ not included in Eqs. (181) and (182). Physically, that is the point at which the nuclear matter finds it easier to go forward and become two nuclei than to return to being a single undeformed nucleus. Because of its shape in Fig. 28, this peak is called the **saddle point**.

For nuclei of different sizes, the saddle point in the potential energy occurs at different points on the path to fission [Fig. 29(a)]. For a nucleus with the critical value $Z^2/A = 49$, the undeformed spherical shape with $\epsilon = 0$ is at the saddle point–the path to fission is all downhill from there. On the other hand, a nucleus with a very small fissionability parameter, $Z^2/A \ll 49$, must be pulled almost completely in two before it prefers to fission instead of going back. (**Scission** is when the fragments actually separate.) While this state cannot really be described by an ellipsoidal shape, it is certainly equivalent to a large departure from sphericity: $\Delta R \approx R$, or $\epsilon \approx 1$. Thus the saddle point may be said to occur at some critical eccentricity $\epsilon_{\rm crit}$ that varies with the fissionability parameter:

$$\epsilon_{\rm crit} \approx 1.15\left(1 - \frac{Z^2/A}{49}\right) \tag{189}$$

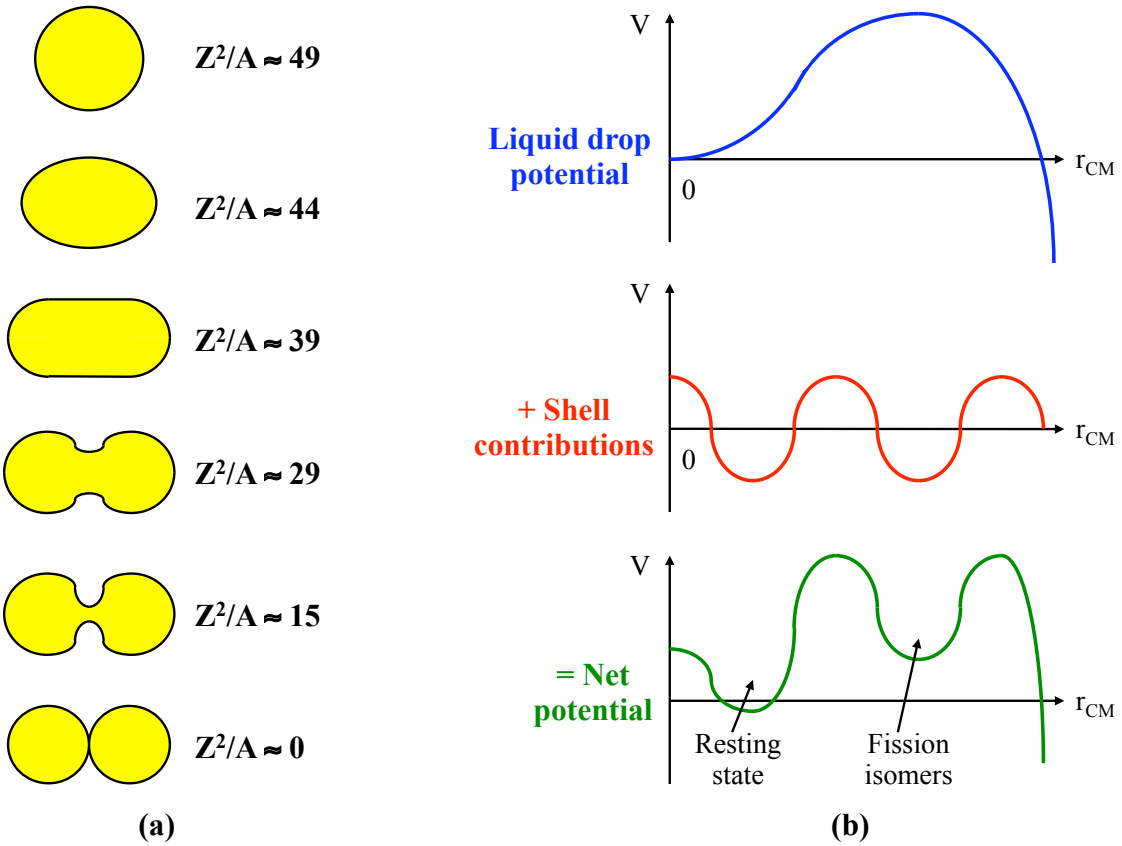

Figure 29. More detailed depiction of nuclear deformations and potential barrier en route to fission. **(a)** Nuclear shapes on path to fission, showing where saddle point occurs for different values of Z^2/A. **(b)** Liquid drop $V(r)$ + shell $V(r)$ = double barrier with peaks V_{B1} and V_{B2}. Fission isomers are nuclei that are temporarily trapped in energetic states between the two peaks and hence are more likely to undergo fission, since they need only tunnel through the final peak.

From the physical arguments above, the coefficient in Eq. (189) should be ~ 1; 1.15 gives the best agreement with experiments. Inserting Eq. (189) into Eq. (182) yields the peak potential energy

$$V_B \;\approx\; 9A^{2/3}\left(1-\frac{Z^2/A}{49}\right)^3 \;\text{MeV} \;+\; (\Delta V_B)_{\text{other}} \tag{190}$$

An extra term $(\Delta V_B)_{\text{other}}$ has been added to account for pairing effects. The pairing energy between nucleons varies slightly as a nucleus is distorted, making the barrier $\sim$0.4 MeV higher for odd-odd nuclei, unchanged for even-odd nuclei, and $\sim$0.4 MeV lower for even-even nuclei. Equation (190) holds primarily for values of $\frac{Z^2/A}{49}$ greater than 2/3 or so, because that is when the underlying assumption of an ellipsoidal saddle-point shape is most valid. The barrier height is approximately 6 MeV for ^{235}U and rapidly decreases for higher elements.

The region around the saddle point may be modeled as an inverted parabola and written like an upside-down simple harmonic oscillator potential. The peak value V_B occurs at some separation $r_{CM} = r_B$ between the two fission fragments. ω_B would be the oscillation frequency within the harmonic oscillator potential if it were upright. As it is, ω_B defines the barrier curvature, or more importantly the barrier thickness; a parabolic barrier with a smaller ω_B curves less rapidly and hence is thicker and more difficult to penetrate. Using these definitions and $\rho \equiv r_{CM} - r_B$, the radial position relative to the fission barrier peak, the barrier energy minus the initial energy E is

$$V(r_{CM}) - E \;=\; V(r_{CM}) - V(0) - \frac{1}{2}\hbar\omega_{\text{vibr}} \;=\; V_B - \frac{1}{2}m_r\omega_B^2(r_{CM}-r_B)^2 \;=\; V_B - \frac{1}{2}m_r\omega_B^2\rho^2 \tag{191}$$

Using this parabolic approximation, the potential barrier exceeds the initial energy in the region

$$-\rho_o < \rho < +\rho_o, \qquad \text{where} \quad \rho_o \;\equiv\; \sqrt{\frac{2V_B}{m_r\omega_B^2}} \tag{192}$$

The half-width ρ_o of the fission barrier may be estimated from the separation between the centers of the fission fragments at the saddle point, $r_{CM} = r_B$. Inserting Eq. (189) into Eq. (185) yields

$$\rho_o \;\approx\; r_B \;-0 \;\approx\; 2.8\,A^{1/3}\left(1-\frac{Z^2/A}{49}\right) \;\text{fm} \tag{193}$$

This half-width is approximately 5 fm for uranium and plutonium.

By convention, the barrier curvature is usually multiplied by $\hbar$ and written as an energy. Using Eq. (192) and (184), this barrier curvature energy is

$$\hbar\omega_B \;=\; \sqrt{\frac{2V_B}{m_r}}\,\frac{\hbar}{\rho_o} \;\approx\; \frac{18.3}{\rho_{o,\,\text{fm}}}\sqrt{\frac{V_{B,\,\text{MeV}}}{A}} \;\text{MeV} \tag{194}$$

Typical values of $\rho_o \approx 5$ fm, $V_B \approx 6$ MeV, and $A \sim 238$ for uranium and plutonium produce a barrier curvature $\hbar\omega_B \approx 0.6$ MeV. Indeed, the barrier curvatures for heavy nuclei are ~ 0.5 MeV.

Shell effects alter the potential somewhat from what has been calculated so far. As a nucleus becomes more and more distended, energy shells close, open, and close again, producing an energy contribution that is a periodic function of r_{CM} [Fig. 29(b)]. As discussed in Section 1.4, shell effects typically contribute a few hundredths of an MeV per nucleon, amounting to around 3.5 MeV for uranium and plutonium. Since this is comparable to the barrier height, adding the shell contribution to the single-humped barrier obtained from the liquid drop model produces a double-humped barrier [Fig. 29(b)]. These shell effects also shift the resting state of large nuclei from spherical ($r_{CM} = 0$) to somewhat distorted ($r_{CM} \neq 0$), as has already been mentioned in Section 1.4.

The consequences of the double hump will be explored soon, but in brief, they are not so drastic that we must throw out our previous calculations of the barrier. Either the calculations can be extended to include the two humps explicitly, or the parameters can be modified somewhat to treat the two peaks together as effectively one hump.

Spontaneous Fission

During spontaneous fission, the fragments must tunnel through the region where $V > E$ from Eq. (191). As with quantum tunneling in α decay, the WKB approximation from Eq. (76) can be used to find the transmission probability T through the fission barrier:

$$\begin{aligned} T &= \exp\left\{-\frac{2}{\hbar}\int_{-\rho_o}^{\rho_o} d\rho\sqrt{2m_r[V(\rho)-E]}\right\} = \exp\left\{-\frac{4}{\hbar}\int_{0}^{\rho_o} d\rho\sqrt{2m_r[V(\rho)-E]}\right\} \quad \text{(symmetrical barrier)} \\ &= \exp\left(-\frac{4m_r\omega_B}{\hbar}\int_0^{\rho_o} d\rho\sqrt{\rho_o^2-\rho^2}\right) = \exp\left(-\frac{4m_r\omega_B}{\hbar}\,\frac{\pi\rho_o^2}{4}\right) \\ &= \exp\left[-\frac{2\pi(V_B-E)}{\hbar\omega_B}\right] \end{aligned} \tag{195}$$

The WKB approximation and hence Eq. (195) are only valid for particle energies significantly below the barrier peak, or for $\frac{2\pi(V_B-E)}{\hbar\omega_B} \gg 1$. To ensure that the transmission probability T goes to 1 for energies far above the barrier peak ($\frac{2\pi(V_B-E)}{\hbar\omega_B} \ll 1$), Eq. (195) can be modified:

$$T = \frac{1}{\exp[2\pi(V_B-E)/\hbar\omega_B]+1} \tag{196}$$

For all but fairly short-lived elements, $2\pi V_B/\hbar\omega_B \gg 1$ is valid and Eq. (195) may be used.

As noted earlier, a large nucleus vibrates with an energy $\hbar\omega_{\text{vibr}} \sim 1$ MeV. Thus the frequency with which the nucleus becomes distorted and encounters the fission barrier is $f = \omega_{\text{vibr}}/2\pi$. By analogy with α decay, the half-life due to spontaneous fission may be written in terms of the frequency of encounters with the barrier and the probability T of transmission through the barrier:

$$\begin{aligned} \tau_{1/2} &= \frac{\ln 2}{T}\,\frac{2\pi}{\omega_{\text{vibr}}} = 2.8\times10^{-21}\exp\left(\frac{2\pi V_B}{\hbar\omega_B}\right)\ \text{sec} \\ &\approx 2.8\times10^{-21}\exp\left\{\frac{2\pi}{(\hbar\omega_B)_{\text{MeV}}}\left[9A^{2/3}\left(1-\frac{Z^2/A}{49}\right)^3+(\Delta V_B)_{\text{other}}\right]\right\}\ \text{sec} \end{aligned} \tag{197}$$

where Eq. (190) was used; $(\Delta V_B)_{\text{other}}$ can include shell as well as pairing effects [Fig. 30(a)]. Figure 30(b) compares measured spontaneous fission half-lives to Eq. (197) with $\hbar\omega_B \approx 0.42$ MeV and $(\Delta V_B)_{\text{other}}$ =+/-0.4 MeV for odd-odd/even-even nuclei. For elements like uranium and plutonium, the half-life for α decay is much shorter and dominates over spontaneous fission (e.g., $\tau_{1/2,\,\alpha} \approx 7000$ years vs. $\tau_{1/2,\,\text{fission}} \approx 2\times10^{11}$ years for ^{240}Pu). However, spontaneous fission surpasses α decay as the dominant decay mode for many nuclei with $Z^2/A > 39$, or $Z > 100$. Even though the fission barrier does not cease to exist until $Z \approx 125$ as found earlier, tunneling of fission fragments or α particles through the potential barrier effectively ends the periodic table by $Z \approx 108$.

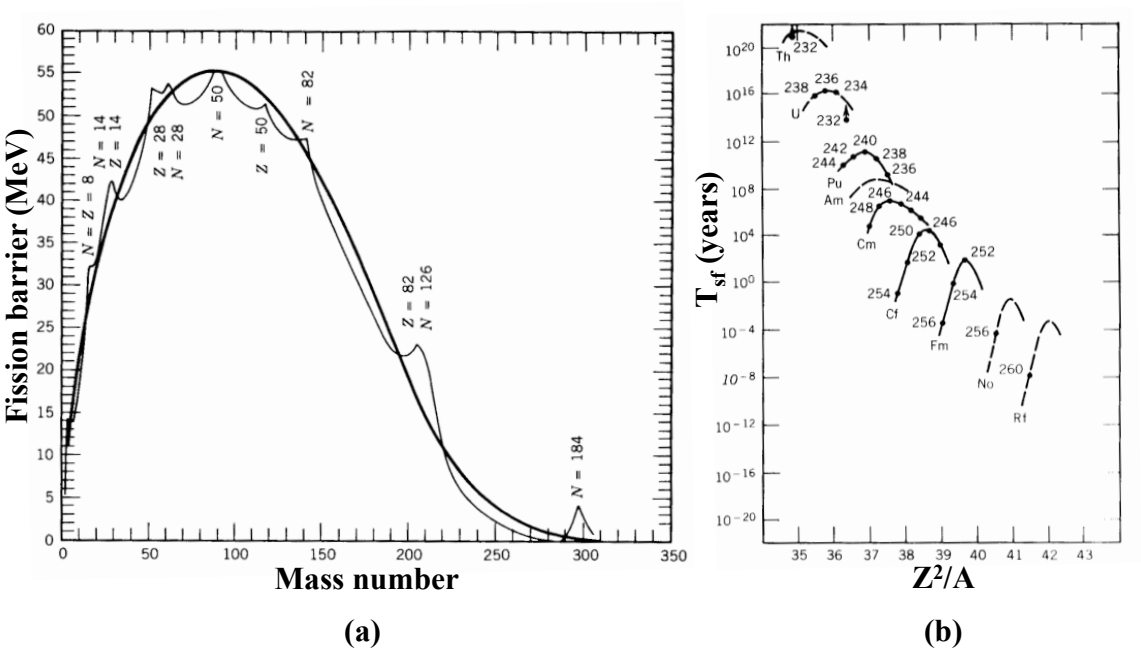

Figure 30. Fissionability of different nuclei. **(a)** Fission barrier height V_B for the most stable isobar of each mass number A. The darker curve is based on the liquid drop model from Eq. (190), while the lighter curve includes shell corrections. **(b)** Spontaneous fission half-life $\tau_{1/2}$ vs. fissionability parameter Z^2/A for different nuclei.

If it is desired to explicitly include the two humps of the barrier, they may be modeled as two inverted parabolas with respective peaks V_{B1} and V_{B2} and curvatures ω_{B1} and ω_{B2}. Assuming the energy is significantly below the peaks and neglecting resonance effects between the humps, the net transmission probability is simply the product of probabilities like Eq. (195) for each hump:

$$T \;=\; \exp\left[-\frac{2\pi(V_{B1}-E)}{\hbar\omega_{B1}} \;-\; \frac{2\pi(V_{B2}-E)}{\hbar\omega_{B2}}\right] \tag{198}$$

One consequence of the double-humped barrier is that nuclei can become temporarily stuck between the humps [Fig. 29(b)]. Nuclei in this state are very distended, with more energy than the undistorted ground state but not enough to go over the final fission barrier. The lifetime of such states is limited by tunneling back through the first hump to the resting state (releasing the excess energy as gamma rays) or tunneling through the second hump to undergo fission. These **fission isomer** states are halfway toward fission and thus more likely to fission than the ground state.

Neutron-Induced Fission

Fission reactors and bombs use the neutrons emitted by one fission to produce more fission events, thereby creating a chain reaction. Such applications require information about the number and energies of neutrons emitted in fission, which we have already examined. They also require information about neutron-induced fission reaction cross sections, which we will now investigate.

Unlike for charged particles in fusion reactions, there is no Coulomb energy barrier for a neutron to enter a nucleus. When a neutron falls into a nuclear potential well, its energy increases by an amount equal to the binding energy of an additional nucleon for that nucleus, typically several MeV. For example, Eq. (19) shows that a neutron added to ^{235}U to form ^{236}U gains an energy

$$S_n\left(^{236}\mathrm{U}\right) \;=\; \left[M\left(^{235}\mathrm{U}\right) - M\left(^{236}\mathrm{U}\right)\right]c^2 \;=\; 6.5\ \mathrm{MeV} \tag{199}$$

This is the same as the energy S_n required to separate one neutron from ^{236}U. Since this energy is larger than the fission barrier height $V_B = 6.2$ MeV from Eq. (190) for the compound nucleus ^{236}U, even a neutron with zero initial energy can cause ^{235}U to immediately undergo fission [Fig. 31(a)]. In contrast, a neutron added to ^{238}U to form ^{239}U gains an energy

$$S_n\left(^{239}\mathrm{U}\right) \;=\; \left[M\left(^{238}\mathrm{U}\right) - M\left(^{239}\mathrm{U}\right)\right]c^2 \;=\; 4.8\ \mathrm{MeV} \tag{200}$$

This energy is ~ 1.8 MeV less than the barrier height $V_B = 6.6$ MeV of ^{239}U from Eq. (190), so neutrons bombarding ^{238}U must have an energy greater than a threshold energy ~ 1.8 MeV to trigger fission [Fig. 31(b)]. The fundamental cause of this difference between ^{235}U and ^{238}U is the pairing energy difference between even-even and even-odd nuclei. Using Eq. (19), whereas neutron absorption changes the even-odd nucleus ^{235}U to the even-even nucleus ^{236}U and hence releases an extra ~ 0.6 MeV, it changes the even-even nucleus ^{238}U to an even-odd nucleus ^{239}U and thus consumes ~ 0.6 MeV. This accounts for most of the difference between neutron addition energies in the two different uranium isotopes. Moreover, from Eq. (190), an even-even compound nucleus like ^{236}U has a fission barrier which is ~ 0.4 MeV lower than that of an even-odd but otherwise comparable nucleus, such as ^{239}U.

With an extra pair of neutrons and an extra pair of protons, ^{239}Pu closely resembles ^{235}U. $S_n \approx 6.5$ MeV is gained by adding a neutron to ^{239}Pu, whereas the fission barrier for ^{240}Pu is only $V_B = 6.0$ MeV. Therefore ^{239}Pu can also be fissioned by neutrons with essentially zero initial energy.

From Eq. (33) with $a \sim 5$/MeV for heavy nuclei, exciting a uranium or plutonium nucleus by $S_n = 6.5$ MeV yields an effective nuclear temperature of $k_B T_{\mathrm{nuc}} = \sqrt{S_n/a} \sim 1.1$ MeV. This temperature of the initial excited nucleus is comparable to the ~ 1.3 MeV temperature of the resulting fission fragments as found from the prompt neutron energy spectrum [Eq. (177)].

Calculating neutron-induced fission cross sections for ^{235}U and ^{239}Pu requires several parameters. As just shown, neutron absorption excites these nuclei by an energy $S_n \approx 6.5$ MeV. Equation (37) predicted that the average spacing between the energy levels of such highly excited nuclei is $D \sim 1$ eV. This agrees with the measured values $D = 0.6$ eV for ^{235}U+n and $D = 2.3$ eV for ^{239}Pu+n.

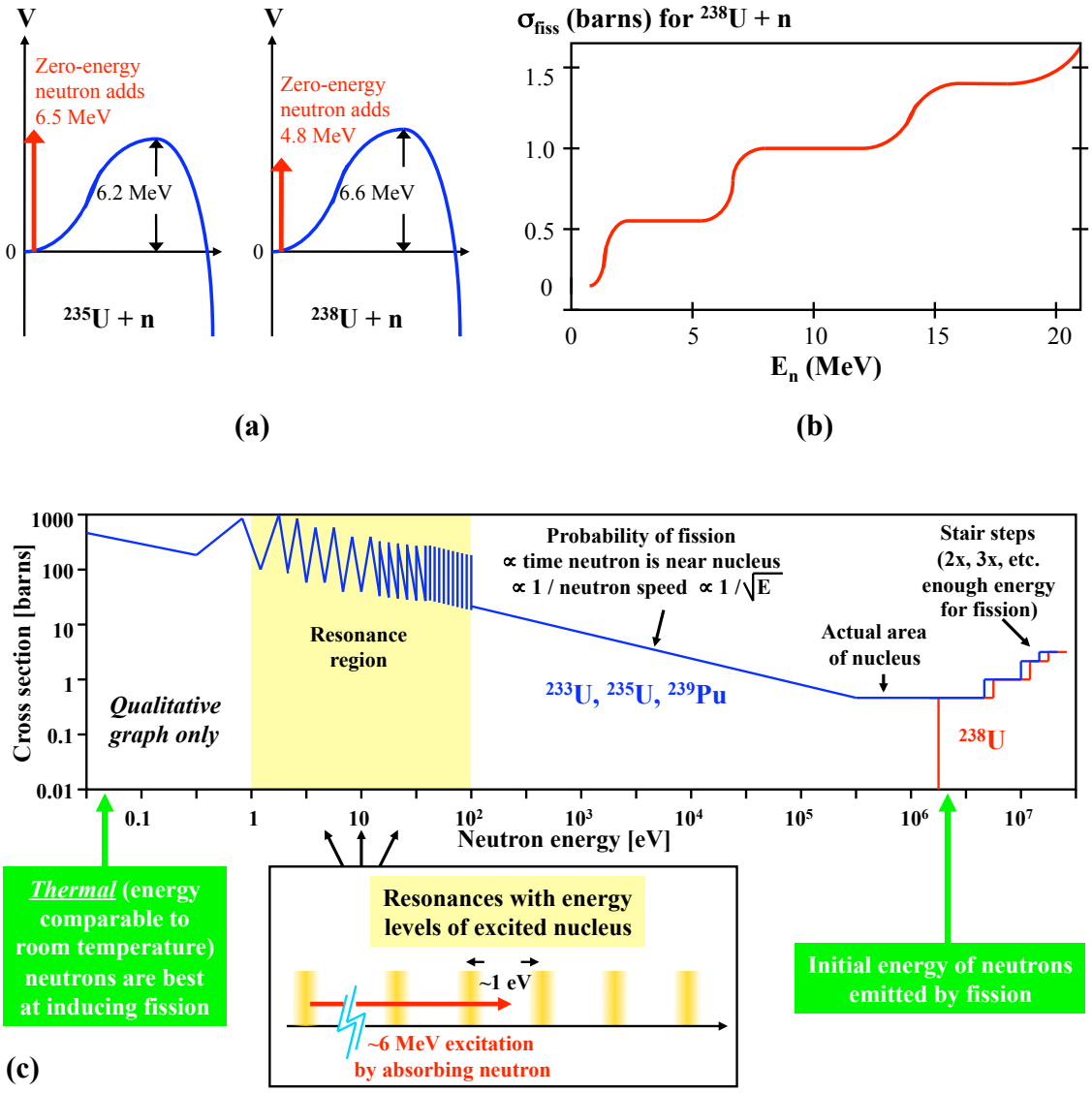

Figure 31. Neutron-induced fission. **(a)** Fission barrier height V_B and neutron addition energy S_n for ^{235}U and ^{238}U isotopes. **(b)** Neutron-induced fission cross section σ_{fiss} for ^{238}U. **(c)** Neutron-induced fission cross section σ_{fiss} for ^{233}U, ^{235}U, ^{239}Pu, and ^{238}U.

Fission cross sections depend on the initial neutron energy E_n. After gaining the absorption energy S_n, a neutron with initial energy $E_n \approx 0$ eV is at some random point between the excited energy levels of the compound nucleus [Fig. 31(c) bottom center]. The first resonance that can be excited by neutron absorption occurs at an initial neutron energy E_{r1} that is less than the spacing D between adjacent levels ($E_{r1} \approx 0.29$ eV for ^{235}U and ^{239}Pu). Additional resonances occur roughly at multiples of D beyond that, at $E_n \approx E_{r1} + nD$ eV, where n is an integer. Of course, this is a crude approximation, since D is only the *average* spacing and the actual spacing can vary somewhat between different levels. It becomes difficult to resolve resonances at energies $E > 100$ eV because their widths correspond to very small fractions of the bombarding neutron energy.

Using Eq. (129), the width for the fission process is

$$\Gamma_f \;=\; T_f \frac{D}{2\pi} \;\approx\; \frac{D}{2\pi} \tag{201}$$

since the transmission probability through the fission barrier [Eq. (196)] is $T_f \approx 1$ when the energy is ~ 0.3 MeV above the barrier. The quoted value of $D \approx 0.6$ eV for ^{235}U+n gives a fission width $\Gamma_f \approx 0.1$ eV. Using Eq. (128), the corresponding time τ_f required for fission is roughly

$$\tau_f \;\approx\; \frac{\hbar}{\Gamma_f} \;\approx\; 7 \times 10^{-15} \text{ sec} \tag{202}$$

This result confirms the fission time from Fig. 25. The fission time is $\sim 10^7$ longer than the period of an individual nucleon as found from Eq. (41), or $\sim 10^6$ longer than the period for nuclear vibrations from Eq. (188). Physically, the fission time is so long because it takes a while for the energy of the added neutron to be redistributed within the nucleus in the right way to cause fission.

From Eq. (130), the transmission probability for a neutron entering or leaving the nucleus is

$$T_n \;\approx\; 4\frac{k_{n,\text{ outside}}}{k_{n,\text{ inside}}} \;=\; 4\sqrt{\frac{E_{n,\text{ outside}}}{E_{n,\text{ inside}}}} \tag{203}$$

if the neutron's energies outside and inside the nucleus are such that $E_{n,\text{ outside}} \ll E_{n,\text{ inside}}$.

Using Eqs. (129) and (203), the width for neutron emission or absorption is

$$\Gamma_n \;=\; T_n \frac{D}{2\pi} \;\approx\; \frac{2}{\pi} D \sqrt{\frac{E_{n,\text{ outside}}}{E_{n,\text{ inside}}}} \tag{204}$$

Note that $\Gamma_n \ll \Gamma_f$ because $E_{n,\text{ outside}} \ll E_{n,\text{ inside}}$. When ^{235}U or ^{239}Pu absorbs a neutron, fission is much more probable than re-emission of the neutron.

The fission cross section [Fig. 31(c)] is found from Eqs. (134), (201), and (204). The spin factor G_s differs among the resonances but for simplicity is assumed to have a uniform value $G_s \approx 1/2$. Using $E \ll E_r$ and $E_r \gg \Gamma_f \gg \Gamma_n$, the cross section in the energy range below the resonances is

$$\begin{aligned}
\sigma_{nf} \;&=\; \frac{\pi}{k^2} \sum_{\text{resonances}} G_s \frac{\Gamma_n \Gamma_f}{(E-E_r)^2 + \frac{1}{4}(\Gamma_f + \Gamma_n)^2} \;\approx\; \frac{\pi}{k^2} \sum_{\text{resonances}} G_s \frac{\Gamma_n \Gamma_f}{E_r^2} \\
&\approx\; \frac{\pi}{k^2} \sqrt{\frac{E_{n,\text{ outside}}}{E_{n,\text{ inside}}}} \frac{D^2}{2\pi^2} \left[\frac{1}{E_{r1}^2} + \frac{1}{(E_{r1}+D)^2} + \frac{1}{(E_{r1}+2D)^2} + ... \right] \\
&\approx\; \frac{33\, D^2}{\sqrt{S_{n,\text{ MeV}}}\sqrt{E_{n,\text{ eV}}}} \left[\frac{1}{E_{r1}^2} + \frac{1}{(E_{r1}+D)^2} + \frac{1}{(E_{r1}+2D)^2} + ... \right] \text{ barn}
\end{aligned} \tag{205}$$

Inserting $S_n = 6.5$ MeV, $E_{r1} = 0.29$ eV, and $D = 0.6$ eV (for ^{235}U) or 2.3 eV (for ^{239}Pu) yields

$$\sigma_{nf} \;\approx\; \frac{85}{\sqrt{E_{n,\text{ eV}}}} \text{ barn} \quad \text{for } ^{235}\text{U} \qquad\qquad \sigma_{nf} \;\approx\; \frac{140}{\sqrt{E_{n,\text{ eV}}}} \text{ barn} \quad \text{for } ^{239}\text{Pu} \tag{206}$$

Fission cross sections are famed for being inversely proportional to the neutron velocity v_n, $\sigma_{nf} \propto 1/\sqrt{E_n} \propto 1/v_n$. Physically, this just means that the reaction cross section is proportional to the time a neutron spends near a nucleus. The constants in Eq. (206) are not actually constant but rather may vary by $\sim 20\%$ over the energy range. Of great importance for fission reactors are the thermal (room-temperature, $E = 0.025$ eV) values, 584 barns for ^{235}U and 742 barns for ^{239}Pu.

Neglecting contributions from other resonances, Eq. (134) gives the cross section at a resonance peak ($E - E_r = 0$, with $G_s \approx 1/2$, $\Gamma_f \gg \Gamma_n$, and $S_n = 6.5$ MeV for ^{235}U+n and ^{239}Pu+n):

$$\begin{aligned}
(\sigma_{nf})_{\text{peaks}} \;&=\; \frac{\pi}{k^2} G_s \frac{4\Gamma_n \Gamma_f}{(\Gamma_f + \Gamma_n)^2} \;\approx\; 4\frac{\pi}{k^2} g_s \frac{\Gamma_n}{\Gamma_f} \;\approx\; 8\frac{\pi}{k^2} \sqrt{\frac{E_{n,\text{ outside}}}{E_{n,\text{ inside}}}} \\
&\approx\; \frac{5200}{\sqrt{S_{n,\text{ MeV}}}\sqrt{E_{n,\text{ eV}}}} \text{ barn} \;\approx\; \frac{2000}{\sqrt{E_{n,\text{ eV}}}} \text{ barn}
\end{aligned} \tag{207}$$

Thus the resonance peaks also vary as $1/v_n$, although in reality there is some fluctuation around this trend since different resonances may have somewhat different values of G_s and other parameters.

Above $\sim$ 100 eV the resonances tend to blur together, producing an average fission cross section that may be found from Eqs. (135) and (204) with $G_s \approx 1/2$, $\Gamma_f \gg \Gamma_n$, and $S_n = 6.5$ MeV:

$$\begin{aligned} \langle \sigma_{nf} \rangle &= \frac{\pi}{k^2} \left\langle G_s \frac{\Gamma_a \Gamma_b}{\Gamma} \right\rangle \frac{2\pi}{\langle D \rangle} \approx \frac{\pi}{k^2} \pi \frac{\langle \Gamma_n \rangle}{\langle D \rangle} \approx 2 \frac{\pi}{k^2} \sqrt{\frac{E_{n,\text{ outside}}}{E_{n,\text{ inside}}}} \\ &\approx \frac{1300}{\sqrt{S_{n,\text{ MeV}}} \sqrt{E_{n,\text{ eV}}}} \text{ barn} \approx \frac{500}{\sqrt{E_{n,\text{ eV}}}} \text{ barn} \end{aligned} \tag{208}$$

Therefore the $1/v_n$ variation continues up through higher and higher energies.

At very high energies, the quantum cross section π/k^2 of the bombarding neutron becomes smaller than the cross-sectional area πR^2 of the nucleus. Using Eq. (125) and $\pi R^2 \approx \pi (0.12)^2 A^{2/3}$ barns ≈ 1.7 barns for uranium and plutonium, this occurs at $E_n \sim 0.4$ MeV. Above this energy, the cross section no longer falls like $1/v_n$ but instead hovers around 1-2 barns [Fig. 31(c)]. A giant resonance increases the cross section by $\sim 20\%$ around $E_n = 2$ MeV.

Another very high-energy phenomenon occurs when $E_n + S_n$ exceeds multiples of the fission barrier energy. When $E_n + S_n > 2V_B$, the bombarding neutron can escape from the nucleus yet leave behind enough energy to still cause the nucleus to undergo fission. Similarly, when $E_n + S_n > 3V_B$, the bombarding neutron and one other neutron can escape from the nucleus while still imparting enough energy to trigger fission. **First-chance fission** is fission that occurs upon simple absorption of a neutron, **second-chance fission** happens after absorption and re-emission of the neutron, **third-chance fission** occurs after absorption of one neutron and emission of two, and so forth. At the threshold for second-chance fission ($\sim$ 7 MeV for ^{235}U and ^{239}Pu), the total fission cross section becomes the sum of approximately equal cross sections ($\sim \pi R^2$) for first- and second-chance fission and therefore roughly doubles. The total fission cross section increases by a similar step size at the threshold for third-chance fission ($\sim$ 13 MeV for ^{235}U and ^{239}Pu).

Figure 31(b) shows the fission cross section for ^{238}U. As noted previously, the threshold for first-chance fission of ^{238}U is around 1.4 MeV. At this point, the cross section smoothly rises to ~ 0.5 barn, a value roughly comparable to but somewhat smaller than πR^2 of the nucleus. Since this energy is too high for resonance or $1/v$ effects, the cross section above the threshold is essentially flat. However, the cross section does increase in stair steps of the value ~ 0.5 barn at the thresholds for second- and third-chance fission (6.5 and 14 MeV). Above this point, the input energies become so large and so disruptive to the nucleus that the stairstep structure becomes more confused.

The neutrons that are produced by fission have very high energies ($E \sim 2$ MeV), yet neutrons with very low energies ($E \ll 1$ eV) have the highest cross sections for inducing ^{235}U and ^{239}Pu fission. This mismatch makes it more difficult to produce a fission chain reaction, in which neutrons from one fission induce other reactions, which then induce still more reactions. To overcome this problem, most fission reactors mix uranium with a **moderator** material that slows down neutrons but does not absorb them. Section 4.4 will examine the properties of moderators in more detail. **Fast reactors** and fission bombs are designed to sustain chain reactions without a moderator, simply relying on the $\sim 1 - 2$ barn fission cross sections at neutron energies of 1-2 MeV.

The energy for fission can also be provided by a charged particle or a gamma ray. For practical applications, however, these processes are much less important than neutron-induced fission, because they require more energy and have smaller cross sections.

4 Radiation Shielding

Different types of radiation–alpha particles and other nuclei, beta particles, gamma rays, and neutrons–lose energy by different mechanisms when they pass through matter (Fig. 32). Analysis of these mechanisms permits one to calculate the range of radiation in shielding materials [1, 2, 9].

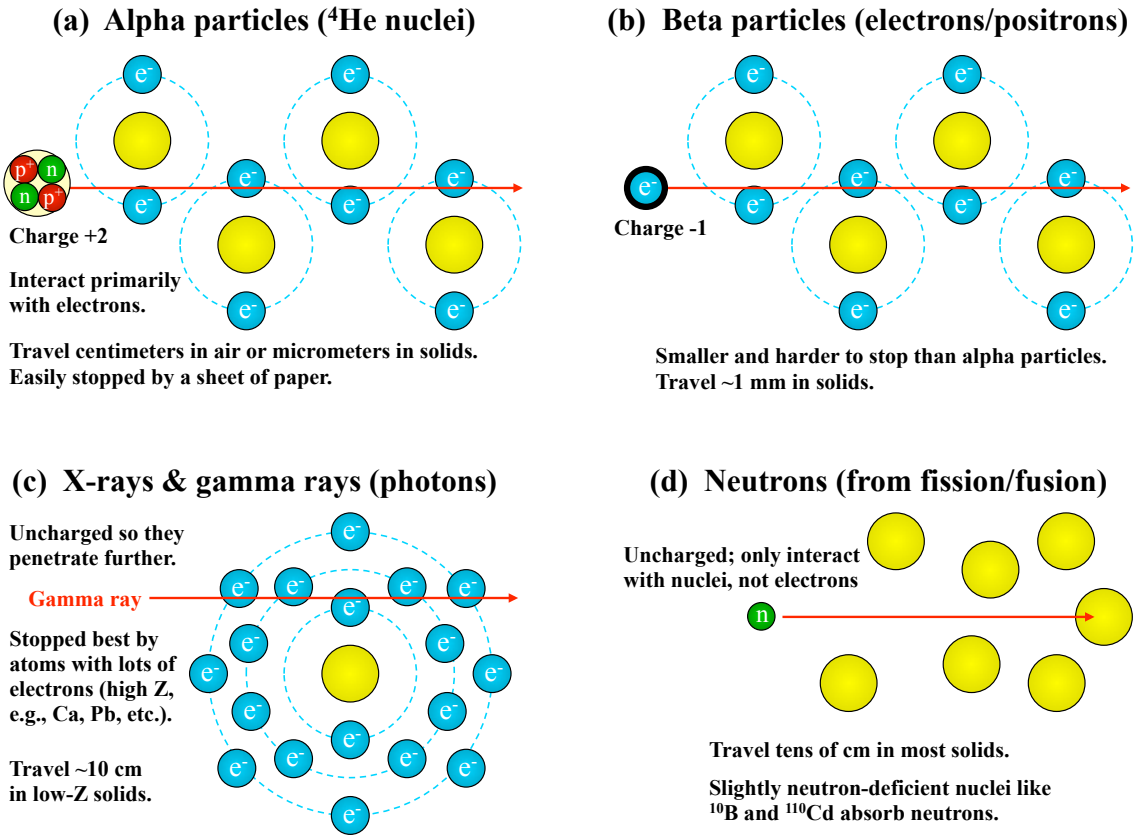

Figure 32. Energy loss by (a) alpha particles, (b) beta particles, (c) gamma rays, and (d) neutrons passing through matter.

4.1 Alpha Particles and Other Nuclei

Energetic nuclei such as protons, alpha particles, and fission fragments are slowed by their interactions with electrons in matter. As shown in Fig. 33, a nucleus with charge z and velocity v passing by an electron with impact parameter b exerts a sidewise force F on the electron for a time Δt:

$$F \approx \frac{ze^2}{4\pi\epsilon_o b^2} \qquad \text{for } \Delta t \approx \frac{2b}{v} \tag{209}$$

In that interaction, the nucleus transfers to the electron a momentum Δp and energy ΔE:

$$\Delta p \approx F\,\Delta t \approx \frac{ze^2}{2\pi\epsilon_o v b} \qquad \Longrightarrow \qquad \Delta E = \frac{(\Delta p)^2}{2m_e} \approx \frac{z^2 e^4}{8\pi^2\epsilon_o^2 m_e v^2 b^2} \tag{210}$$

Collisions with nuclei of mass M_i instead of electrons in the shielding material would have a factor of M_i in place of m_e in the denominator of ΔE in Eq. (210), so their effect is negligible.

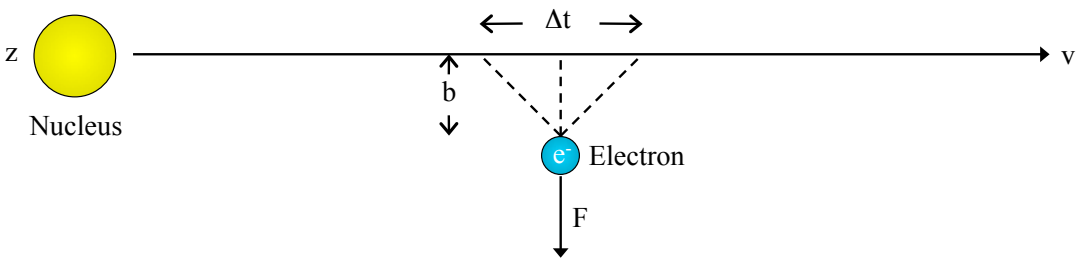

Figure 33. Energy loss by charged particles. An energetic nucleus with charge z and velocity v passing by an electron with impact parameter b exerts a sideways force F on the electron for time Δt. The change in the nucleus's trajectory is negligible, due to its far greater mass.

Shielding material with atomic number Z and N atoms per volume has NZ electrons per volume. The energy lost per path length by a high-energy nucleus interacting with all these electrons is

$$-\frac{dE}{dx} \;=\; NZ\int_{b_{\rm min}}^{b_{\rm max}} \Delta E\; 2\pi b\; db \;\approx\; \frac{z^2e^4NZ}{4\pi\epsilon_o^2 m_e v^2}\int_{b_{\rm min}}^{b_{\rm max}}\frac{db}{b} \;\approx\; \frac{z^2e^4NZ}{4\pi\epsilon_o^2 m_e v^2}\ln\left(\frac{b_{\rm max}}{b_{\rm min}}\right) \tag{211}$$

The minimum impact parameter at which such interactions can occur is determined by the Heisenberg uncertainty relation $(\Delta x)(\Delta p) \sim \hbar$ and the maximum relativistic momentum $p_{\rm max} = \gamma m_e v$ that could be imparted (where $\gamma \equiv (1 - v^2/c^2)^{-1/2}$ from *Classical Mechanics* ?.?):

$$b_{\rm min} \;\approx\; \frac{\hbar}{(\Delta p)_{\rm max}} \;\approx\; \frac{\hbar}{\gamma m_e v} \tag{212}$$

As the impact parameter increases, the transferred energy becomes smaller and smaller. The maximum impact parameter occurs when this energy is just enough to successfully ionize an orbital electron from an atom of shielding material, $(\Delta E)_{\rm min} = I$, where the minimum ionization energy of an atom is typically $I \sim 10Z$ eV. Using the other Heisenberg relation, $(\Delta t)(\Delta E) \sim \hbar$, this minimum energy may be related to the maximum effective collision time $(\Delta t)_{\rm max} \sim b_{\rm max}/(\gamma v)$ (which includes relativistic time dilation by the factor γ):

$$(\Delta t)_{\rm max} \;\approx\; \frac{b_{\rm max}}{\gamma v} \;=\; \frac{\hbar}{\Delta E_{\rm min}} \;=\; \frac{\hbar}{I} \qquad\Longrightarrow\qquad b_{\rm max} \;\approx\; \frac{\hbar\gamma v}{I} \tag{213}$$

Inserting Eqs. (212) and (213) into Eq. (211) yields

$$-\frac{dE}{dx} \;=\; \frac{z^2e^4NZ}{4\pi\epsilon_o^2 m_e v^2}\ln\left(\frac{\gamma^2 m_e v^2}{I}\right) \tag{214}$$

More detailed calculations modify Eq. (214) somewhat [1, 9], with $\beta \equiv v/c$:

$$-\frac{dE}{dx} \;=\; \frac{z^2e^4NZ}{4\pi\epsilon_o^2 m_e v^2}\left[\ln\left(\frac{2\gamma^2 m_e v^2}{I}\right) - \beta^2\right] \qquad \textbf{Bethe formula for slowing of energetic nuclei} \tag{215}$$

Equation (215) breaks down at low energies when the now slowly moving nucleus begins to capture electrons that shield part of its charge. Neglecting this and relativistic effects for $E \ll m_i c^2$, defining $L \equiv \ln(2\gamma^2 m_e v^2/I) - \beta^2 \approx \ln(2m_e v^2/I)$, and integrating using Eq. (215), the total range of an energetic nucleus is

$$x \;=\; \int_0^E \frac{dx}{dE}\,dE \;=\; \frac{8\pi\epsilon_o^2 m_e}{z^2e^4NZm_i}\int_0^E \frac{E\,dE}{L} \;\approx\; \frac{4\pi\epsilon_o^2 m_e E^2}{z^2e^4NZ\,\langle L\rangle\, m_i}\,, \tag{216}$$

utilizing a representative value $\langle L \rangle$. In a typical solid with a density on the order of Avogadro's number $N \sim N_A \sim 6 \times 10^{23}$ atoms/cm^3, Eq. (216) shows that α particles have a range on the order of microns, depending on the precise values of E, Z, and $\langle L \rangle$. Even in air their range is only centimeters. It is much easier to shield against α particles than other forms of radiation.

The range is proportional to m_i/z^2, so a proton has the same range as an alpha particle when their velocities are equal, or when the proton's energy $E = m_i v^2/2$ is 1/4 of the alpha particle's energy. Also, for comparable atomic densities N, $x \propto 1/Z$ due to the increased number of electrons.

Fission fragments begin with very high $z \sim 30$ and $E \sim 70$ MeV and have $\sim 1/2$ the range of 5-MeV α particles. As the fragments acquire electrons, z drops so rapidly that $-dE/dx$ from Eq. (215) actually decreases as the fragments slow, despite the energy loss's $1/v^2$ dependence.

4.2 Beta Particles

Like energetic nuclei, beta particles are slowed by collisions with electrons. However, the Bethe Eq. (215) is modified because the incident and target particle masses are now the same [9]:

$$\left(-\frac{dE}{dx}\right)_{\rm col} = \frac{e^4 N Z}{8\pi\epsilon_o^2 m_e v^2}\left[\ln\left(\frac{\gamma^2 m_e v^2 E}{2I^2}\right) - \frac{\ln 2}{\gamma}\left(2 - \frac{1}{\gamma}\right) + \frac{1}{\gamma^2} + \frac{1}{8}\left(1 - \frac{1}{\gamma}\right)^2\right] \quad (217)$$

Beta particles also lose energy by a second mechanism, bremsstrahlung radiation. The power lost due to bremsstrahlung by an electron moving through an ion population is (*Plasma Physics* 1.3):

$$\left(-\frac{dE}{dt}\right)_{\rm rad} \approx \frac{Z^2 e^6 N}{24\pi^2 \epsilon_o^3 c^3 m_e^2 b_{\rm min}} \quad (218)$$

For relativistic electrons, the minimum impact parameter (including $\gamma = E/m_e c^2$) is

$$b_{\rm min} = \frac{2\hbar}{\gamma m_e v} = \frac{m_e c^2}{E}\frac{2\hbar}{m_e v} \quad (219)$$

Using Eqs. (218) and (219), the energy loss per length due to bremsstrahlung radiation is

$$\left(-\frac{dE}{dx}\right)_{\rm rad} = \frac{1}{v}\left(-\frac{dE}{dt}\right)_{\rm rad} \approx \frac{Z^2 N e^6 E}{48\pi^2 \epsilon_o^3 c^5 m_e^2 \hbar} \approx 4\alpha_{fs} r_e^2 Z^2 N E \quad (220)$$

Because the bremsstrahlung loss varies like $\sim 1/m^2$ with the mass of the energetic particle, it is far smaller for energetic nuclei and hence was safely neglected in Section 4.1.

More precise calculations of bremsstrahlung [9] modify Eq. (220) to yield

$$\left(-\frac{dE}{dx}\right)_{\rm rad} \approx 4\alpha_{fs} r_e^2 Z^2 N E\left[\ln\left(\frac{2E}{m_e c^2}\right) - \frac{1}{3}\right] \quad (221)$$

Writing Eq. (221) as $(-dE/dx)_{\rm rad} = NE\sigma_{\rm brem}$, the bremsstrahlung cross section is

$$\sigma_{\rm brem} \approx 4\alpha_{fs} r_e^2 Z^2\left[\ln\left(\frac{2E}{m_e c^2}\right) - \frac{1}{3}\right] \quad (222)$$

The ratio of radiative to collisional losses from Eqs. (221) and (217) is

$$\frac{(dE/dx)_{\rm rad}}{(dE/dx)_{\rm col}} \approx \frac{EZ}{m_e c^2}\frac{2}{\pi}\alpha_{fs}\frac{\ln(2E/m_e c^2)}{\ln(E^3/2I^2 m_e c^2)} \approx \frac{E_{\rm MeV} Z}{700}\,, \quad (223)$$

using the logarithm ratio $\sim 1/7$ for typical E (~ 5 MeV) and I (~ 500 eV for $Z \sim 50$). Thus bremsstrahlung is negligible compared to collisional losses unless both E and Z are very large. (Indeed, bremsstrahlung X-ray generators impact a high-energy electron beam on a high-Z material.) A third energy loss mechanism, Cerenkov radiation, is even smaller (*Electromagnetism* ?.?).

By expressing Eq. (217) as $(-dE/dx)_{\rm col} \sim E/x$ and using $N \sim N_A$, $v \approx c$, and ~ 20 as a representative value for the term in brackets, the characteristic range x of beta particles in a solid is $\sim 3E_{\rm MeV}/Z$ mm, or on the order of a millimeter for typical energies and atomic numbers.

4.3 Gamma Rays

Gamma rays are absorbed or scattered in matter by three different mechanisms, depending on the energy E_γ of the gamma rays: the photoelectric effect, Compton scattering, and pair production.

The **photoelectric effect** predominates at low energies (E_γ less than ~ 0.5 MeV or so, depending on the Z of the matter). It occurs when a gamma ray is absorbed by an atomic electron, which uses the excess of E_γ over its own binding energy to escape the atom. For conservation of momentum, the electron must be initially bound to an atom, so this effect generally occurs with the innermost atomic electrons, which are most tightly bound. The innermost K-shell (1s) electrons of an atom have orbital radius $r = r_{\text{Bohr}}/Z$ [using Eq. (164)] and binding energy $E = Z^2 E_{\text{Bohr}}$ [using Eq. (163)]. Physically, one would expect the photoelectric absorption cross section to vary like $\sigma_{\text{photo}} \sim 2\pi r^2 \alpha_{\text{fs}} f(E/E_\gamma)$. This result includes a factor of 2 for the two K-shell electrons, πr^2 for the cross section of the electron orbit, α_{fs} for the coupling of the photon to the electron, and some function $f(E_{Bohr}/E_\gamma)$ that decreases at high photon energies where the electrons seem less tightly bound by comparison. Detailed calculations of the cross section per atom [8] confirm this intuition:

$$\sigma_{\text{photo}} \approx \frac{2^8}{3}\,\pi r^2\,\alpha_{\text{fs}}\left(\frac{E}{E_\gamma}\right)^{7/2} = \frac{2^8}{3}\,\pi r_{\text{Bohr}}^2\,\alpha_{\text{fs}}\,Z^5\left(\frac{E_{\text{Bohr}}}{E_\gamma}\right)^{7/2} \approx 5.5\times 10^7\,Z^5\left(\frac{13.6\text{ eV}}{E_\gamma}\right)^{7/2}\text{ b} \quad (224)$$

As shown in Fig. 34(a), the measured cross section $\sigma_{\text{photo}}(E_\gamma)$ jumps when E_γ increases past the binding energy $E_n = 13.6$ eV $(Z - \text{screening})^2/n^2$ of each atomic electron shell, producing edges named for each shell: the K edge, L edge, etc. Because the electron must appear tightly bound relative to the photon energy, the dominant shell is usually the innermost shell whose energy is accessible with E_γ, and the photoelectric effect becomes negligible for $E_\gamma \gg E_{\text{K-shell}} = 13.6Z^2$ eV. Lower-energy X-rays (fluorescence) are produced just after photoelectric absorption when a higher atomic electron falls into the vacant state, but such X-rays are usually absorbed near their point of origin. Sometimes the electrons in several different shells play musical chairs to decide which one will actually be ejected by the photoelectric effect, a process called **Auger emission**.

Compton scattering is dominant at medium energies (E_γ between ~ 0.5 MeV and ~ 10 MeV or so, depending on Z). In Compton scattering, the gamma ray scatters off a nearly free electron, traveling off in a new direction and leaving a bit of its energy with the electron. An atom's outer electrons, whose binding energies are negligible compared to E_γ, are thus more important than inner electrons for Compton scattering, in contrast to the situation for the photoelectric effect. *Relativistic Quantum Field Theory* 2.2.1 discusses Compton scattering in detail and calculates the cross section per electron. Assuming Z electrons per atom, the cross section per atom is:

$$\sigma_{\text{Compton}} \sim Z\pi r_e^2 \frac{m_e c^2}{E_\gamma} \quad (225)$$

Pair production, in which a gamma ray splits into an electron and a positron, predominates at high energies (E_γ above ~ 10 MeV or so, depending on Z). The Coulomb field of a nucleus facilitates this process, and the recoil of the nucleus allows momentum to be conserved. Neglecting the very small amount of energy imparted to the nucleus, the gamma ray energy is converted into kinetic and rest energy of the electron-positron pair: $E_\gamma = \text{KE}_{\text{e}^-} + \text{KE}_{\text{e}^+} + 2m_e c^2$. Thus pair production requires a gamma ray energy $E_\gamma > 2m_e c^2 = 1.022$ MeV. The produced positron subsequently annihilates with a nearby electron, producing two ~ 511 keV photons.

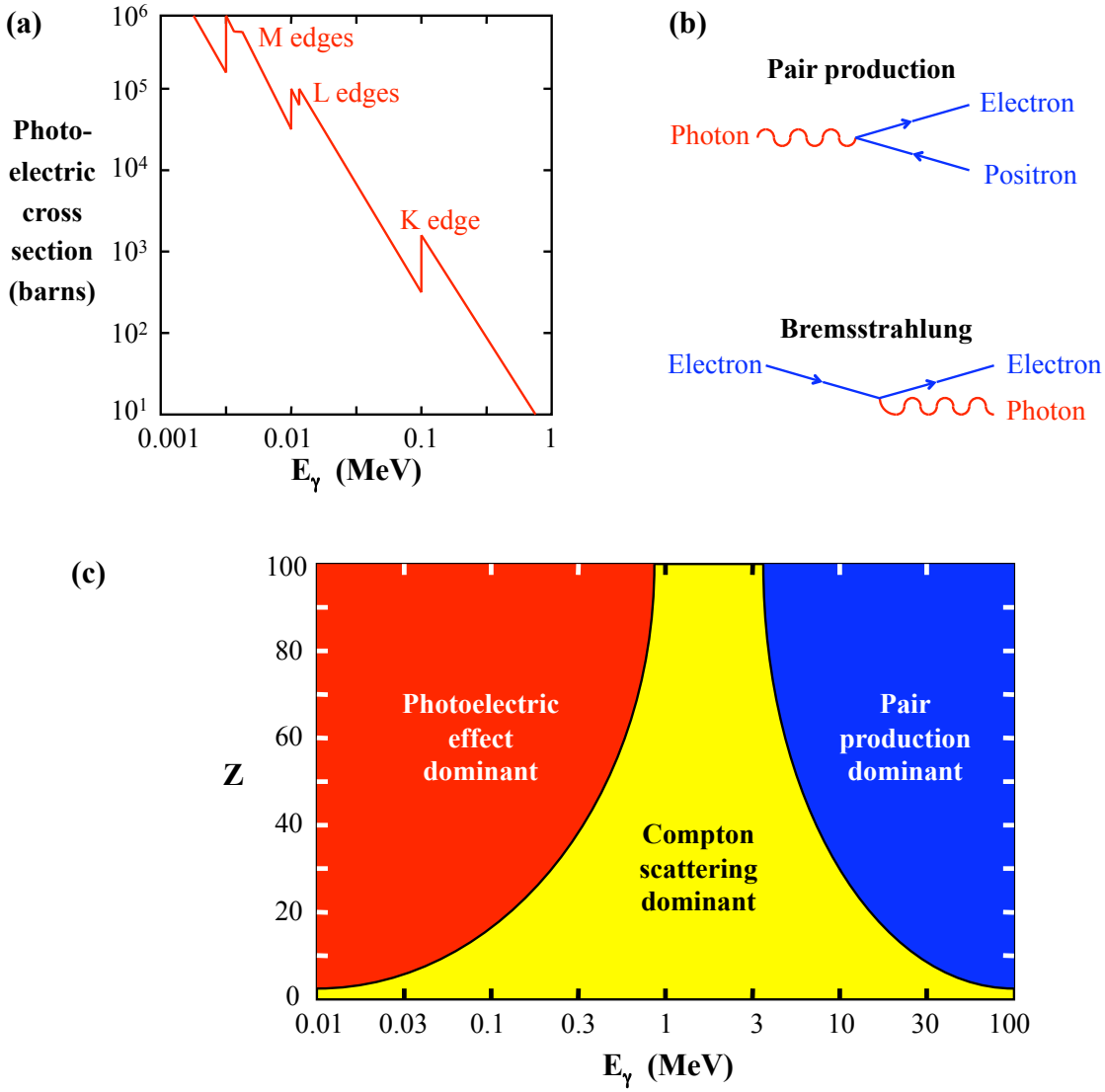

Figure 34. Energy loss by gamma rays. (a) The photoelectric cross section $\sigma_{\rm photo}$ vs. gamma ray energy E_γ for lead. **(b)** Pair production is closely related to bremsstrahlung. **(c)** Plot of shielding material Z vs. gamma ray energy E_γ, showing the regimes in which the photoelectric effect, Compton scattering, and pair production predominate.

Figure 34(b) shows that pair production ($\gamma \to {\rm e}^- + {\rm e}^+$) is closely related to the bremsstrahlung process (${\rm e}^- \to {\rm e}^- + \gamma$). Thus one would expect the pair production cross section to be comparable to the bremsstrahlung cross section from Eq. (222). Indeed, detailed calculations [8] give

$$\sigma_{\rm pair} \approx \frac{28}{9}\alpha_{fs} r_e^2 Z^2 \left[\ln\left(\frac{2E_\gamma}{m_e c^2}\right) - \frac{109}{42}\right] \tag{226}$$

Using Eqs. (224) and (225), one can find the values of Z and E_γ at which $\sigma_{\rm photo} \approx \sigma_{\rm Compton}$:

$$Z \approx \left[\frac{3}{2^8}\left(\frac{r_e}{r_{\rm Bohr}}\right)^2 \frac{1}{\alpha_{fs}} \frac{m_e c^2}{E_{\rm Bohr}^{7/2}}\right]^{1/4} E_\gamma^{5/8} \approx 100\, E_{\gamma,\,{\rm MeV}}^{5/8} \tag{227}$$

Similarly, Eqs. (225) and (226) show that $\sigma_{\rm Compton} \approx \sigma_{\rm pair}$ when

$$Z \sim \frac{\pi}{\alpha_{fs}} \frac{m_e c^2}{E_\gamma} \sim \frac{200}{E_{\gamma,\,\rm MeV}} \tag{228}$$

Figure 34(c) uses Eqs. (227) and (228) to plot Z vs. E_γ, showing the regions in which the photoelectric effect, Compton scattering, and pair production predominate.

Unlike other forms of radiation, gamma rays are attenuated by losing actual particles, not just energy per particle. Photons are absorbed or scattered out of the beam by the above processes, causing exponential attenuation of the intensity of a beam of gamma rays passing through matter:

$$I = I_o e^{-\mu x}\,, \qquad \text{where} \qquad \mu \equiv N(\sigma_{\rm photo} + \sigma_{\rm Compton} + \sigma_{\rm pair}) \tag{229}$$

For example, for 5-MeV gamma rays, Compton scattering predominates and has a cross section $\sigma_{\rm Compton} \sim Z\pi r_e^2/10 \sim 2.5 \times 10^{-26} Z$ cm^2. In a typical solid with $\sim N_A \sim 6 \times 10^{23}$ nuclei/cm^3, such gamma rays have an effective path length of $\sim 70/Z$ cm. Therefore the characteristic path length of gamma rays is of the order of 10 cm in typical low-Z materials. Because of the Z-dependence of $\sigma_{\rm photo}$, $\sigma_{\rm Compton}$, and $\sigma_{\rm pair}$, high-Z materials provide the best shielding from γ rays.

4.4 Neutrons

Neutrons only interact with nuclei in matter. Such interactions can include:

- **Inelastic scattering.** Neutrons with enough energy to excite nuclei ($\sim$ 1 MeV or more) can be inelastically scattered by nuclei in matter, with the excitation energy generally being emitted as gamma rays when the nuclei return to their ground states.
- **Elastic scattering.** Neutrons of any energy can be elastically scattered by nuclei. In the lab frame in which a neutron strikes a nucleus that is initially at rest, part of the neutron's initial kinetic energy is transferred to the nucleus. Lower-mass nuclei have less inertia and therefore absorb more of the neutron's energy, reducing or **moderating** the neutron energy and sometimes leading to recoil nuclei with enough kinetic energy to constitute secondary radiation of heavy charged particles. Low-mass nuclei that do not readily absorb neutrons (such as deuterium and ^{12}C) are used as moderators to slow neutrons inside fission reactors. After many collisions, the neutrons are slowed until their average kinetic energy is the same as the thermal energy $\sim k_B T$ of the surrounding matter, or .025 eV for room temperature matter. **Thermal neutrons** that have reached this state are in equilibrium with their surroundings and on average do not lose additional energy from further collisions. In addition to slowing neutrons down, collisions scatter the neutrons, leading to spatial diffusion.
- **Neutron absorption.** Certain slightly neutron-deficient nuclei such as ^{10}B and ^{110}Cd readily absorb neutrons, becoming heavier isotopes and emitting the excess energy as gamma rays. Such nuclei are useful for neutron shielding or absorbing excess neutrons in fission reactors.
- **Nuclear reactions.** As discussed in Section 3.3, neutrons within a certain energy range can trigger fission or other reactions when they strike certain nuclei.

In a typical solid with $N_A \sim 6 \times 10^{23}$ nuclei/cm^3 and a $\sigma \sim 1$ barn $= 10^{24}$ cm^2 cross section for neutron absorption or scattering, neutrons travel $\sim 1/N_A\sigma \sim 60$ cm. Like γ rays, neutrons are uncharged and thus penetrate further than charged particles in matter.

Fission Power gives more information on neutron scattering, absorption, and reactions.

5 Radiation Detection

Nuclear physics experiments and applications frequently require the detection of high-energy particles or electromagnetic radiation. It is convenient to categorize sensors according to whether they detect radiation via electrical signals, light emission, particle tracks, or other techniques [1, 2, 9]. Figure 35 shows various types of radiation detectors.

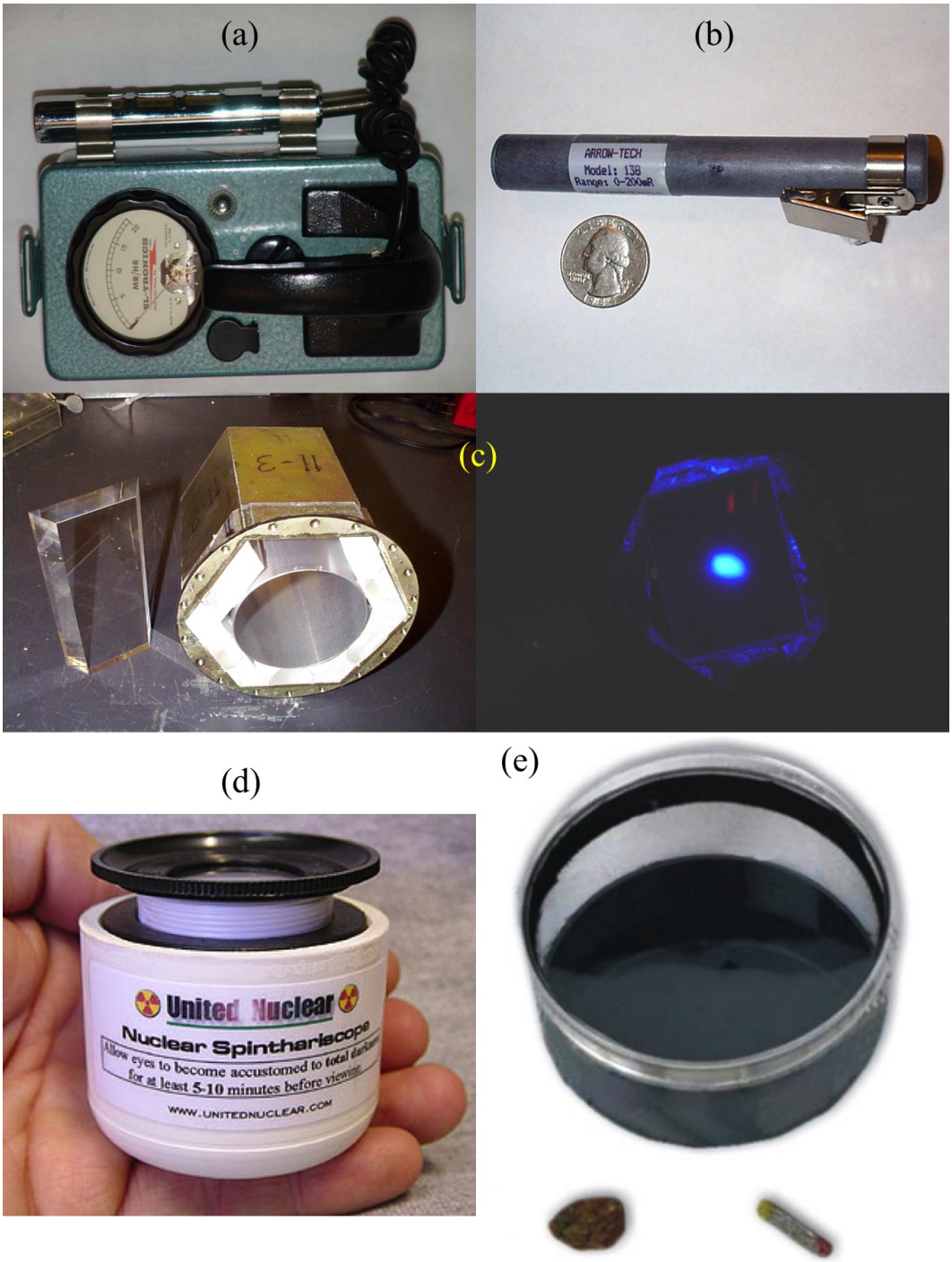

Figure 35. Examples of radiation detectors. **(a)** Geiger-Müller detector. **(b)** Dosimeter. **(c)** Scintillator. **(d)** Spinthariscope. **(e)** Cloud chamber.

5.1 Detection via Electrical Signals

Radiation can be detected via the electrical signals it produces in gas-filled high-voltage tubes [categorized in order of increasing voltage: ionization chambers, proportional counters, and Geiger-Müller counters–see Figs. 35(a) and 36] or semiconductor junction diodes.

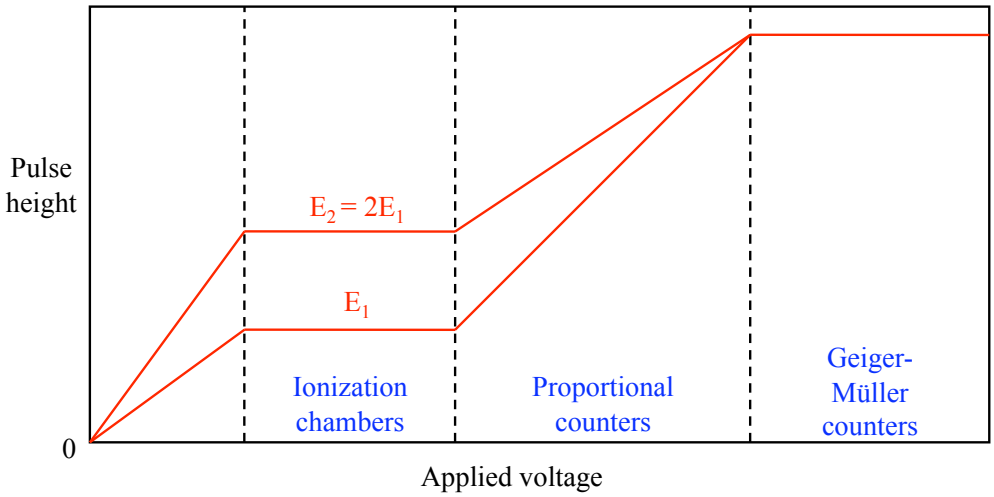

Figure 36. Operating regimes of ionization chambers, proportional counters, and Geiger-Müller counters. The higher the applied voltage in a gas-filled chamber, the larger the electrical pulse that is generated by a passing charged particle. Ionization chambers operate at a low voltage where the pulse height is proportional to the energy absorbed from the charged particle (e.g, E_1 and E_2). Geiger-Müller counters operate at a high voltage where particles of different energies produce the same pulse height. Proportional counters operate in an intermediate regime.

Ionization chambers have a $\sim$ 100 V/cm electric field between an anode and cathode. Energy lost by passing radiation ionizes gas atoms in the chamber (Sections 4.1-4.2). For example, 1 MeV can create $\sim$ 30,000 electron-ion pairs in air (34 eV per pair). In the applied electric field, the electrons drift to the anode within $\sim$ 10 μsec, creating an electric current proportional to the radiation energy loss in the chamber, although individual radiation counts may be too small to detect. Because of their large mass, the ions drift much more slowly than the electrons and can be neglected. Though neutrons do not directly cause ionization, slow neutrons can be detected via triple α decay of ^{11}B in BF_3 gas, while fast neutrons can be detected via the recoil protons they strike in H_2 gas. Alternatively, slow or fast neutrons can be detected via fission in ^{235}U- or ^{238}U-coated electrodes, respectively. **Electroscopes** are simple ionization chambers in which the output is read visually via an electrostatically charged filament that moves as radiation-generated electrons neutralize its charge. Pen-sized electroscopes are especially useful as **dosimeters** for measuring a person's radiation exposure [Fig. 35(b)].

Proportional counters have a $\sim$ 1000 V/cm field that accelerates radiation-induced electrons, which strike atoms and create additional electrons, a process called a **Townsend avalanche**. The measured current is proportional to the number of secondary electrons, which depends on the number of primary electrons, so the output is still proportional to the energy deposited by the radiation. However, the signal amplification of $\sim 10^3 - 10^6$ allows proportional counters to easily detect individual events. The ~ 1 μsec response time reflects the drift time from the primary event to the high-field region near the anode wire. Proportional counters can have either a single anode wire [Fig. 37(a)] or many wires to obtain spatial information [Fig. 37(b)].

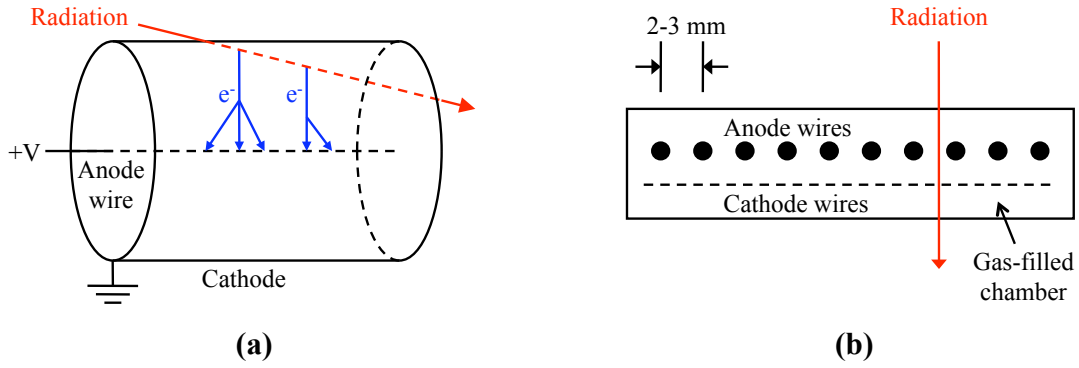

Figure 37. Proportional counters. **(a)** Radiation passing through a cylindrical proportional counter frees some electrons from the gas; the electrons are accelerated toward the anode wire, exciting and freeing more electrons as they go, generating a measurable electrical discharge to the anode. **(b)** Radiation passing through a multiwire proportional counter generates a measurable electrical signal on the nearest wire, so the approximate location of the radiation can be determined.

Geiger-Müller counters [Fig. 35(a)] have an even higher electric field, so that collision-generated photons spread the electron avalanche to the entire tube of gas. This provides a signal amplification of $\sim 10^10$ but no information on the deposited radiation energy. As in proportional counters, the response time is $\sim$ 1 μ sec. Typically the gas is $\sim$ 90% argon with $\sim$ 10% ethanol added as a quencher gas to prevent the discharge from continuing indefinitely [9], so there is a $\sim$ 100 μsec dead time after a pulse before another event can be detected. Using high-Z tube walls permits X-ray detection with $\sim$ 1% efficiency via electrons ejected from the walls. Surrounding a Geiger-Müller tube with paraffin allows detection of neutrons of any energy via recoil protons from the paraffin.

Junction diodes make much more compact detectors, due to the shorter radiation ranges in solids versus gases. Radiation can create an electron-hole pair in the **depletion region** or junction between the n- and p-doped regions of a diode. Only $\sim$ 3 eV is required to create a charge pair, so $\sim$ 10x more charges are created for a given energy than in a gas-filled detector. A $\sim 1-3$ kV reverse bias is generally applied to the diode to separate the electrons and holes and also to maximize the size of the radiation-sensitive depletion region. As with ionization and proportional counters, the induced electric current is proportional to the energy deposited by the radiation. *Semiconductor Devices* ?.? gives more information on diode designs for detectors.

5.2 Detection via Light Emission

Both scintillators and Cerenkov counters use light emission to detect radiation.

Scintillators [Fig. 35(c)] emit light via fluorescence (*Solid State Physics* 5.2). Electrons in scintillator materials have a ground or valence state, an excited or conduction state with energy E_e relative to the ground state, and an intermediate or activator state with energy E_a (Fig. 38). The ground state is well populated and the other states have populations $\sim \exp(-E_e/k_BT)$ or $\sim \exp(-E_a/k_BT)$ that are virtually zero since their energies ($\sim$eV) are much larger than room-temperature thermal energy $k_BT \sim 0.025$ eV. Energy lost by a charged particle (Sections 4.1 and 4.2) can boost an electron from the ground to the excited state [Fig. 38(a)]. When the electron falls back from the excited state, it emits a photon. If there were no activator state, the electron would drop directly to the ground state, emitting a photon of energy E_e. Since this photon energy can boost any of the ground state electrons up to the excited state, the photon would be rapidly absorbed within the scintillator instead of escaping to be detected. With an activator state present, an electron can drop from the excited to the activator state, emitting a photon with energy $E_e - E_a$ [Fig 38(b)] that cannot boost electrons from the populated ground state and hence is not reabsorbed within the scintillator. The excited electron ultimately decays from the activator to the ground state.

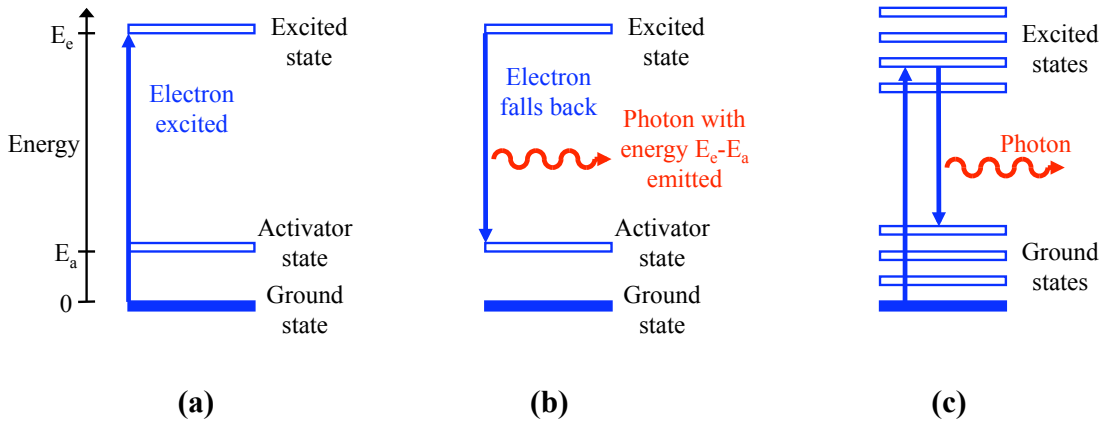

Figure 38. Scintillator energy levels. **(a)** Energy E_e lost by a passing particle can boost an electron from the populated ground state to the unpopulated excited state. **(b)** The excited electron falls to the activator state, emitting a photon of energy $E_e - E_a$ that cannot be reabsorbed within the scintillator, and the electron later drops back to the ground state. **(c)** In an organic scintillator, molecular vibrations split the electronic ground and excited states into many closely spaced levels, some of which can serve as activator states.

An important class of scintillators is inorganic insulators, especially alkali halides like NaI and ZnS. As insulators, these materials have a large band gap (~ 4 eV) between the conduction and valence band states. To create activator states, thallium or silver impurities are added, denoted as NaI(Tl) and ZnS(Ag). NaI(Tl) is excited by $E_e = 4.10$ eV (a photon wavelength of 303 nm) and emits photons with $E_e - E_a = 3.02$ eV (410 nm). To prevent reflection or absorption at crystal faces, large single crystals are used. NaI readily absorbs water vapor from the air, changing from a transparent crystal to an opaque powder, so it must be kept sealed.

Another class of scintillators is organic molecules with vibration levels as in Fig. 38(c). Several "ground states" are ~ 0.1 eV apart, while excited states are ~ 0.1 eV apart from each other but a few eV higher than the ground states. Some of the electrons do not participate much in bonding and can be excited to these higher states. The upper ground states function as an activator state, making the peak absorption and emission energies different. Organic scintillator materials include anthracene, benzene-like liquids, and plastics (which are especially convenient).

A photomultiplier tube or PMT (*Optics and Quantum Electronics* ?.?) can be placed next to a scintillator or connected to it via a light pipe. A good PMT can detect a particle that loses as little as 4 keV in a scintillator. PMTs generally work better with visible light than ultraviolet light.

Some old watches used a mixture of ZnS(Ag) and radium as luminous if somewhat dangerous paint. Similarly, a **spinthariscope** is a low-power optical microscope focused on a screen containing ZnS(Ag) and an alpha emitter, permitting one to observe flashes of light from each decay [Fig. 35(d)].

The scintillation pulse, height, and material can indicate a particle's type and energy. Scintillators can detect gamma rays indirectly via the energetic Compton electrons they produce. High-Z materials are especially conducive for this purpose (Section 4.3) and iodine has $Z = 53$, so NaI is a good scintillator for gamma ray detection. By adding Cd or B to a scintillator, neutrons can be detected via scintillation light produced by energetic recoil nuclei.

Cerenkov counters measure electromagnetic Cerenkov radiation, which is emitted when a charged particle's velocity v exceeds the speed of light c/n in a medium with index of refraction n. Cerenkov radiation is the optical equivalent of a sonic boom and is emitted at an angle $\cos\theta = 1/n\beta$ relative to the particle's trajectory (*Electromagnetism* ?.?). Although Cerenkov radiation is ~ 100x weaker in the visible spectrum than scintillation light, its emission angle is useful for measuring the velocity of charged particles traveling in a particular direction. A CO_2 chamber with variable temperature 25-50^{o}C and pressure 1-200 atm can achieve $n = 1.0004 - 1.21$ for this purpose.

5.3 Detection via Particle Tracks

Several detection methods involve observing the physical tracks left by radiation passing through suitable media, including certain solids, photographic film, cloud chambers, and bubble chambers.

Solids. Massive, high-energy, high-Z ionizing particles like fission fragments and other energetic nuclei can leave tracks in solid materials that are electrical insulators. An ionizing particle can destroy the lattice in a crystalline solid, creating a microscopic hole along its path. In amorphous solids like plastics, an ionizing particle can leave a track by breaking polymer chains or creating chemically reactive molecules. This technique is especially useful for dating rocks or meteorites by microscopically counting the number of tracks left by fission fragments from spontaneous fission of certain impurities and considering the half life and initial amount of those impurities.

Photographic film is the oldest radiation detection method, dating back to Becquerel in 1896. Because the blackening of film is proportional to the product of the radiation intensity and exposure time, radiation workers can wear film badges to monitor their cumulative personal exposure. Stacked layers of film with a high density of silver bromide can be used to trace individual particle tracks through the layers. The particle energy loss $|dE/dx|$ from Section 4 can be measured since higher values yield more developable grains per length, up to some saturation value $|dE/dx|_{\text{sat}}$. Likewise, the range of a track can be related to the particle type and initial energy as described in Section 4. Several additions can also be made to film-based detectors for special purposes: a reinforcing screen that emits secondary light or electrons in response to the primary radiation, shielding material that blocks radiation of certain types or energies, or impurities such as boron, bismuth, or uranium that enhance or reduce the response to particular types of radiation.

Cloud chambers [Fig. 35(e)] contain a vapor that is **supersaturated**, or on the verge of condensing into droplets. A charged particle passing through the chamber leaves a visible trail of condensed droplets momentarily suspended in space. By observing the curvature of the trails in an applied $\sim 1 - 5$ Tesla magnetic field, one can measure the momentum of the particles. **Continuous cloud chambers** create a vertical temperature gradient between a heated top and a cold bottom containing dry ice; the mixture of gas and vapor (usually air and alcohol) in the chamber is supersaturated within some temperature layer. An intense (e.g., xenon) light is often used to visualize the droplet trails, especially against a black background. **Intermittent cloud chambers** use adiabatic expansion with a piston to cool a gas, creating a supersaturated vapor for ~ 0.1 sec after the expansion. Cloud chambers of either type can be cleared of old tracks using an electric field, and stereo photographs are helpful to document and reconstruct all the tracks.

Bubble chambers, in contrast, contain a liquid (hydrogen, deuterium, freon, propane, etc.) on the verge of boiling, so a passing charged particle leaves a visible trail of bubbles. Because the material is much denser than in a cloud chamber, it can absorb more of a particle's energy, enabling clearer signals and more accurate measurements. Advantages over film include simpler material composition and reusability. Typically the liquid is decompressed within ~ 10 msec, lowering its boiling point close to the actual temperature, intense lights flash ~ 1 msec later to visualize particle tracks, and then the liquid is recompressed, all within a ~ 1 sec cycle. As with a cloud chamber, stereo photographs are commonly taken, and particles can be analyzed by their range and track curvature in a magnetic field. Bubble chambers with diameters of $\sim 3 - 4$ m are used to identify the products of particle collisions at major accelerators like CERN and Fermilab.

5.4 Miscellaneous Detection Methods

Polarimeters measure the polarization of particle spins. The polarization of nucleons can be assessed from their interactions with a spinless target such as ^{4}He. The polarization of electrons can be found by scattering them off a polarized electron target (e.g., a magnetic material); the Pauli principle suppresses scattering of parallel spins relative to antiparallel spins by over a factor of 10. Gamma ray polarization can be determined by Compton scattering off a polarized electron target, since the scattering angle depends on the polarization of the photons and electrons.

Spectrometers measure the energy of particles. An applied magnetic field bends the trajectory of charged particles, with lower-energy particles having more curvature than higher-energy particles (*Plasma Physics and Fusion* 1.4). Figure 39(a) shows a magnetic spectrometer that gives the best energy resolution for charged particles. Particles from a source are bent by a magnetic field and impact different areas of a detector array or photographic film depending on their energy. On the other hand, the magnetic lens spectrometer in Fig. 39(b) has the best luminosity, since particles emitted over a wide range of angles from the source converge on the detector if they have the appropriate energy. Gamma rays with energies greater than $2m_ec^2$ can be analyzed by using a magnetic spectrometer to measure the energies of electrons and positrons they create via pair production. Gamma rays of lower energy can be analyzed by measuring their Bragg scattering angle from calcite or other crystals (*Electromagnetism* ?.?).

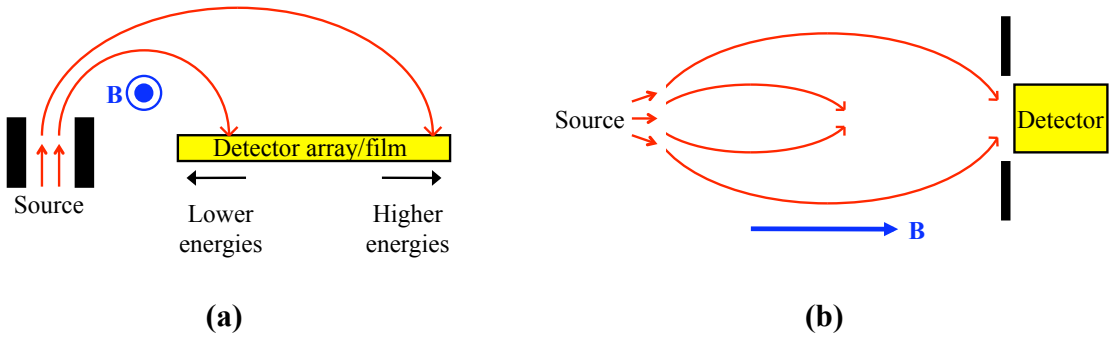

Figure 39. Magnetic spectrometers for charged particles. (a) The best energy resolution is achieved by letting particles from a source curve around a perpendicular magnetic field **B** and impact on a detector array or film. A particle's energy affects its trajectory's curvature and hence the impact location on the detector. **(b)** The best luminosity is achieved by using an axial magnetic field to focus all particles of a certain energy onto a detector. Particles of other energies do not have the correct curvature to reach the detector. The magnetic field can be varied to detect different energies.

Detector arrays can form images from X or gamma rays. Semiconductor arrays are replacing film for X-ray imaging (*Semiconductor Devices* ?.?). For gamma rays, a gamma camera channels radiation through holes in a lead screen to a scintillator plate, behind which is an array of photomultiplier tubes (Fig. 40).

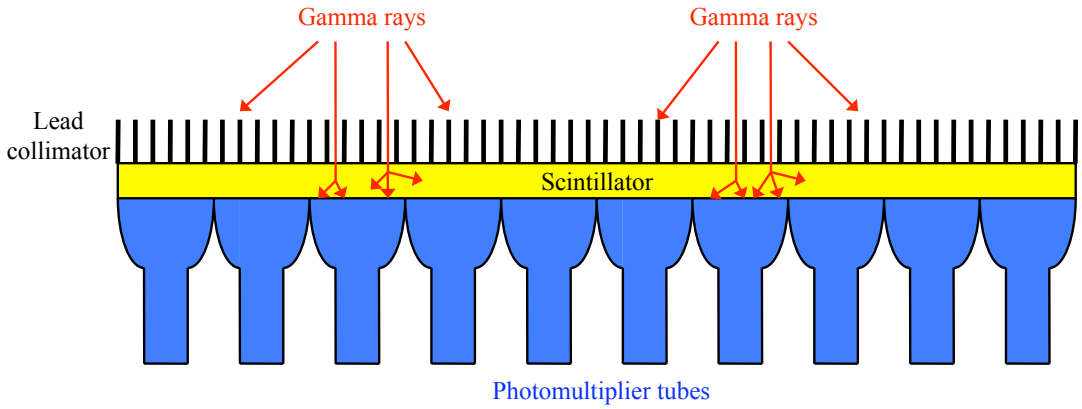

Figure 40. Gamma camera. Gamma rays traveling in the appropriate direction pass through the lead collimator channels and enter a scintillator plate, where they produce secondary photons that are detected by the nearest photomultiplier tubes in a two-dimensional array.

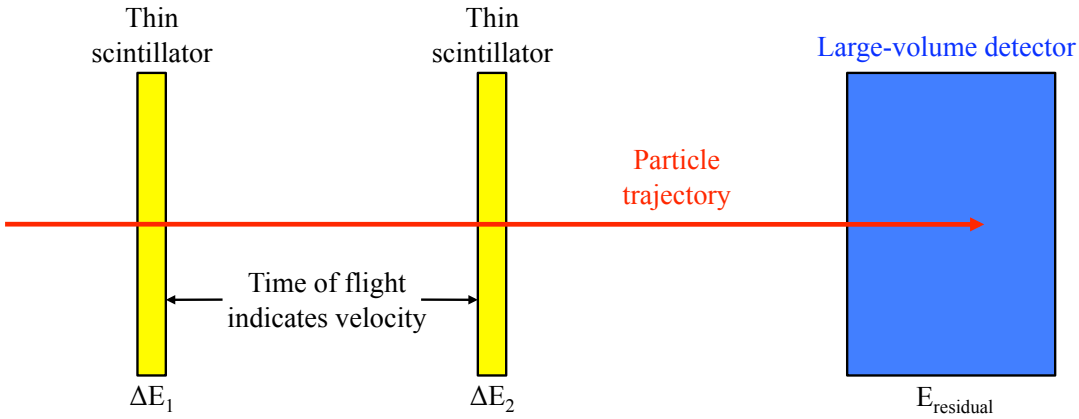

Figure 41. Counter telescope for identifying particles. The particles' energy is found by summing the energy losses, $E = \Delta E_1 + \Delta E_2 + E_{\text{residual}}$, and their velocity can be determined from the time of flight between the two thin scintillators. The particles' mass can be found using their energy and velocity, while their charge can be determined by the energy loss rate in the detectors.

Counter telescopes are a series of detectors and are especially useful for identifying particles. For example, Fig. 41 shows a counter telescope composed of two thin detectors (such as thin plastic scintillators) followed by a large detector such as a large-volume scintillator. Particles lose relatively small amounts of energy ΔE_1 and ΔE_2 in the two thin detectors before expending their remaining energy in the large detector. The three energy depositions and the time-of-flight between the two thin detectors provide a great deal of information on the particles. Coincident signals in all three detectors are measured relative to uncorrelated background noise.

6 Some Applications of Nuclear Physics

This section will cover applications of nuclear physics to medicine and materials analysis. Applications to fission and fusion power are treated in separate summaries.

6.1 Radiation Units and Medical Effects

First we will consider the units for measuring radiation and the medical effects of different amounts of radiation. The quantities can be expressed in either the old units that were used in the early days of nuclear physics or the newer metric units [1, 2, 9, 10].

The **activity** of a radioactive source indicates the number of nuclear decays per second. The new unit of activity is the Becquerel (Bq), equivalent to one decay per second. Originally activity was expressed in terms of the Curie (Ci), the activity of 1 gram of ^{226}Ra, approximately 3.7×10^{10} Bq. Eventually the activity of a radioactive source goes to zero as the nuclei decay to stable forms. However, before ultimately decreasing, the activity may actually increase initially if the daughter products of the primary decay are themselves radioactive.

The **exposure** indicates the ionization that radiation creates within a given mass of air, including secondary charged particles. The new unit is simply Coulombs/kg. The old unit, the Roentgen (R), is 1 esu of charge per cm^3 of air at standard temperature and pressure (STP). One Roentgen is equivalent to 2.58×10^{-4} C/kg or 2.08×10^9 charges/cm^3 of STP air.

The **absorbed dose** is the energy that radiation deposits within a given mass of material, or the energy density deposited per mass density. It is usually applied to biological organisms or tissues. The new unit, the Gray (Gy), is one J/kg. The old unit, the rad (radiation absorbed dose), is 100 erg/g or 0.01 Gy. Assuming one charge per ion and an average energy of 34 eV to produce an ion in air, 1 R = 0.88 rad, so Roentgens and rads are roughly equivalent.

Radiation generally damages biological material by ionizing molecules within the material, creating free radicals with unpaired electrons (like H· or OH·) that undergo destructive chemical reactions with DNA and other essential cellular components. The degree of biological damage depends on the specific type of radiation as well as the absorbed dose. Radiation that deposits its energy over a short path length (such as alpha particles) does more damage within each cell than radiation that gradually loses energy over a long path length (like gamma rays), depositing very little energy within any given cell. The relative destructiveness is taken into account by assigning a **weighting factor** W_R to different types of radiation:

W_R = 1	for X, γ, β, and muon radiation	5	for $<$ 10 keV neutrons
2	for $<$ 2 MeV protons	10	for 10-100 keV neutrons
5	for $>$ 2 MeV protons	20	for 100 keV-2 MeV neutrons
20	for alpha particles	10	for 2-20 MeV neutrons
		5	for $>$ 20 MeV neutrons

The **equivalent dose**, the absorbed dose multiplied by the weighting factor W_R, is a measure of the biological damage done by the radiation. If the absorbed dose is in Grays, the equivalent dose is then in Sieverts (Sv). In older units, if the absorbed dose is in rads, the equivalent dose is in rem (Roentgen equivalent in man), where 1 rem = 0.01 Sv. In practice, the Sv is so large that radiation doses typically get measured in milli-Sievert (mSv) or even smaller units. The convenient thing about the older unit, the rem, is that it is smaller and therefore closer to typical doses.

Sometimes these definitions are carried even further to calculate an **effective dose**, which takes into account not only the weighting factor for different radiation types but also a weighting factor for the different radiation sensitivities of various organs and tissues.

Table 2 lists the typical annual doses from various radiation sources. At 4 km altitude where there is less atmosphere to screen out cosmic rays, the cosmic ray dose can be up to 10 times higher than the sea level value, so living in the mountains or flying a great deal increases the dose. Potassium is an essential nutrient, and $\sim 1.2 \times 10^{-4}$ of natural potassium is ^{40}K, a beta emitter with a half-life of 1.85 billion years that contributes roughly half the dose from all ingested radionuclei. Depending on the local geology and building materials, γ rays from rocks (particularly granite) can give a sizeable dose. Gaseous alpha-emitting radon isotopes from the decay of ^{233}Th and uranium inside the earth can seep into basements and add a significant dose to the lungs. The total annual dose from these factors is $\sim 2-3$ mSv = 0.2-0.3 rem. In the U.S., the recommended maximum annual dose is 5 mSv = 0.5 rem for the general public and 50 mSv = 5 rem for radiation workers.

Radiation source	**New units**	**Old units**
Cosmic rays (at sea level)	0.25 mSv	25 mrem
Ingested ^{40}K	0.17 mSv	17 mrem
Other radionuclei in body	~ 0.2 mSv	20 mrem
γ rays from rocks	$\sim 0.2-0.4$ mSv	20-40 mrem
Radon gas	~ 1 mSv	~ 100 mrem
Medical X-rays	~ 0.5 mSv	~ 50 mrem
Nuclear power and weapons tests	< 0.005 mSv	< 0.5 mrem
Total	2-3 mSv	0.2-0.3 rem

Table 2. Typical annual radiation dose for general public.

Either cumulative or acute (short-term intense) radiation can cause biological damage. Radiation-induced mutations in proto-oncogenes or tumor suppressor genes can make cells cancerous; the lifetime risk of fatal cancer from cumulative radiation exposure increases by ~ 0.05/Sv $= 5 \times 10^{-4}$/rem. For example, a person exposed to 0.3 rem/year for 75 years has a $\sim 1\%$ chance of fatal cancer, not including the effects of chemical carcinogens, oncogenic viruses, or inherited oncogenic mutations. Acute radiation doses can damage DNA enough to kill cells or trigger apoptosis (cell suicide). Rapidly dividing cells such as those in Table 3 are more sensitive to radiation-induced DNA damage than other cells in the body. Whole-body doses over ~ 3 Sv = 300 rem are generally fatal unless there is intensive medical treatment such as transfusions, antibiotics, and bone marrow transplants. Antioxidants like sulfhydryl compounds minimize free radical formation and therefore increase resistance to acute radiation doses, but they have only been used experimentally.

Tissue type	**New units**	**Old units**	**Effects**
White blood cells	0.5 Sv	50 rem	Weakened immune response for several days
Gastrointestinal	1 Sv	100 rem	Vomiting within hours
tract lining	4 Sv	400 rem	GI tract bacteria released into bloodstream
Bone marrow	2 Sv	200 rem	Fatigue and anemia (no red blood cells produced)
			No immune system (no white blood cells produced)
Ovaries/testes	< 1 Sv	< 100 rem	Mutations in offspring
	3 Sv	300 rem	Sterility
Fetus	< 0.25 Sv	< 25 rem	Birth defects or miscarriage
Hair follicles	3 Sv	300 rem	Loss of hair within 2 weeks
Skin	1 Sv	100 rem	Radiation burns

Table 3. Approximate thresholds for radiation damage to most sensitive tissue types.

6.2 Diagnostic Nuclear Medicine

Nuclear physics techniques, including X-rays, radioisotopes, positron-emission tomography, and nuclear magnetic resonance, can be used to image organs and diagnose medical problems (Fig. 42) [2, 10].

X-rays [Fig. 42(a)] have been used since their discovery to photograph bones within the body, since bone is dense with high-Z calcium and hence attenuates X-rays much more than soft tissue does. Disadvantages of plain X-ray photography or **radiography** are that (1) it yields a two-dimensional image with no depth information and (2) it has difficulty distinguishing between soft tissue types, for example to spot a tumor. To extend the capabilities of radiography, nonradioactive, high-Z atoms that strongly attenuate X-rays can be temporarily added as a contrast medium in tissues of interest. For instance, swallowing a viscous drink containing barium makes the gastrointestinal tract stand out in X-ray photographs. A further elaboration of radiography is **Computerized Axial Tomography (CAT)**, in which a source emitting a fan of narrow X-ray beams rotates around the patient, while an array of X-ray detectors rings the patient. (When X-ray detectors were more expensive, the detector array was smaller and would also rotate to remain on the opposite side of the patient from the X-ray source.) Computers can process all of the detector data to produce three-dimensional images or two-dimensional image "slices" through the patient.

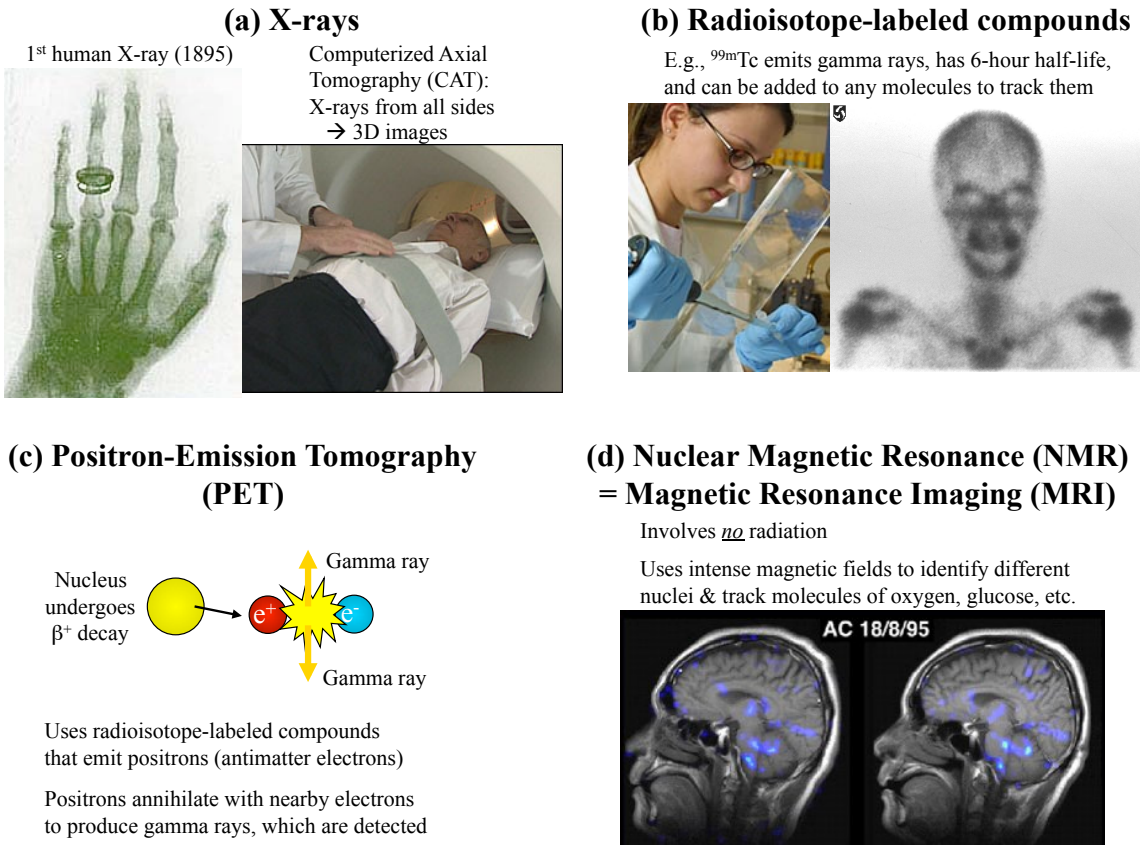

Figure 42. Diagnostic nuclear medical techniques include (a) X-rays, (b) radioisotope-labeled compounds, (c) positron-emission tomography, and (d) nuclear magnetic resonance.

Radioisotope-labeled compounds taken up by certain tissues can help image those tissues or measure their physiological activity [Fig. 42(b)]. ^{99m}Tc, a technicium isomer, is ideal for this purpose since it can be added to almost any compound, it only emits a 140-keV photon that can readily escape the body and be detected, and its half-life is just 6 hours, thus minimizing the dose to the patient. Saline passed through a charge-exchange column with ^{99}Mo can "milk" the ^{99m}Tc decay product:

$$^{99}\text{Mo} \xrightarrow{66\text{ hr}} {}^{99m}\text{Tc} \tag{230}$$

Thus availability in hospitals is determined by the longer 66-hour half-life of the ^{99}Mo instead of the actual 6-hour half-life of the technicium. ^{99}Mo can be obtained as a fission product [near the low-mass peak of Fig. 26(a)] or it can be bred by bombarding ^{98}Mo with neutrons. A collimated scintillation detector can be scanned back and forth near a labelled organ to produce an image, or for faster imaging, an array of many collimated detectors can be used as a gamma-ray camera. Millimeter-scale lateral and depth resolution is possible with properly designed detectors.

Other radioisotopes serve specialized diagnostic functions. For example, ^{201}Tl is used as a potassium analog for cardiac and other studies, although its 68-80 keV photons are more difficult to detect than the higher-energy photons from ^{99m}Tc. Moreover, iodine is readily taken up by the thyroid gland, so a simple counter held near the neck after consumption of radioactive iodine can measure thyroid activity. ^{123}I, which can be produced in a cyclotron and decays with a 13-hour half-life via electron capture with emission of only a 159-keV photon, is good for this purpose. An alternative isotope is ^{132}I, which has only a 2.3-hour half-life but can be milked from the 78-hour-half-life fission product ^{132}Te via a solvent that dissolves iodine but not tellurium. Sodium iodohippurate containing radioactive iodine is excreted by the kidneys and thus can also be used to measure kidney function via a simple counter. Finally, brain tumors often breech the blood-brain barrier, so radio-labeled impurities added to the blood stream can accumulate there and identify the tumor.

Positron-Emission Tomography (PET) also employs radioisotope-labeled compounds, but the radioisotope undergoes β^+ decay, and the emitted positron promptly annihilates with a nearby electron to produce back-to-back 511-keV photons [Fig. 42(c)]. The patient is surrounded with an array of detectors, whose data is used to produce a three-dimensional image of the distribution of the radio-labelled compound. Suitable radioisotopes are biologically relevant elements that have fewer neutrons than normal, making them unstable to β^+ decay. They include ^{11}C ($\tau_{1/2} = 20$ min), ^{13}N ($\tau_{1/2} = 10$ min), ^{15}O ($\tau_{1/2} = 2$ min), and ^{18}F ($\tau_{1/2} = 110$ min). For example, $^{15}O_2$ or ^{18}F-labelled glucose are useful for visualizing blood flow to organs such as the brain. Because of their very short half-lives, these isotopes must be made at the medical facility in a cyclotron.

Nuclear Magnetic Resonance (NMR), or **Magnetic Resonance Imaging (MRI)**, involves no radiation [Fig. 42(d)]. The patient is placed in a strong static magnetic field $\mathbf{B_o}$, which causes a Zeeman splitting of nuclear spin states by an energy ΔE that depends on $\mathbf{B_o}$ and the nuclear spin J. Different nuclides have different characteristic ΔE values for a given $\mathbf{B_o}$; ^{1}H, ^{13}C (present as 1.1% of natural carbon or administered artificially), and ^{17}O (0.038% of natural oxygen or administered artificially) are particularly easy to recognize. A second magnetic field $\mathbf{B_1}$ that oscillates at frequency f is applied perpendicular to $\mathbf{B_o}$. If f matches the resonance frequency of a certain nuclide, $f = \Delta E/h$, this perturbation facilitates transitions between spin states, causing detectable energy absorption from the $\mathbf{B_1}$ field. (See *Nonrelativistic Quantum Physics* ?.? for more details.) Monitoring absorption vs. frequency indicates the identities and amounts of various nuclides, while their location can be deduced if $\mathbf{B_o}$ and hence the resonance frequencies vary spatially within the patient. NMR fields have no known deleterious physiological effects, although there should be no metal objects in or near the patient. Functional NMR may replace PET since it offers the same real-time three-dimensional imaging capabilities without radiation exposure.

6.3 Therapeutic Nuclear Medicine

Because cancer cells divide rapidly and are therefore very sensitive to radiation damage, radiation is often used (usually with surgery and/or chemotherapy) to treat cancer (Fig. 43) [10]. Radiation delivery methods such as external beam radiotherapy, brachytherapy, direct radioisotope administration, and radioimmunotherapy strive to minimize the dose to the rest of the patient's tissues. Antiemetics such as prochlorperazine can minimize radiation sickness nausea during radiotherapy.

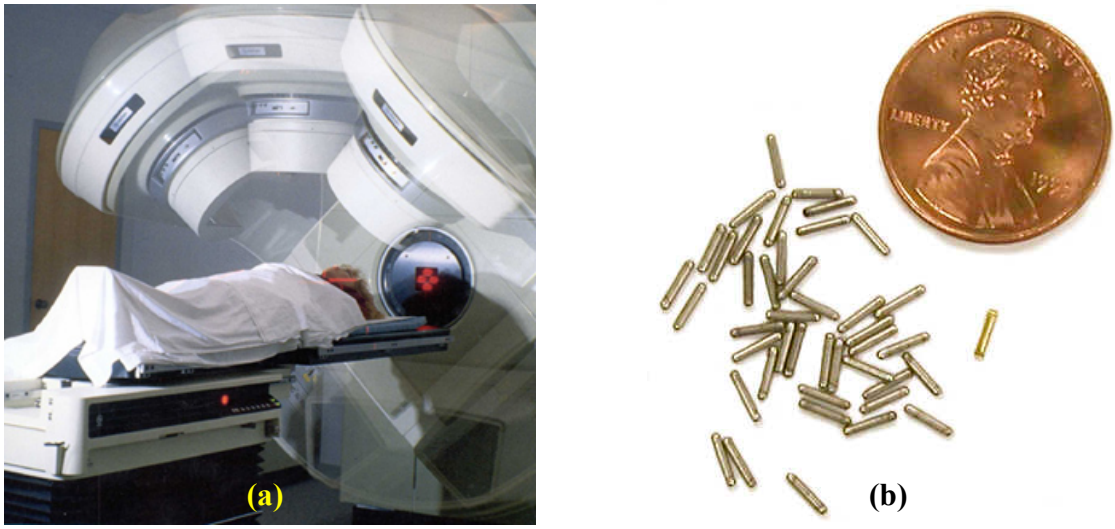

Figure 43. Examples of therapeutic nuclear medical techniques. (a) Radiation beams can be focused on a tumor. **(b)** Sealed radioactive "seeds" can be injected into a tumor, or antibodies can guide radioisotopes to cancer cells.

External beam radiotherapy [Fig. 43(a)] focuses intense radiation on a tumor, usually daily for a few weeks. Beta radiation from an electron accelerator cannot penetrate deeply and therefore is used for surface tumors like skin cancer. Occasionally protons are used instead. X-rays from a bremsstrahlung source or gamma rays from ^{60}Co are commonly used for tumors within the body. Neutron beams damage molecules by direct collisions, not formation of free radicals, and thus are sometimes used on oxygen-starved tumors that are relatively resistant to other forms of radiation.

Brachytherapy involves injecting a sealed radioactive seed [Fig. 43(b)] into a tumor via a needle. A β^- or α-emitting radionuclide is used so that all the energy is deposited in the surrounding tumor. Either the half-life is very short or the seed is removed after a certain period of time. For example, ^{125}I or ^{103}Pd seeds are used to treat prostate cancer.

Direct radioisotope administration is possible when the cancer cells selectively take up a certain element. Since the thyroid gland absorbs iodine, a hyperactive or cancerous thyroid can be destroyed by a sufficient dose of radioactive sodium iodide. ^{131}I, a fission product with an 8-day half-life, is used for this purpose. (Conversely, people in danger of exposure to fission reactor waste or fission bomb fallout should take nonradioactive iodine pills to saturate the thyroid and prevent uptake of ^{131}I, which could cause thyroid cancer in small doses or destroy a normal thyroid gland in larger doses.) Similarly, ^{89}Sr, another fission product with a 53-day half-life, is absorbed by bone cells and thus is used to treat metastatic bone cancer.

Radioimmunotherapy uses radiolabeled antibodies that specifically bind to certain cancer cell types. Suitable antibodies have been developed for leukemia as well as lung, colon, and breast cancers. Depending on the radioisotope label, antibodies can be used for either diagnosis or therapy.

6.4 Other Applications

Other applications of nuclear physics include radioactive dating (Fig. 44), as well as sterilization, smoke detectors, radioisotope thermoelectric generators, neutron activation analysis, and particle-induced X-ray emission (Fig. 45) [1, 2].

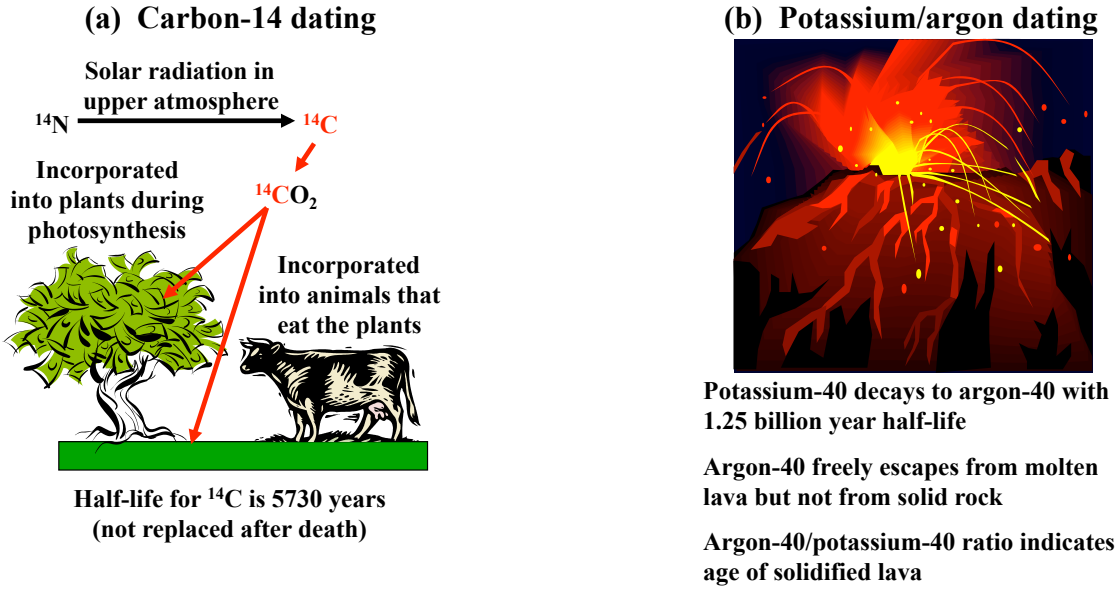

Figure 44. Radioactive dating. (a) Carbon-14 dating. **(b)** Potassium/argon dating.

Radioactive dating (Fig. 44) can be used to determine the age of an object such as a rock or biological material, provided that the object contained a known amount of radioisotope when it was formed. The best-known example is radiocarbon or ^{14}C dating. Cosmic rays transmute some ^{14}N into ^{14}C in the upper atmosphere. Living organisms acquire carbon from atmospheric CO_2 either directly (for plants) or indirectly from other organisms, and approximately 1×10^{-12} of their carbon is ^{14}C. The decay rate of the ^{14}C ($\tau_{1/2} \approx 5730$ years, or 13.5 decays/min per gram of total carbon) is balanced by intake of fresh carbon when an organism is alive, but not after it dies. For samples less than $\sim 50,000$ years old, the ^{14}C content can generally be measured by a radiation counter. For older or unusually small samples with very little ^{14}C, a particle accelerator can be used as a mass spectrometer, distinguishing the charge and mass of different ions vaporized from the sample. Analysis of tree rings and historical records indicates that the rate of ^{14}C formation has remained relatively constant, and thus ^{14}C dating is fairly reliable. However, two problems complicate ^{14}C dating of biological matter formed after $\sim$ 1900 A.D. Burning of fossil fuels, in which all of the ^{14}C has long since decayed, has added carbon to the atmosphere and diluted the relative amount of ^{14}C. On the other hand, above-ground nuclear explosions from 1945 to 1963 added a great deal of ^{14}C to the atmosphere. As shown in Fig. 44(b) and explained in more detail in *Geology* ?.?, longer-lived isotopes such as ^{40}K ($\tau_{1/2} \approx 1.25$ billion years) can be used to date rocks and estimate the age of the earth.

Sterilization of medical products, medical waste, food, or other items [Fig. 45(a)] is frequently accomplished via a high-energy electron beam, X-ray bremsstrahlung, or gamma rays from a source such as ^{60}Co.

(a) Radiation sterilization of medical products, food, etc.

(b) Smoke detectors

Americium-241 emits alpha particles, ionizing air inside the detector and allowing electric current to flow

Smoke particles decrease the current flow and trigger an alarm

(c) Radioisotope Thermoelectric Generators (RTGs)

Convert heat from alpha decay (e.g., ^{238}Pu) into electricity
Small RTGs supply electricity to cardiac pacemakers
Large RTGs on spacecraft exploring outer planets

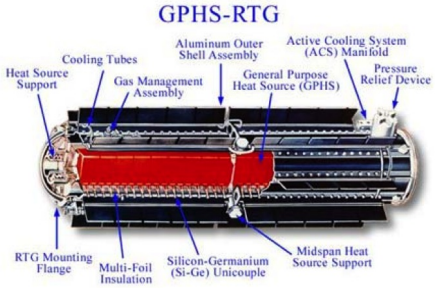

(d) Neutron activation analysis and Particle-Induced X-ray Emission (PIXE)

Identify elements in an object by their response to radiation

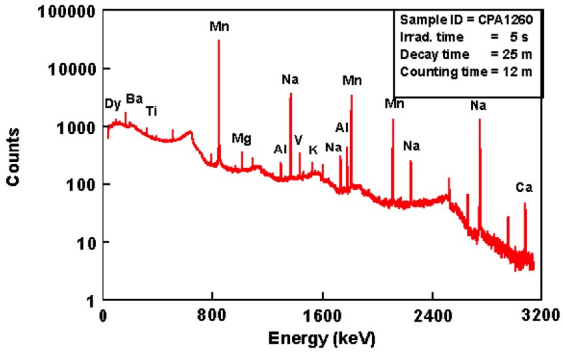

Figure 45. Other applications of nuclear physics include (a) sterilization, (b) smoke detectors, (c) radioisotope thermoelectric generators, and (d) neutron activation analysis and particle-induced X-ray emission.

Smoke detectors [Fig. 45(b)] contain a small amount of ^{241}Am ($\tau_{1/2} \approx 433$ years), which emits 5.6-MeV alpha particles that ionize air, making current flow between two closely spaced electrodes. Smoke contains strongly ionized atoms that collide with the ionized air molecules and decrease the current, triggering an alarm.

Radioisotope Thermoelectric Generators (RTGs) [Fig. 45(c)] are very small nuclear power sources. They use long-lived radioisotopes such as ^{238}Pu, which emits 5.6-MeV alpha particles with a half-life of 86 years, corresponding to a power output of 0.6 Watts/gram. A thermoelectric converter turns the decay heat into electricity. Small RTGs power cardiac pacemakers (~ 300 μW of power), while larger ones power the electronics on spacecraft going to the outer solar system, which don't require full-fledged fission reactors but are too far from the sun to use solar panels.

Neutron Activation Analysis (NAA) [Fig. 45(d)] involves bombarding a sample with thermal neutrons to determine its composition. Neutron capture (n,γ) processes typically create short-lived radioactive nuclei that decay via beta and/or gamma decay. Analysis of all the gamma rays and their energies reveals the types and amounts of various nuclei in the original sample. Other than the low-level, short-lived radioactivity, this method is nondestructive.

Particle-Induced X-ray Emission (PIXE), by comparison, involves bombarding a sample with heavy or light nuclei to determine the composition. The charged bombarding nuclei can remove inner electrons from nuclei in the sample. When outer electrons drop down to fill the vacancies in the inner orbitals, they emit characteristic X-rays that identify the sample nuclei.

References

[1] Emilio Segrè, *Nuclei and Particles* (2nd ed., Benjamin Cummings, Reading, MA, 1977). Expanding on ca. 1950 lecture notes by his mentor Enrico Fermi, Segrè adopts Fermi's concise, physically intuitive style. The result is the best introductory textbook in this field, simultaneously very readable, scientifically detailed, and far-ranging.

[2] Kenneth S. Krane, *Introductory Nuclear Physics* (Wiley, New York, 1988). Another highly readable introductory text, more basic than Segrè but with some good insights nonetheless.

[3] John M. Blatt and Victor F. Weisskopf, *Theoretical Nuclear Physics* (Dover, New York, 1952). An exhaustively detailed yet readable presentation of most aspects of nuclear physics. It only betrays its age in a few places, such as its discussions of the shell model and beta decay.

[4] Amos deShalit and Herman Feshbach, *Theoretical Nuclear Physics Volume I: Nuclear Structure* (Wiley, New York, 1974); Herman Feshbach, *Theoretical Nuclear Physics: Nuclear Reactions* (Wiley, 1992). These two volumes neglect many key topics (α decay, the deuteron, fission, fusion, etc.) despite their combined 1900-page length, and they thoroughly obfuscate other topics, particularly in the second volume. However, they do provide modern, detailed accounts of nuclear models, beta decay, and gamma decay. The first chapter is a helpful overview.

[5] Donald D. Clayton, *Principles of Stellar Evolution and Nucleosynthesis* (University of Chicago Press, 1983). While nuclear physics texts say alarmingly little about fusion reactions, this stellar physics text describes them in a fair amount of detail.

[6] B. Brunelli and G. G. Leotta (eds.), *Muon-Catalyzed Fusion and Fusion with Polarized Nuclei* (Plenum Press, 1987). A decent introduction to muon-catalyzed and spin-polarized fusion.

[7] Cyriel Wagemans, *The Nuclear Fission Process* (CRC Press, 1991). This reference and those it cites are good for filling the gaps in nuclear physics textbooks regarding fission reactions.

[8] V. B. Berestetskii, E. M. Lifshitz, and L. P. Pitaevskii, *Quantum Electrodynamics* (2nd ed., Pergamon Press, New York, 1982). Shares the characteristic strengths and weaknesses of the other texts in the Landau and Lifshitz series. It contains many examples and insights that simply cannot be found elsewhere, though it champions mathematics over physical explanations.

[9] Glenn F. Knoll, *Radiation Detection and Measurement* (3rd ed., Wiley, New York, 2000). Clear but comprehensive, this book lives up to its name.

[10] Wagner, Szabo, and Buchanan (eds.), *Principles of Nuclear Medicine* (2nd ed., Saunders, 1995). Provides thorough coverage of diagnostic and therapeutic nuclear medicine, and it also makes an excellent doorstop.